2014

The Inverse Design Of Hypersonic Flow Paths

Thomas Lawrence
North Carolina Agricultural and Technical State University

The Inverse Design of Hypersonic Flow Paths

Thomas Lawrence

North Carolina A&T State University

A thesis submitted to the graduate faculty

in partial fulfillment of the requirements for the degree of

MASTER OF SCIENCE

Department: Mechanical Engineering

Major: Mechanical Engineering

Major Professor: Dr. Frederick Ferguson

Greensboro, North Carolina

2014

The Graduate School
North Carolina Agricultural and Technical State University
This is to certify that the Master's Thesis of

Thomas Lawrence

has met the thesis requirements of
North Carolina Agricultural and Technical State University

Greensboro, North Carolina
2014

Approved by:

Dr. Frederick Ferguson Major Professor	Dr. John Kizito Committee Member
Dr. Sun Yi Committee Member	Dr. Mookesh Dhanasar Committee Member
Dr. Samuel Owusu-Ofori Department Chair	Dr. Sanjiv Sarin Dean, The Graduate School

Biographical Sketch

Thomas Lawrence was born on November 10, 1987, in Chesapeake, VA. He graduated Magna Cum Laude with his Bachelor of Science degree in Mechanical Engineering in 2010 from North Carolina Agricultural and Technical State University. He is a candidate for the Master of Science degree in Mechanical Engineering.

Dedication

To all family, friends and loved ones who expressed their support of me throughout this experience.

Acknowledgements

First and foremost, I would like to thank God for the mental fortitude and determination that he has instilled within me. I would like to express my gratitude toward my advisor Dr. Frederick Ferguson for his academic guidance and financial support of me. I would also like to thank my committee members, Dr. John Kizito, Dr. Mookesh Dhanasar and Dr. Sun Yi, for lending their time toward the critiquing of this thesis. I express my thanks to Wright-Patterson Air Force Base for allowing me to use their resources. I am grateful for the support I received from my mother, father and younger brother. Your expressions of love toward me did not go unnoticed. I appreciate the words of encouragement from my girlfriend and her family. Thank you all for your appreciation and acceptance of me.

Table of Contents

List of Figures

List of Tables

Nomenclature

1D	One dimensional
2D	Two dimensional
3D	Three Dimensional
$\alpha_1, \alpha_2, \alpha_3$	Control parameters for scramjet model
A_1	Area one
A_2	Area one
A^*	Area at the throat
c_f	Skin friction coefficient
c_p	Specific heat at constant pressure
D_h	Hydrolic diameter
D	Diameter
dA	Change in area
dM	Change in Mach number
dP	Change in pressure
dT	Change in temperature
du	Change in velocity
dx	Change in position
dy	Change in y
dH	Change in Enthalpy
dQ	Change in chemical energy
$d\dot{m}$	Change in mass flow rate
$d\gamma$	Change in specific heat ratio

h	Step size
h_1	Enthalpy one
h_2	Enthalpy two
k_1,l_1,m_1	Function of two variables at the beginning of the interval
k_2,l_2,m_2	Function of two variables at the midpoint of the interval
k_3,l_3,m_3	Function of two variables at the midpoint of the interval
k_4,l_4,m_4	Function of two variables at the end of the interval
L	Length of a given duct
L_{x1}	Length from A_0 to B_0 (see Figure 6.1)
L_{x2}	Length from A_0 to C_0 (see Figure 6.1)
L_{x3}	Length from A_0 to D_0 (see Figure 6.1)
L_{y1}	Height from point B_0 to B_1 (see Figure 6.1)
L_{y2}	Height from point D_0 to D_1 (see Figure 6.1)
L_{y3}	Height from point D_0 to D_2 (see Figure 6.1)
M	Mach number
M_1	Inlet Mach number
M_{i+1}	Mach number at position x_{i+1}
$\dot{m}$	Mass flow rate
N	Number of points
P	Pressure
P_1	Inlet pressure
P^*	Pressure at choked flow conditions
P_{ref}	Reference pressure

P_0	Stagnation pressure
P_{i+1}	Pressure at position x_{i+1}
PV_{old}	Old set of primitive variables
PV_{new}	New set of primitive variables
ρ_1	Density one
ρ_2	Density two
p_1	Pressure one
p_2	Pressure two
T	Temperature
T_0	Stagnation temperature
T^*	Temperature at choked flow conditions
T_{ref}	Reference temperature
τ_w	Wall shear stress
T_1	Inlet Pressure
T_{i+1}	Temperature at position x_{i+1}
u_1	Velocity one
u_2	Velocity two
x_i	Location at position x_i
x_{i+1}	Location at position x_{i+1}
x_n	Location at position x_n
y_i	Value of function y at x_i
y_{i+1}	Value of function y at x_{i+1}
γ	Specific heat ratio

Abbreviations

ATREX	Air-Turbo Ramjet Expander-Cycle
AVUS	Air Vehicle Unstructured Solver
CFD	Computational Fluid Dynamics
CIAM	Central Institute of Aviation Motors
CPGS	Conventional Prompt Global Strike
DARPA	Defense Advanced Research Projects Agency
DoD	Department of Defense (US)
HGV	Hypersonic Glide Vehicle
HPTF	Hypersonic Propulsion Test Facility
IMACS	Institute of Mechanics, Chinese Academy of Sciences
JAPHAR	Joint Airbreathing Propulsion for Hypersonic Application Research
JAXA	Japan Aerospace Exploration Agency
NASA	National Aeronautics and Space Administration
NASP	National Aerospace Plane
ONERA	Office National d'Etudes et de Recherches Aerospatiales
HSGTS	Hypersonic Space and Global Transportation System
HyTECH	Hypersonic Technology
SED	Scramjet Engine Demonstrator
SSTO	Single-Stage-To-Orbit
TBCC	Turbine-Based Combined Cycle
TSTO	Two-Stage-To-Orbit

Abstract

Previous research efforts at North Carolina Agricultural and Technical State University (NCAT), led to the design of a morphing RAM-SCRAMJET model with superior thrust-to-drag performance characteristics. A literature survey, conducted as part of this MS thesis effort, revealed that the morphing RAM-SCRAMJET model has many attractive engineering characteristics and is worthy of a realistic engineering evaluation. The objective of this effort is to improve on the NCAT RAM-SCRAMJET model by incorporating real-world effects into the design process. In accomplishing this goal, a quasi-one-dimensional flow field solver with capabilities of modeling the real-world effects was developed, coded in object oriented FORTRAN, and incorporated into the NCAT original model. The improved quasi-one-dimensional flow field solver is based on the Runge-Kutta 4^{th} order method for solving systems of differential equations. In principle, the new solver allows for the flow field evaluation within arbitrary shaped ducts in which the influences of 'area change', 'friction', 'heating' and 'chemistry' may be of importance. Prior to incorporating the new solver into the NCAT RAM-SCRAMJET model, a detailed validation study was conducted. These tests demonstrated that the 'area change' and 'friction' capabilities performed as expected. Unfortunately, the 'heating' and 'chemistry' capabilities did not, and as such these capabilities were not added to the NCAT model. Now, with improved but limited real-world capability, the NCAT RAM-SCRAMJET model was used to conduct an updated system performance study. Engineering tests were conducted in the Mach number range of 4 through 12. Results showed the improved NCAT scramjet code performs well at low Mach numbers, but did not compare well with independent efforts in the high Mach number region. At this stage, the difference is attributed to the fact that the new flow field solver cannot predict the effects of heating.

`

CHAPTER 1

Introduction

As part of this MS thesis requirement, a literature survey in the field of hypersonic technology was conducted. The goal was to identify all existing research opportunities that may serve the hypersonic aerodynamic needs of the air and space community. Results of this survey showed that hypersonic missiles and aircraft are of interest to the US military forces, and reusable hypersonic access to space vehicles are of interested to the National Air and Space Administrations. An international survey on the importance Hypersonic Aerodynamics was also conducted. The findings of this study are detailed in Chapter 2. NCAT has already embarked on a scramjet design project that will aid in the advancement of hypersonic technology. This chapter highlights NCAT hypersonic research efforts and puts it in perspective in relations to the hypersonic research activities conducted nationally. Also described in this chapter is the motivation behind the current research effort, and if successful, its potential contribution to the field.

1.1 Objective

The objective of this research is to independently validate the scramjet model developed by Dhanasar (Dhanasar, 2009) at North Carolina A&T. This scramjet model, displayed in Figure 1.1, was designed to be a baseline hypersonic propulsion engine model that could help advance hypersonic vehicle technology. Figure 1.1 represents a sample of the capabilities contained within the NCAT scramjet model. The scramjet model grants one the ability to manipulate the geometry with a series of design parameters. The focus of the current MS thesis research is on the development a tool capable of conducting an accurate aerodynamic analysis of arbitrary shaped aerodynamic ducts.

`

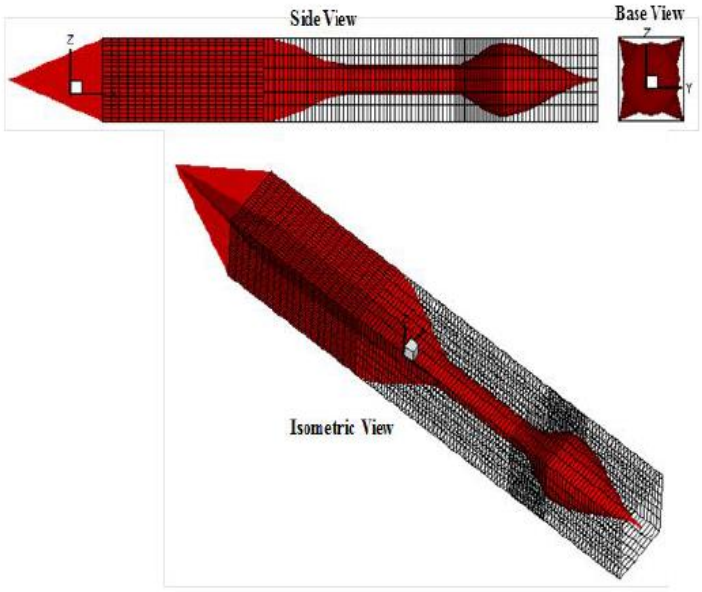

Figure 1.1. Computational model of the morphing ramjet-scramjet engine (Dhanasar, 2009).

One of the design goals of this tool is to provide technical guidance prior to the much needed robust aerodynamic evaluation. As such processes may involve significant expenses and resources, for example, today's computational fluid dynamics (CFD) tool costs the NCAT ME Department $25,000 annually, with no less than six months to turn around a single design.

1.2 Motivation

The lack of a tool with the ability to conduct an accurate aerodynamic analysis without the means of CFD serves as the motivation for this research. A tool capable of providing that analysis would allow one to quickly ensure that a scramjet model is working efficiently prior to doing all the preparation needed for CFD. The construction of the aforementioned tool would be critical in aiding the advancement of hypersonic vehicle technology. Hypersonic vehicle technology is developed mainly for military and space exploration related applications.

1.2.1 Military applications. Hypersonic technology has proved itself useful in the realm of military applications. One future application is the Conventional Prompt Global Strike (CPGS) concept by Boeing ("Defense", 2014).

Figure 1.2. Conventional Prompt Global Strike concept by Boeing ("Defense", 2014).

CGPS is a weapons system that relies on a flight-proven hypersonic configuration and allows rapid, global delivery of weapons within one hour of being launched. Boeing plans on CGPS being a key technology in future operation systems ("Defense", 2014).

The Falcon HTV-3X shown in Figure 1.3 below is a conceptualized hypersonic aircraft model that is designed to take-off from a conventional runway under its turbojet power, accelerate to Mach 6 under combined propulsion and decelerate using its turbojet engine.

Figure 1.3. Falcon HTV-3X conceptual model (Walker, 2008).

`

The combined propulsion, referred to as the Turbine-based combined cycle (TBCC) propulsion system utilized by the HTV-3X is explained in further detail in Figure 1.4 below (Walker, 2008).

Figure 1.4. Turbine-based Combined Cycle Propulsion Concept (Walker, 2008).

TBCC is three-stage engine concept with two flow paths. The upper flow path where the turbojet is located serves as the low-speed flow path while the lower path containing the ramjet/scramjet engine is the high-speed path. Each of the two paths share an inlet and exhaust (Walker, 2008).

1.2.2 Space exploration applications. The need for more inexpensive means of space travel can be met by advances in hypersonic technology. The Hypersonic Space and Global Transportation System (HSGTS), pictured in Figure 1.5, is a flight vehicle concept to help reduce space launch costs relative to expendable rockets (Bowcutt, 2011).

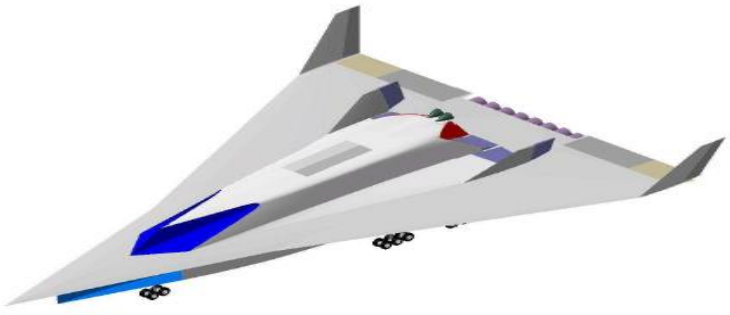

Figure 1.5. Hypersonic Space and Global Transportation System (HSGTS) (Bowcutt, 2011).

The HSGTS was designed to be a two-stage-to-orbit (TSTO), reusable vehicle that was capable of taking off and landing horizontally. During takeoff and landing, air breathing propulsion would be employed while rocket propulsion would be used for space travel. The technology integrated into the HSGTS will allow it to achieve conventional airplane-like operations (Bowcutt, 2011).

1.3 Problem Statement

The scramjet model developed by Dhanasar was comprised of seven main sections. Those sections, depicted in Figure 1.6, included the forebody, inlet, isolator, transition zone, combustor, diffuser and nozzle.

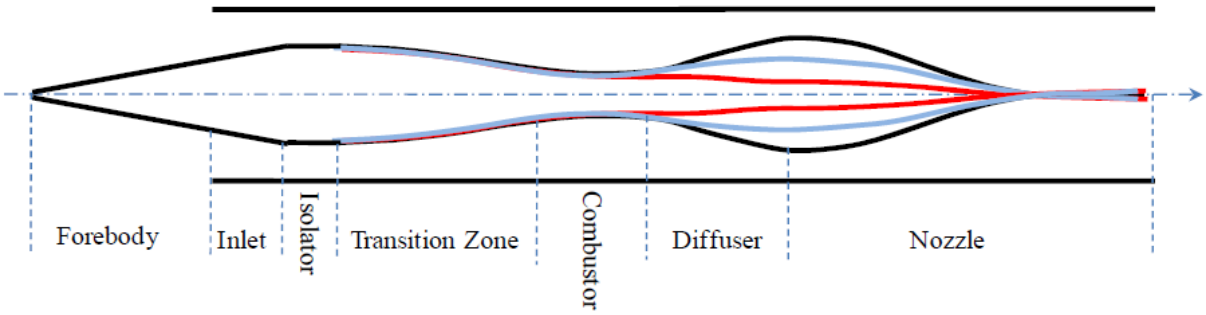

Figure 1.6. Ramjet-scramjet propulsion model (Dhanasar, 2009).

The focus of this thesis is on the forebody, inlet and isolator sections. Using FORTRAN, a quasi-1D flow solver implementing the Runge-Kutta 4th order method is developed to independently validate the forebody, inlet and isolator sections of the scramjet model provided by Dhanasar. The flow solver is capable of providing accurate preliminary analysis of ducts of various shapes without the hassle of using CFD.

1.4 Thesis Outline

The results of a literature review is presented in Chapter 2 of this thesis. The literature review focuses on hypersonic programs in the United States as well as international programs.

Chapter 3 details the scramjet design efforts at NCAT. Chapter 4 explains the methodology behind the Runge-Kutta 4th order solver. In Chapter 5, the Runge-Kutta solver is validated and compared with results obtained from the literature review. Chapter 6 demonstrates the implantation of the Runge-Kutta 4th order solver as tool to quantitatively validate Dhanasar's scramjet model. Finally, in Chapter 7, a conclusion is made along with future work suggestions.

`

CHAPTER 2

Literature Review

An international survey on the importance of hypersonic aerodynamics was conducted. Efforts made by the United States, Russia, France, Australia, Japan and China are presented. Over the years, the United States has shown its technical prowess in field of hypersonics by producing the world's fastest and most sustaining scramjet engines. The Russians, French, Australians, Japanese and Chinese have made monumental contributions toward the creation of scramjet missiles and hypersonic air-breathing flight models. This chapter summarizes the results of the international survey as they relate to this MS thesis.

2.1 Literature Survey

A literature survey was conducted that focuses on hypersonic propulsion programs both domestically, in the United States, and internationally. The international section of the literature review focuses on programs in Russia, France, Australia, Japan and China.

2.1.1 Programs in the United States. There have been numerous successful scramjet programs in the United States since the 1960s (Curran, 2001). During the 1960s, there was an increased availability of funds for space related studies. Unfortunately, this was coupled along with a sharp decline in resources for aeronautical research. This lead to the focus on hydrogen-fueled scramjet work using single-stage-to-orbit (SSTO) concepts (Curran, 2001). Scramjet programs spearheaded by government organizations like NASA, DARPA and the US Air Force rose to the occasion.

2.1.1.1 NASA/DARPA National Aerospace Plane (NASP) program. In the 1960s, the US Air Force initiated first aerospace plane program (Chase, 1995). The aerospace plane program considered an air breathing, hydrogen-fueled aerospace vehicle that could be controlled

`

and reused like an airplane. Single-stage-to-orbit (SSTO) and two-stage-to-orbit (TSTO) aerospace plane concepts were also considered (Chase, 1995). This concept came about as a result of the dwindling of aerospace resources. The ideals of this concept were instrumental in the creation of the National Aerospace Plane (NASP) program (Curran, 2001). An illustration of the NASP concept vehicle is displayed in Figure 2.1.

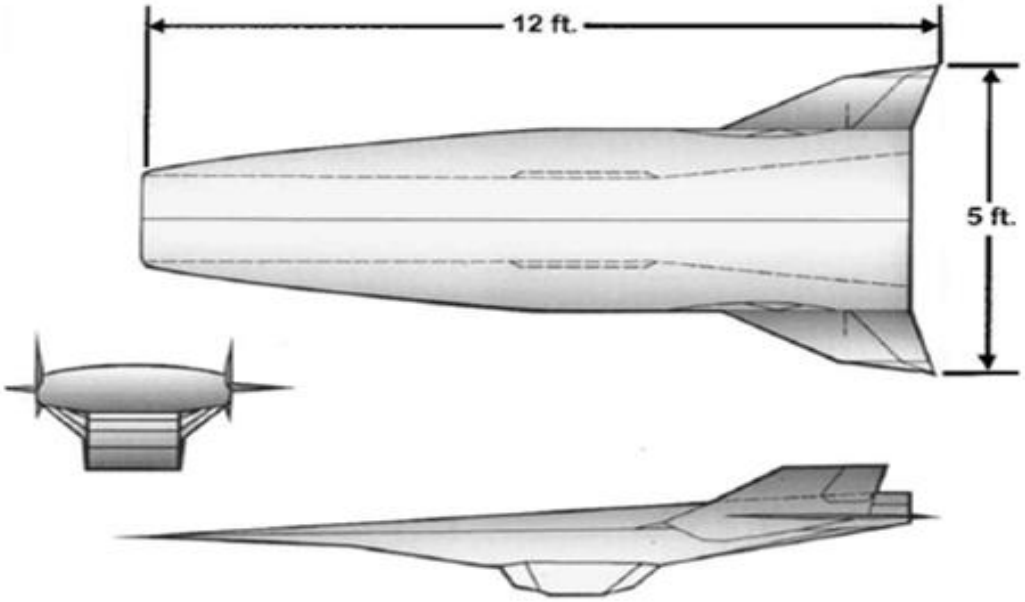

Figure 2.1. NASA Hyper-X research vehicle (Curran, 2001).

NASP was established in 1986 by NASA and the DoD with DARPA as the lead agency (Curran, 2001). NASP was envisioned as an air breathing, hydrogen-fueled SSTO vehicle that would revolutionize space transportation and reduce costs compared to rocket launch vehicles (Chase, 1995). The NASP initiative was an attempt to increase the speed of air breathing aircraft to Mach 25 (Barthelemy, 1989). The goal of NASP was to develop an aircraft with the ability to use conventional airfields and accelerate to hypersonic speeds. It would be capable of delivering useful payloads to space and return to Earth with propulsive methods while having the operability and flexibility of a conventional airplane (Barthelemy, 1989). NASP was terminated

in 1993 (Chase, 1995). One of the biggest criticisms of the NASP program was that the scramjet engine tests were limited to simulated flights in wind tunnels (Harsha, 2005). The termination of NASP ultimately lead to the creation of the Hyper-X program.

2.1.1.2 NASA X-43A program. The Hyper-X program was approved by NASA in July 1996 and started in September 1996 (McClinton, 1997). This program stemmed mostly from the NASP program and set out to conduct numerous flight test programs. The design and manufacture phase for Hyper-X was initiated in March 1997 (Harsha, 2005). One program that emerged from the Hyper-X program was NASA's X-43A program. An artist's conception of the X-43 can be observed below in Figure 2.2.

Figure 2.2. Artist conception of the X-43A in flight ("Spinoff", 1999).

The X-43A had notable flight tests that took place in the early 2000s. Its initial flight test on June 2, 1991 was unsuccessful due to an overload of the booster's control surfaces (Harsha, 2005). March 27, 2004 marked the first successful flight test of the X-43A as it maintained Mach 7 flight under the power of its own scramjet engine for approximately 10 seconds. This lead to a successful Mach 10 flight that took place later that year on November 16, 2004 (Harsha, 2005).

The X-43A flight tests represented the highest speeds reached by a vehicle powered by an air breathing engine in the atmosphere.

2.1.1.3 US Air Force/DARPA X-51A SED program. Upon the termination of the NASP program in 1993, the US Air Force initiated the HyTECH (Hypersonic Technology) program in 1995 as a follow-up (Mercier, 1998). The overall goal of HyTECH was to demonstrate the operability, performance and structural durability of an expendable liquid hydrocarbon-fueled scramjet propulsion system that operates from Mach 4 to Mach 8 (Mercier, 1998).

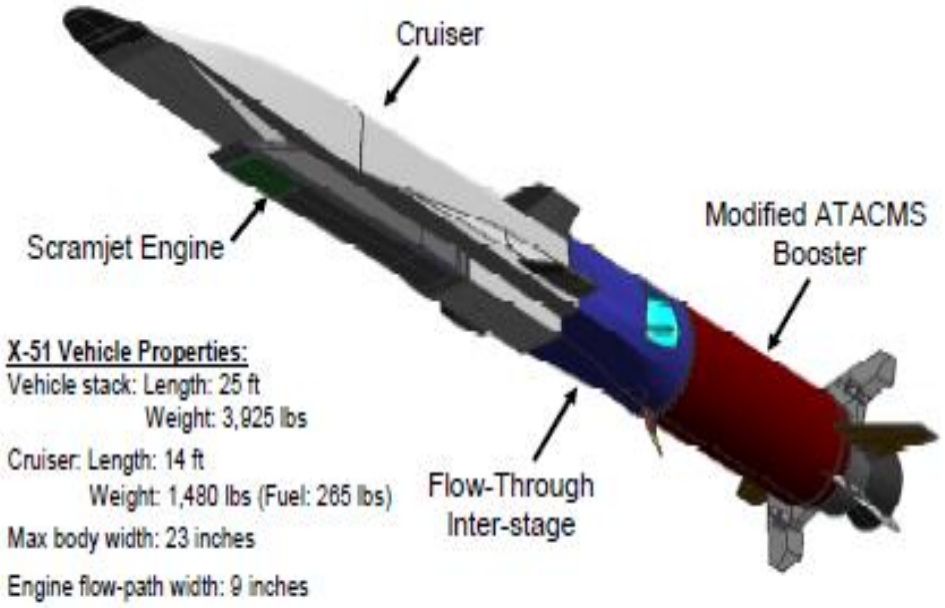

Figure 2.3. X-51 SED vehicle concept (Hank, 2008).

The X-51A Scramjet Engine Demonstrator (SED) program emerged from the HyTECH program in July 2005 (Hank, 2008). A concept model of the X-51A is displayed in Figure 2.3. The main program objective of the X-51A program was to flight test the US Air Force HyTECH scramjet engine, using hydrocarbon fuel, by accelerating a vehicle from boost, at approximately Mach 4.5 to Mach 6.5 (Hank, 2008). A flight test for the X-51A was conducted on May 1, 2013. A booster rocket was used to accelerate the X-51A to Mach 4.8. Once Mach 4.8 was reached, the

booster separated allowing the X-51A to fly under its own scramjet engine. The X-51A was able to reach a speed of Mach 5.1 and maintain flight for 240 seconds until it ran out of fuel (Rosenburg, 2013). The X-51A broke the world record for the longest air-breathing hypersonic flight. It is considered to be the most successful air-breathing hypersonic flight to date (Rosenburg, 2013).

2.1.2 International Programs. Several programs dedicated to the advancement of hypersonic, air-breathing propulsion have been initiated since the 1960s (Curran, 2001). Development programs from Russia, France, Australia and Japan are highlighted in this section of the literature review.

2.1.2.1 Russian programs. Russian scramjet research and development has been in progress for many decades (Curran, 2001). There is a limited availability of documentation in the English language. Due to the increased participation in international conferences, much of the fundamental work became available during the 1990s.

The institution known as the Central Institute of Aviation Motors (CIAM) led many of Russia's attempts at air-breathing hypersonic flight (Curran, 2001). The Kholod, displayed in Figure 2.4, was a major accomplishment of CIAM in 1991 (Curran, 2001)

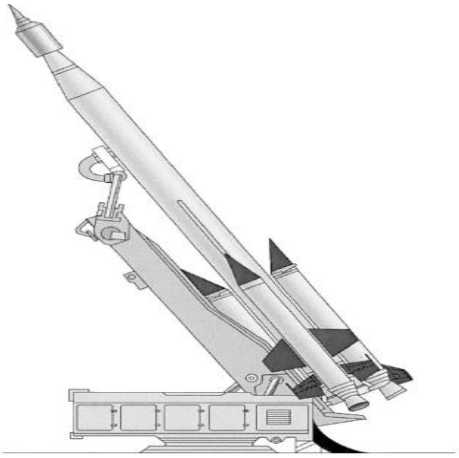

Figure 2.4. HFL Kholod concept illustration (Curran, 2001).

The Kholod was an axisymmetric dual-mode ramjet with an SA-5 surface-to-air missile used as a non-separable booster. The Kholod also utilized a support structure known as the Hypersonic Flying Laboratory (HFL) that was used a launching device (Curran, 2001).

On November of 1991, the HFL Kholod had its first successful flight test. (Bouchez, 2005) The engine was able to operate between Mach 3.5 – 5.7 demonstrating both subsonic and supersonic combustion modes. A second test for the HFL Kholod was conducted on November of 1992 with the help of ONERA, a French aerospace center (Bouchez, 2005). The second test provided results that were very similar to the first test. ONERA and CIAM collaborated once again for a third HFL Kholod flight test, however, the engine did not operate due to HFL system issues (Curran, 2001). A fourth test was conducted by CIAM and NASA on February 12, 1998 (Bouchez, 2005). Prior to the test, the SA-5 missile was modified demonstrate the full supersonic combustion mode to Mach 6.5. The engine data obtained from the test showed that flight speed varied from Mach 3.5 – 6.4, thus showing an improvement from the previous tests (Curran, 2001).

2.1.2.2 French programs. The French have been working scramjet programs since the early 1960s. ESOPE was a French program dedicated to the development of air-breathing hypersonic technology that was established in 1966 (Curran, 2001). ESOPE developed an axisymmetric engine with an annular combustor that utilized a dual-mode scramjet concept (Curran, 2001). Due to limited resources, this engine could only be ground tested. Two tests were conducted between 1970 and 1972. The first test demonstrated the need for improved fuel injection and mixing. For the second test, modifications were made and engine performance was much improved (Curran, 2001). The program was terminated in 1972 in favor of the development of the integral rocket ramjet engine (Curran, 2001).

`

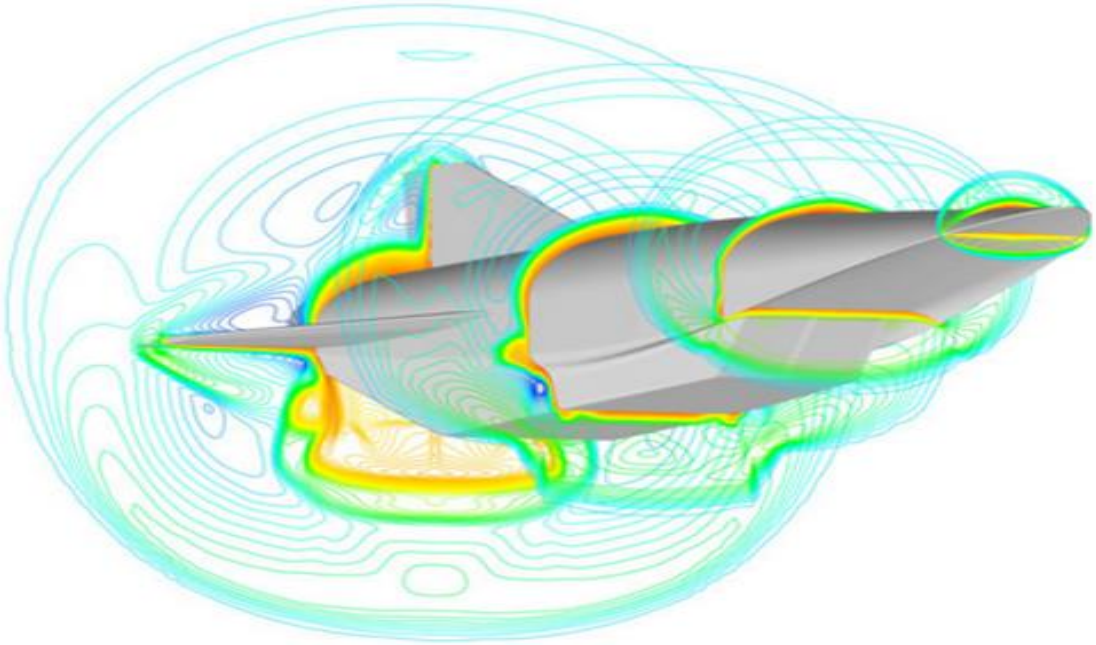

Figure 2.5. JAPHAR concept illustration ("JAPHAR", 2009).

Two other notable programs include PREPHA and the Joint Air-breathing Propulsion for Hypersonic Application Research (JAPHAR). PREPHA was established in 1992 as a follow-up to ESOPE. PREPHA focused primarily on hydrogen-fueled scramjet technology. (Curran, 2001) JAPHAR was a joint program between France and Germany that was initiated in 1997. An illustration of a concept vehicle from the JAPHAR program is displayed above in Figure 2.5. Its objective was to advance hydrogen-fueled dual-mode scramjet technology with the goal of testing a vehicle between Mach 4 and Mach 8. (Eggers, 2001)

2.1.2.3 Australian programs. Hypersonic propulsion work in Australia started in 1981 with the T3 hypersonic impulse facility at the Australian National University (Curran, 2001). This work transitioned to the T4 shock tunnel at the University of Queensland. The shock tunnel is capable of simulating orbital flight conditions (Curran, 2001).

One of Australia's most significant flight programs was the HyShot program established in 2001 (Curran, 2001). A concept illustration of HyShot is shown in Figure 2.6 below. The

objective of HyShot was to obtain the correlation between flight- and ground-test supersonic combustion data (Curran, 2001). HyShot was a missile based program that consisted of a series of flight tests of a simplified supersonic combustion experiment.

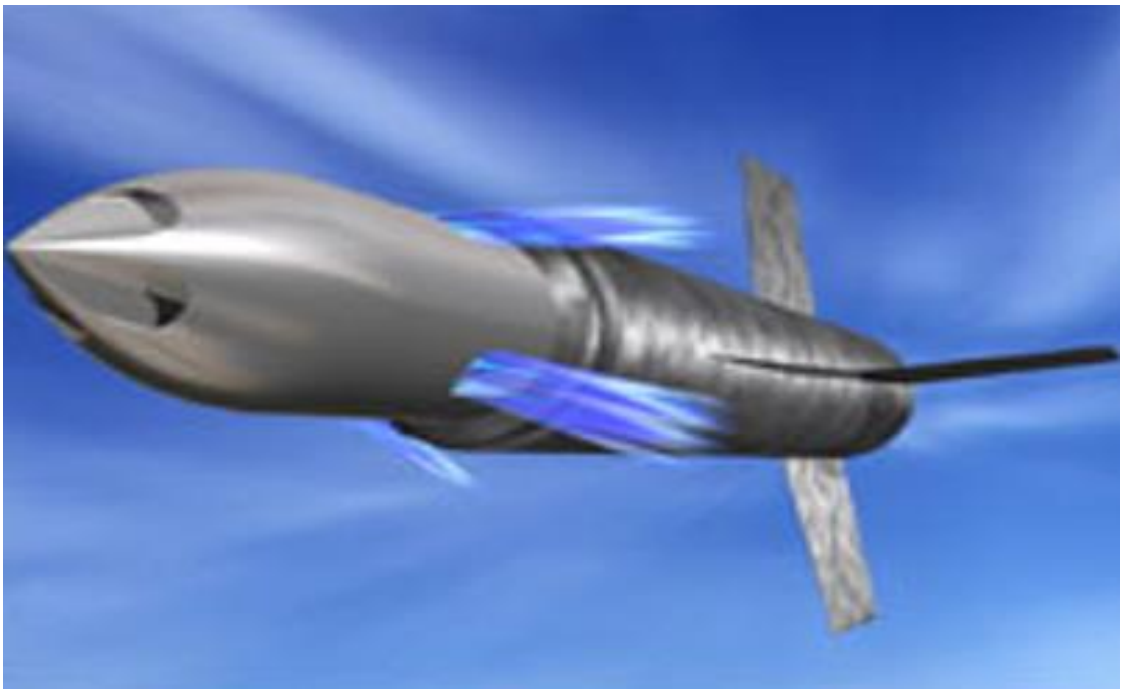

Figure 2.6. HyShot concept illustration ("Revolutionary", 2006).

In the HyShot experiments, a scramjet coupled along with a rocket is fired with a highly parabolic trajectory. During the nearly vertical re-entry portion of the trajectory, the scramjet experiment is conducted (Curran, 2001). The first HyShot launch took place on October 30, 2001 and was unsuccessful. The failure of the first experiment was due to the fins of the rocket breaking away during the first minute of flight. This problem was resolved by replacing the smaller fins with larger ones (Rosenburg, 2002). HyShot II was conducted on July 30, 2002 and was successful. This run led to two other successful runs (HyShot III and IV) along with others planned for the upcoming years (Curran, 2001).

2.1.2.4 Japanese programs. Efforts toward the advancement of hypersonic air-breathing propulsion and reusable launch systems have been directed by the Japan Aerospace Exploration

Agency (JAXA). Japanese research emphasized the development of air-breathing propulsion systems for space access (Dhanasar, 2009).

Figure 2.7. ATREX concept illustration (Sato, 2003).

A notable Japanese program was the Air-Turbo Ramjet Expander-Cycle (ATREX). The main objective of ATREX was to achieve Mach 6 flight at an altitude of 30 km (Sato, 2003). This program considered a TSTO concept. Development studies for ATREX have been conducted since 1988 by way of ground firing tests and wind tunnel tests (Sato, 2003).

2.1.2.5 Chinese programs. Since the end of the 1950s, China showed its interest in the development of hypersonic related technologies (Lin, 1991). This section highlights a few of the efforts made by the Chinese.

In the late 1970s, the People's Republic of China began development of the C-101 (Fry, 2004). The C-101 was designed to be a shore-based, supersonic, anti-ship missile and achieved a maximum cruise speed of Mach 1.8. It could also be launched from air and ship platforms. The

requirements of high speed and long range resulted in a large missile with two solid propellant boosters and two ramjet engines (Fry, 2004).

The C-301, was later developed to trump its predecessor, the C-101, with increased speed with a longer range. The C-301 variant was fitted with four boosters. It resembles a scaled-up C-101, but has a thicker fuselage. Although first seen in a Beijing display in November 1988, export versions were not released until the early 1990's (Fry, 2004). The missile employs four solid propellant boosters located above and below each ramjet engine. The two ramjets are mounted on narrow pylons extending from the sides of the fuselage. The C-301 cruises at Mach 2 with adjustable cruising altitudes and exhibits twice the range of the C-101 (Fry, 2004).

In order to understand the fundamental phenomena of scramjet, studies on supersonic combustion have been conducted in IMCAS (Institute of Mechanics, Chinese Academy of Sciences) since 1994. A hypersonic propulsion test facility (HPTF) was constructed that dedicated itself to the fundamental studies of scramjets with the support of IMCAS (Fry, 2004).

In recent news, the new hypersonic glide vehicle (HGV), dubbed the WU-14 was allegedly spotted flying at record-breaking speeds during a flight test on January 9, 2014 ("Missile", 2014). Its hypersonic speed range reportedly lies between Mach 5 and Mach 10. HGVs are designed for precise targeting and rapid delivery of weapons while also acting as a countermeasure toward hostile defenses ("China", 2014).

`

CHAPTER 3

Scramjet Design at NC A&T

It is of interest to note that the MS thesis research conducted herein is a relatively small part of a larger hypersonic research effort at NCAT. The NCAT hypersonic research program is supported by the Air Force Research Laboratory at Wright Patterson Air Force Base. This chapter describes the NCAT Hypersonic research efforts from a historic perspective, and highlights its challenges and accomplishments in relations to the motivation and objectives this MS thesis.

3.1 Inverse Design of a Baseline Tip-To-Tail Scramjet

An inverse design of a baseline tip-to-tail scramjet was developed by Dhanasar at NCAT (Dhanasar, 2009). A schematic of this scramjet model is pictured below in Figure 3.1. The inverse design implied that the scramjet model was shaped by the physics of the flow field it was subjected to. In other words, this scramjet model was deigned to yield the ideal scramjet configuration for a particular given flow field.

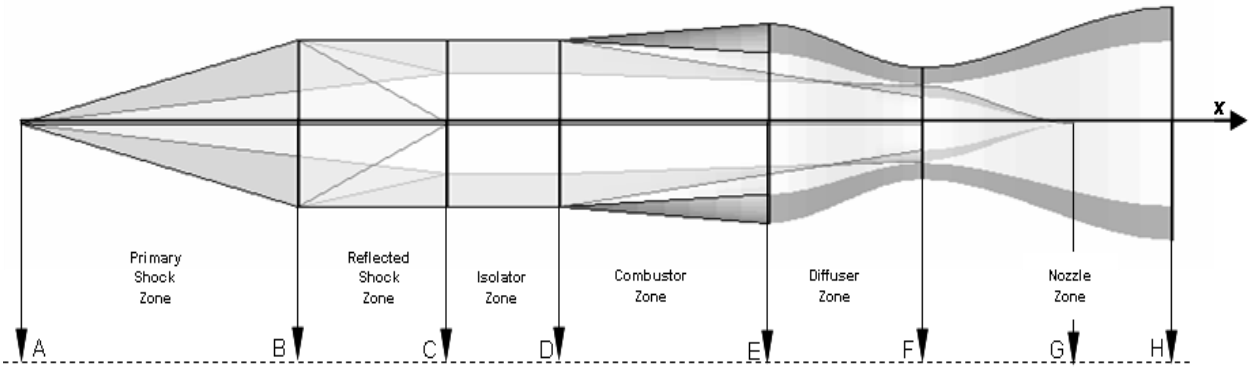

Figure 3.1. Tip-to-tail scramjet model (Dhanasar, 2009).

An incoming hypersonic flow field makes contact with the leading edge at A-Station creating a shock. The initial shock reflects from the upper section of B-station, known as the cowl lip, towards the reflection point at C-Station. The reflected shock directs itself toward the

isolator creating a series of weak oblique shocks, commonly referred to as a shock train (Dhanasar, 2009). Using the Waverider approach (Grant, 2010) along with 2D flow fields a 3D model was developed. A figure of the 3D scramjet model shown is shown in Figure 3.3 (Dhanasar, 2009).

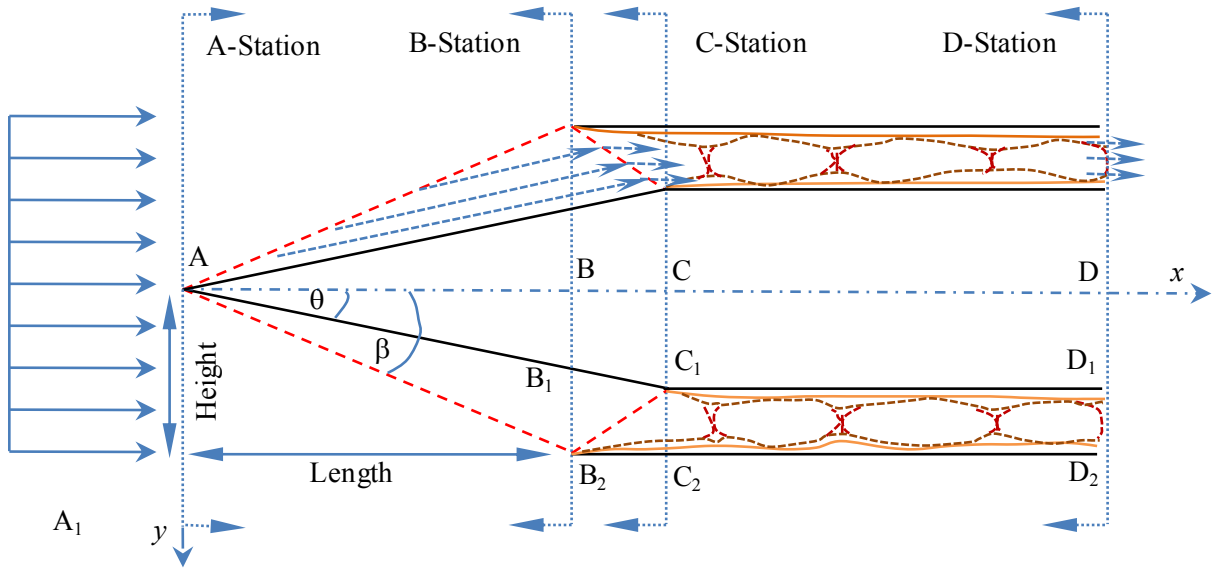

Figure 3.2. 2-D cross-section of the forebody-inlet-isolator section (Dhanasar, 2009).

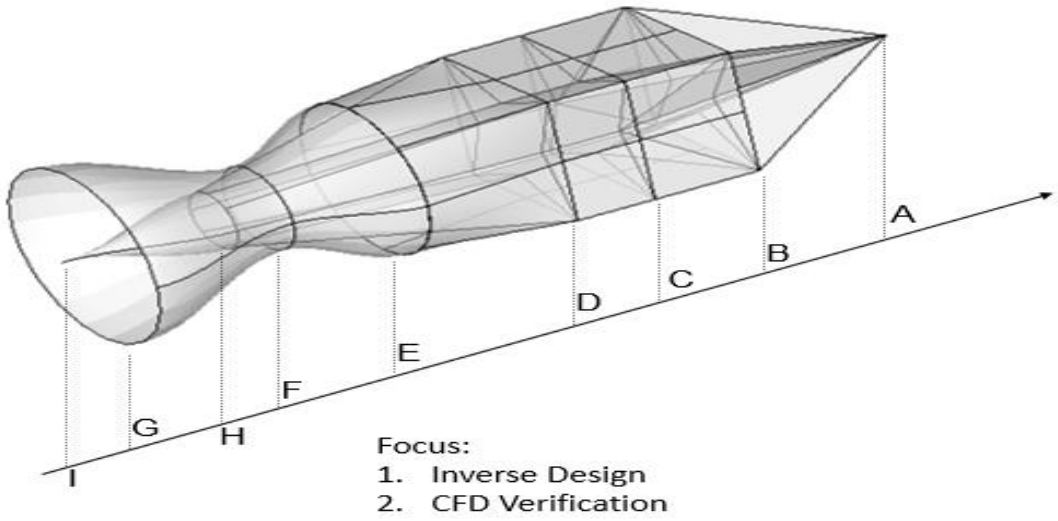

Figure 3.3. Complete 3-D scramjet model (Dhanasar, 2009).

3.1.1 Past CFD validation studies. Grant (Grant, 2010), a former master's student at North Carolina A&T, conducted a qualitative validation of the hypersonic flow field associated with an inlet that was inversely generated by Dhanasar (Dhanasar, 2009). Since Grant was conducting a qualitative analysis, he was only concerned with making sure the correct physics within the inlet was captured relative to similar studies. The inlet is illustrated in Figure 3.4 below.

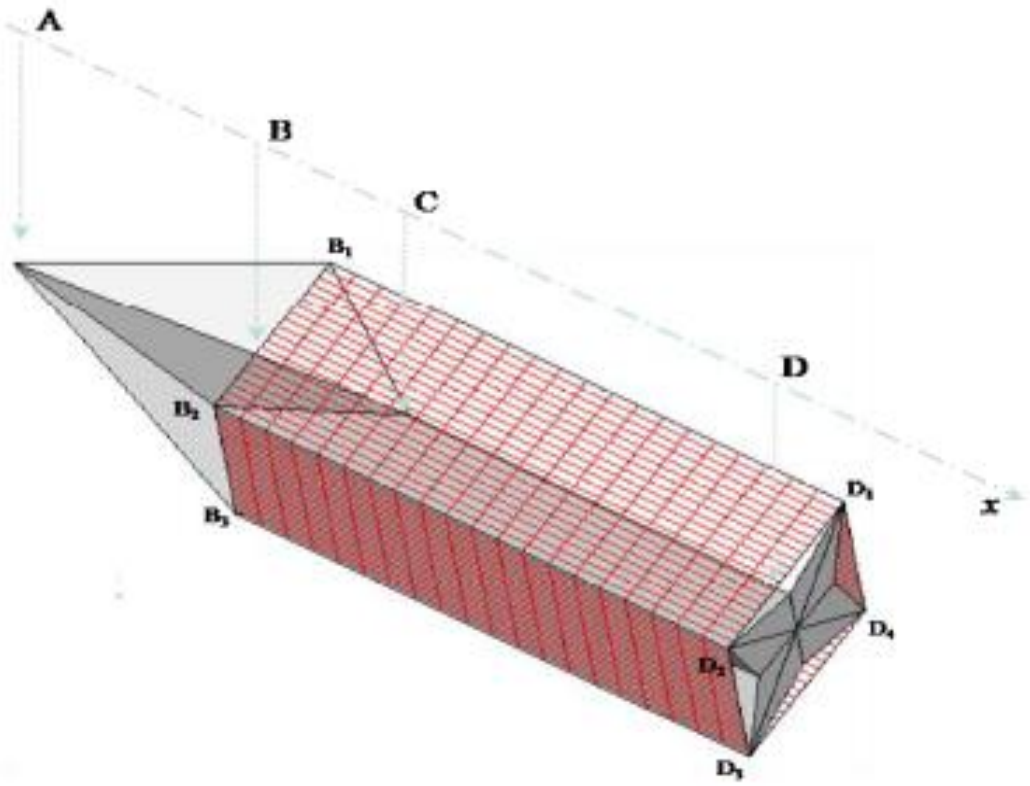

Figure 3.4. 4-point star inlet (Dhanasar, 2009).

In an effort to reduce computational costs, a piece of the 4-point star inlet pictured in Figure 3.4 above was independently validated. Each 4-point star inlet geometry was made of four individual components known as streamtubes. A typical streamtube associated with the 4-point star inlet is shown below in Figure 3.5.

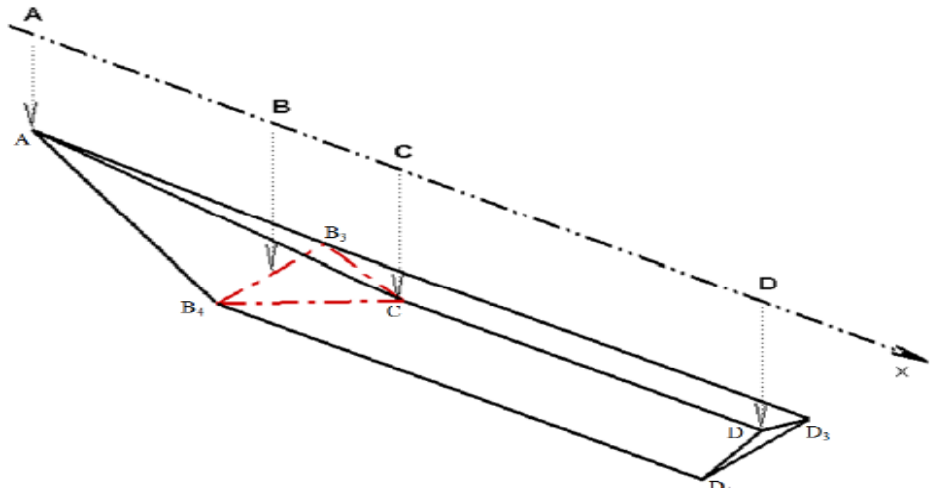

Figure 3.5. Waverider derived stream tube (Dhanasar, 2009).

3.3.1.1 2-D CFD study. Using GAMBIT, a grid generation software, the geometry of the streamtube of interest was formulated along with the grids associated with the geometry. The 2-D grid generation of the streamtube is shown in Figure 3.6. Using FLUENT, a well-known CFD software, flow field evaluations for the streamtube were made. The stream tube was constructed with a wedge angle of 17.5 degrees and evaluated at a free stream Mach number of 6.0 with an altitude of 30 km. This 2D study took viscous effects into account. The results for the 2D evaluations are described in Figures 3.7 and 3.8 in the form of Mach number and pressure contours, respectively (Grant, 2010).

The results of this 2D viscous evaluation showed that the expected flow field behaviors were recovered. In both illustrations of Figures 3.7 and 3.8, the primary and reflected shocks are recovered, and the primary flow field at the inlet is uniform. In Figure 3.7, a concentration of the Mach contour at the boundaries inside the streamtube indicated that boundary layers were developed. In the case of Figure 3.8, a weak shock train can be observed in the isolator (Grant, 2010). The analysis showed that the 2D model of the 4-point star-shaped forebody performed as designed.

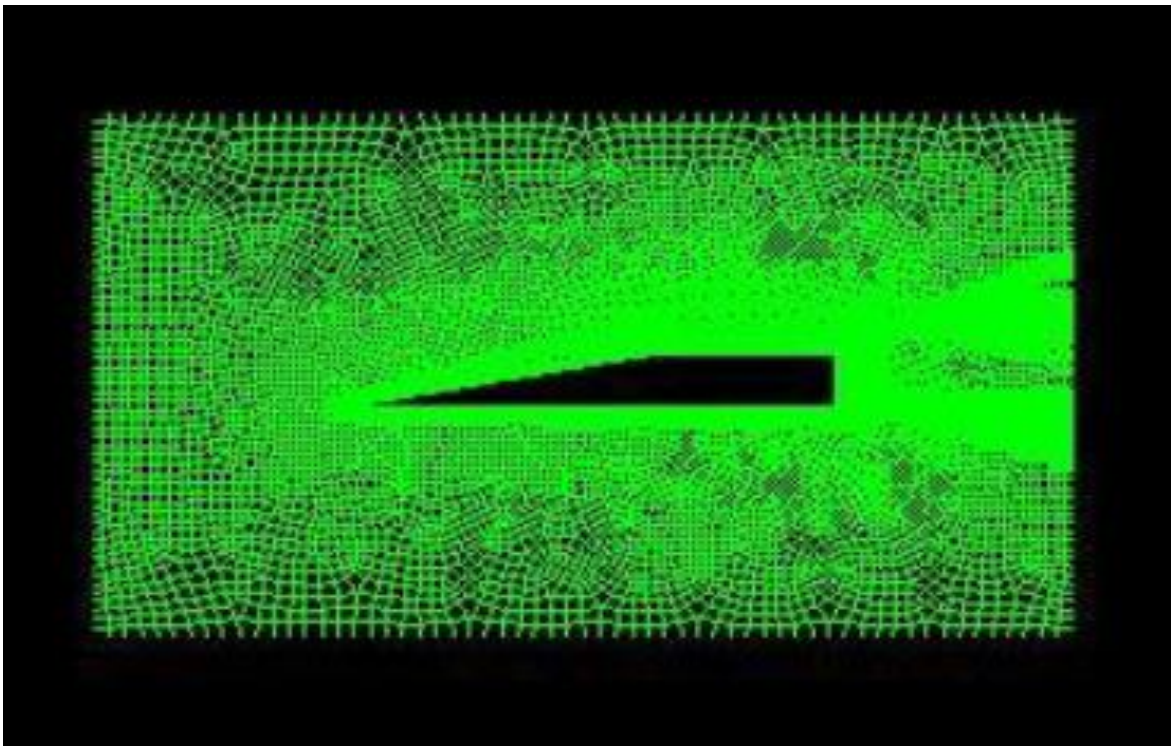

Figure 3.6. 2D grid of the streamtube (Grant, 2010).

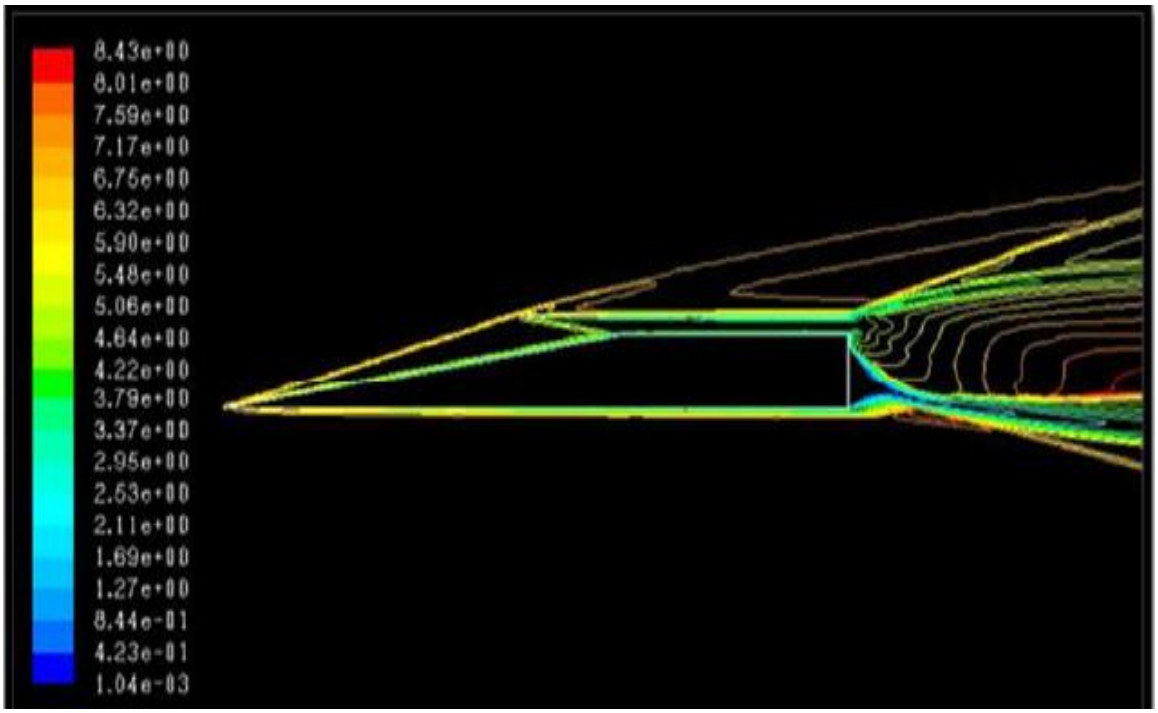

Figure 3.7. Mach 6 free stream with contours of Mach number (Grant, 2010).

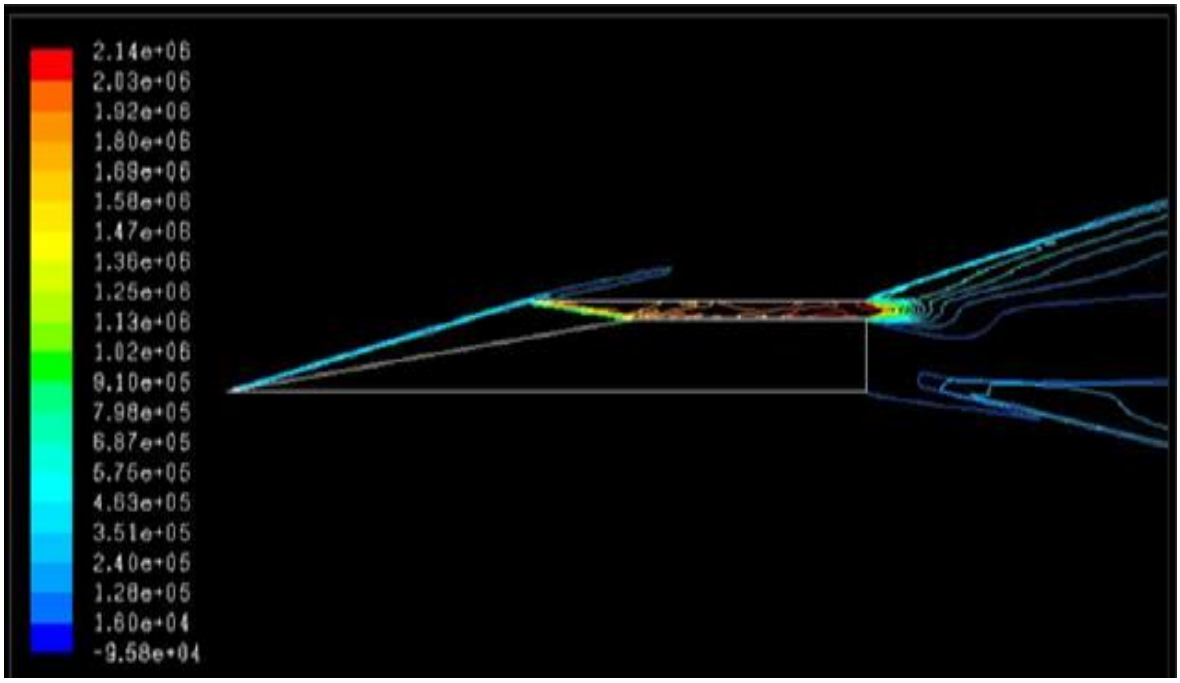

Figure 3.8. Mach 6 free stream with contours of pressure (Grant, 2010).

3.3.1.2 3-D CFD study. The promising 2-D viscous results from FLUENT prompted Grant to continue along with a 3-D CFD study. A 3-D grid of the streamtube was constructed in GAMBIT and is shown in Figure 3.9 below. Similar to the 2-D study, the stream tube was constructed with a wedge angle of 17.5 degrees and evaluated at a free stream Mach number of 6.0 with an altitude of 30 km for the 3-D study. Viscous effects were also taken into account.

The result from the 3-D study is depicted Figure 3.10. Figure 3.10 represents the Mach number distribution along the centerline geometry of the stream tube. The viscous result came out to be inconclusive and unsatisfactory. No convergence in any of the flow field variables was obtained. Due to the lack of computational resources larger grid sizes could not be tested (Grant, 2010).

The next 3D CFD evaluation was conducted using the Air Vehicle Unstructured Solver (AVUS) and Gridgen CFD software tools. The grid generation software, Gridgen, was used primarily to produce high quality grids. Using Gridgen, a set of grids were developed that

incorporated 24 layers of prism-like cells along the wall boundaries of the streamtubes. Illustrations of the 24 prism layers that were incorporated in the unstructured grid used in this analysis are presented in Figure 3.11.

Once the grids were developed, the grid information along with the free stream data and CFD model information were assigned and submitted to AVUS for flow field evaluation. The streamtube was evaluated at the same free stream Mach number, altitude and wedge angle as the previous 3D CFD study. 3D Euler results from the AVUS CFD study are presented in Figures 3.12 and 3.13 in the form of 2D data slices. Figures 3.12 and 3.13 illustrate 2D slices of the forebody-inlet Mach number and pressure distribution along the centerline plane of scramjet inlet, respectively.

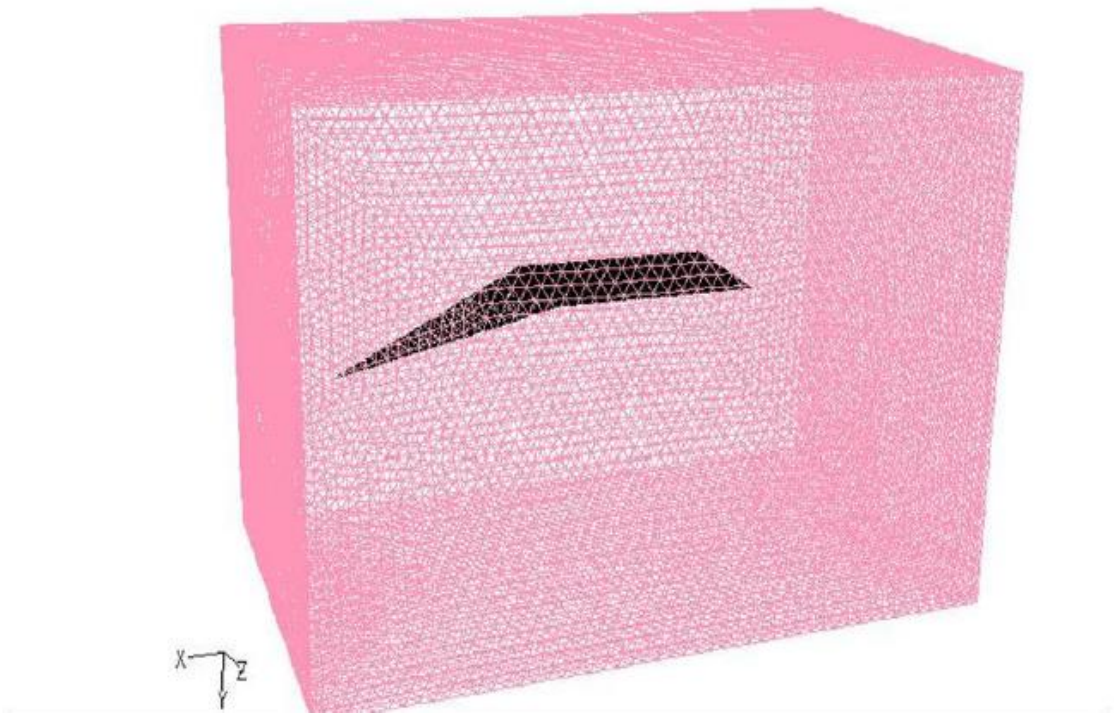

Figure 3.9. 3D grid of the streamtube (Grant, 2010).

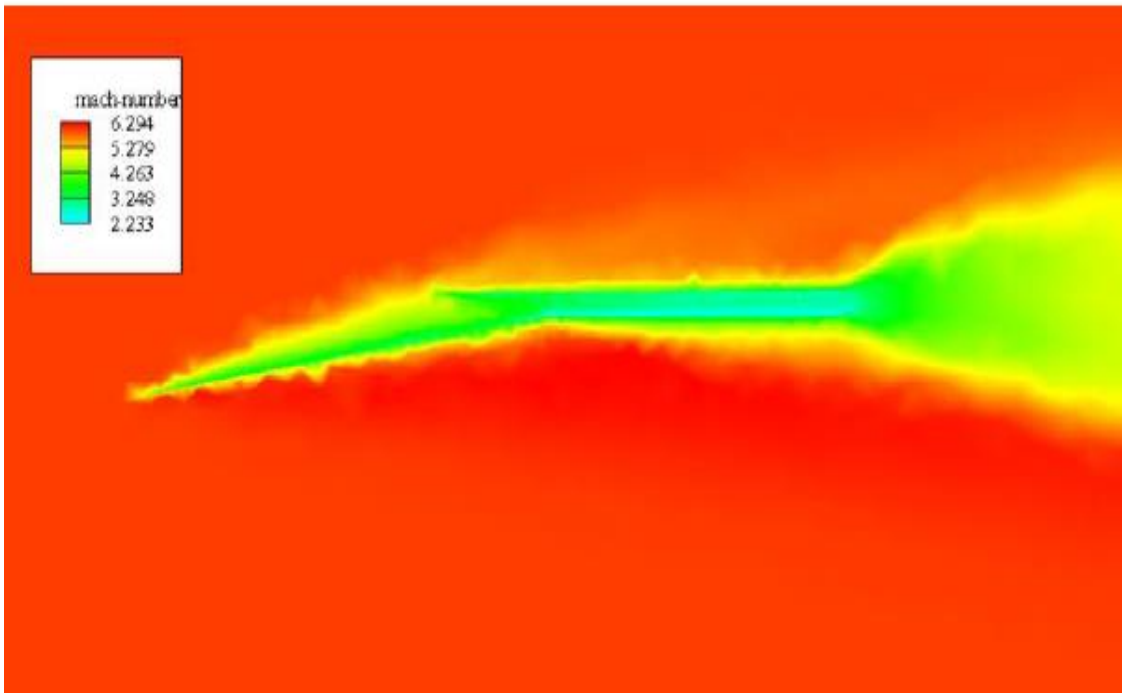

Figure 3.10. 3D Mach 6 contours of Mach number, centerline z-axis (Grant, 2010).

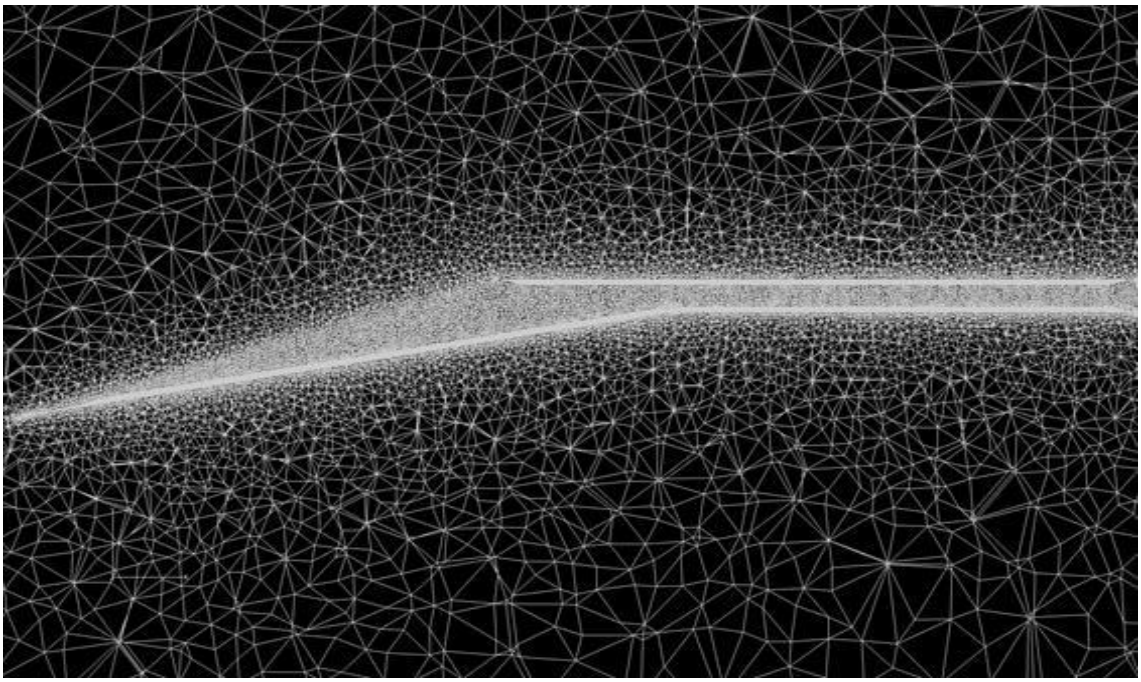

Figure 3.11. Cross-sectional illustration of the grid created in Gridgen (Grant, 2010).

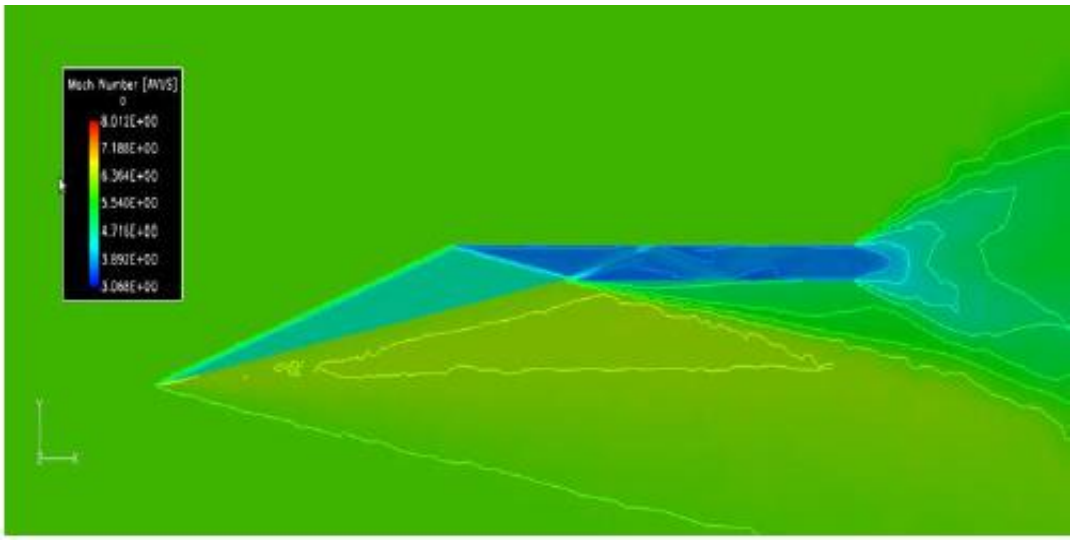

Figure 3.12. 3D contours of Mach number, centerline z-axis (Grant, 2010).

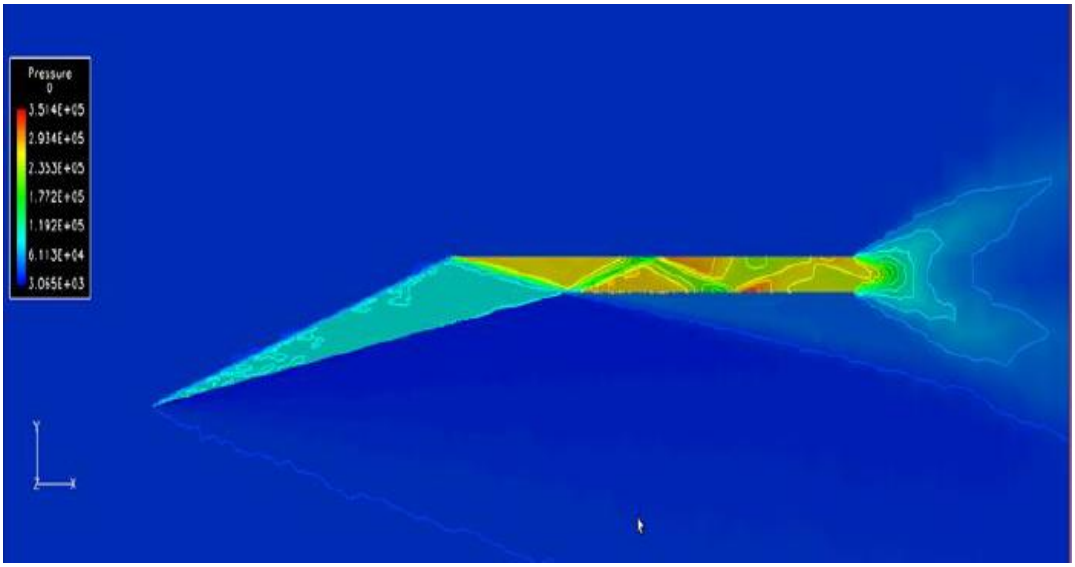

Figure 3.13. 3D contours of pressure, centerline z-axis (Grant, 2010).

As noted in Figures 3.12 and 3.13, the Mach number and pressure distribution between the primary and reflected shock waves is uniform, respectively. This information came in as expected. Figure 3.13 showed distinct evidence of an oblique shock train in the isolator.

In an effort to demonstrate that the internal flow field within the scramjet forebody is truly 2D in nature, a plot of density contours with 2D data slices along the z-axis was developed. The density contour plot is illustrated in Figure 3.14 below (Grant, 2010). This result indicates

that there are no movements in the z-directions, and confirms that the flow field is truly two-dimensional.

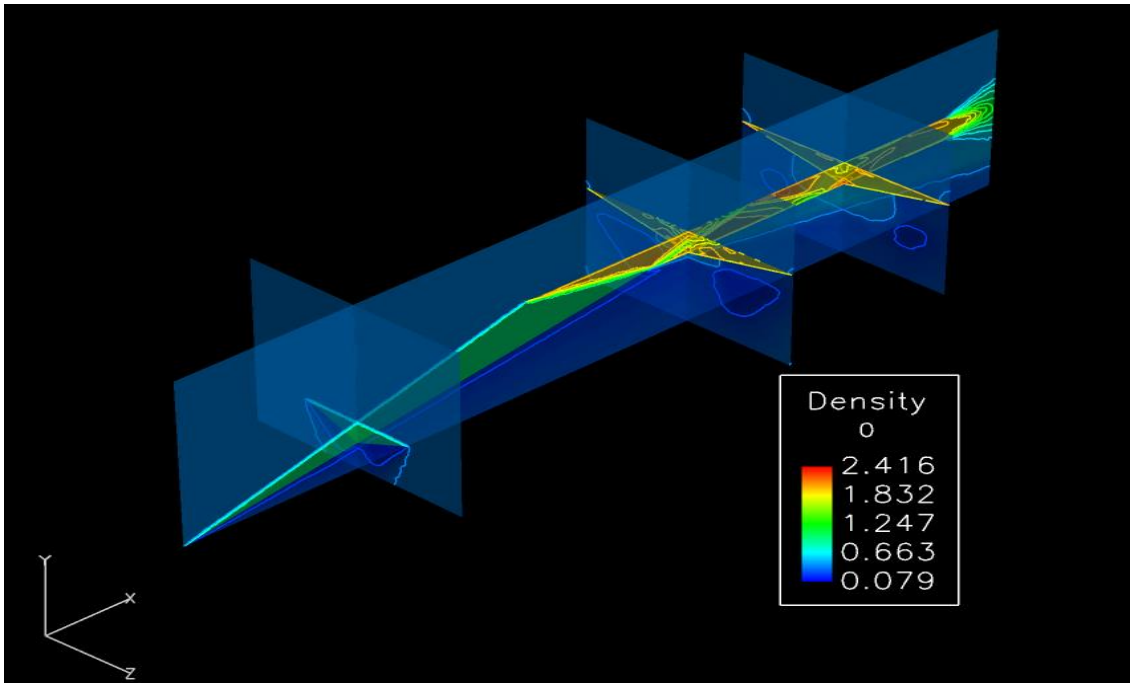

Figure 3.14. Flow visualization demonstration, contours of density at Mach 6 (Grant, 2010).

A similar CFD study was carried out by a colleague, Nastassja Dasque, in 2008 (Ferguson, 2009). In her study, Dasque conducted a Mach 5 inviscid analysis of the complete four-point-star configuration. The results from the analysis are presented in Figures 3.15 and 3.16 (Ferguson, 2009).

The results shown in Figures 3.15 and 3.16 bear a strong resemblance to the results generated by this study, as seen in Figures 3.12 and 3.13. Both sets of results recover the primary and reflective oblique shock waves. Also, there are no strong oblique or normal shock waves in the isolator. Although these two sets of data bear a strong resemblance to each other, there is one major difference. Dasque's results do not recover the oblique shock train in the isolator. This is due to the fact that Dasque modeled all four stream tubes in her analysis. A consequence of this choice reduces the number of grid points in the isolator available to capture minute disturbances in the flow field (Grant, 2010).

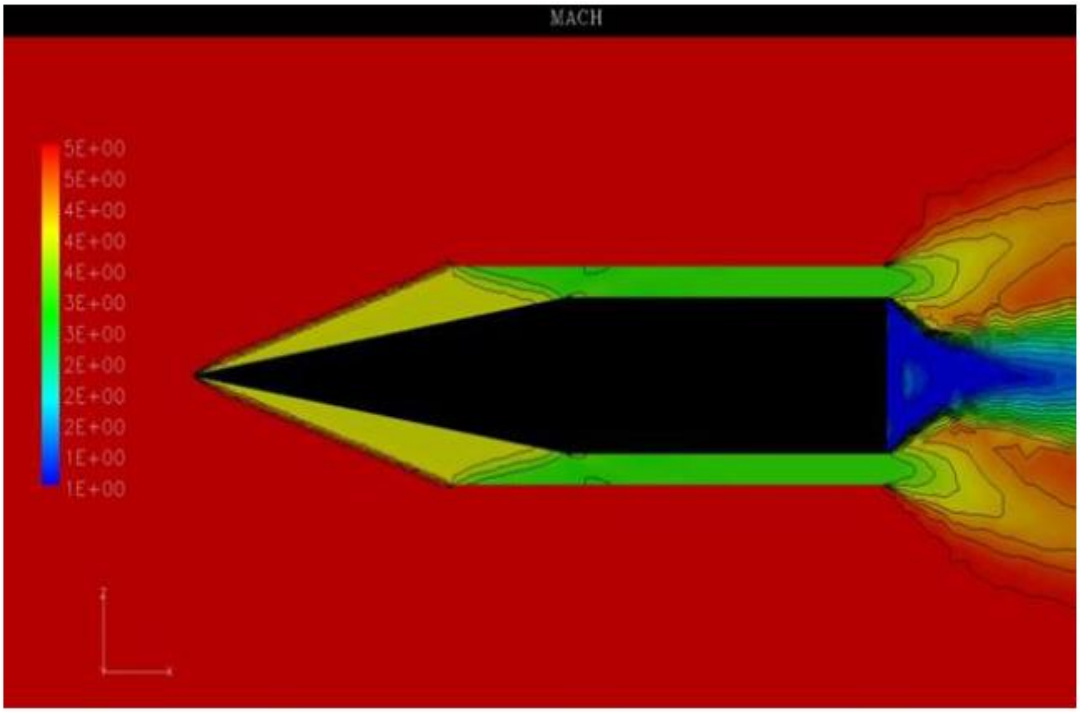

Figure 3.15. Independent validation; contours of Mach number (Grant, 2010).

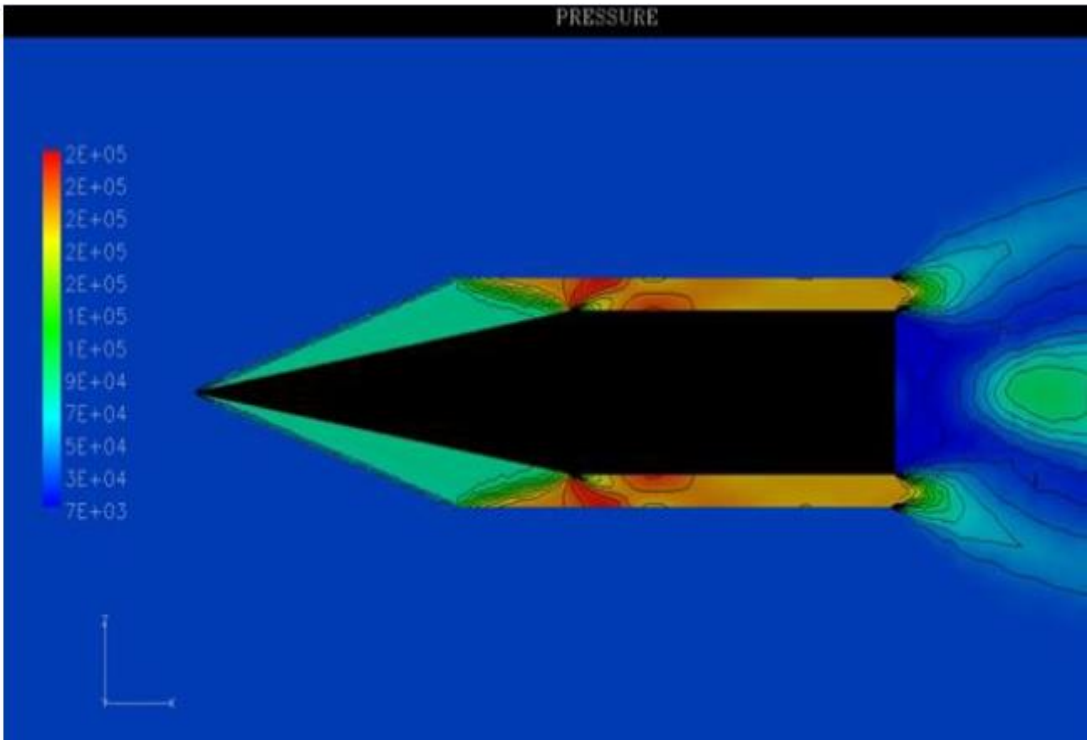

Figure 3.16. Independent validation; contours of pressure (Grant, 2010).

3.3.1.3 Pros and cons of CFD. The use of CFD over time has proved beneficial to the advancement of hypersonic air-breathing propulsion. Some advantages of CFD include: the delivery of accurate results, ability to capture phenomenon that some numerical schemes have difficulty with and modeling can be constructed at a full scale. Despite the power of CFD, it has limitations. Pre-processing times can be rather lengthy and prolong the data collection process. Before anything is done, grids must be generated to simulate the region of interest. With millions of cells to analyze, the limitation of computational resources becomes more apparent. The entire analysis could take days or weeks to accomplish depending on the computer's resources. It is necessary to ensure that the model of interest is tested thoroughly prior to being analyzed by CFD. The quasi-1D solver mentioned in the objective of this thesis can guarantee that the model is working efficiently before CFD analysis is conducted.

CHAPTER 4

Methodology

The objective of this MS thesis is to use the quasi-1D fluid dynamic equations to evaluate the fluid flow in arbitrary shaped ducts under the influence of aerodynamic heating, friction, mass addition and other fluid dynamic interactions of interest to scramjet designs. Consequently, it becomes important to review the quasi-1D fluid dynamic theory and the appropriate assumptions that this theory is built on. This chapter presents the framework upon which the quasi-1D fluid dynamic equations are built and highlights its use in this thesis. Also, in this chapter, the available analytical solutions of the quasi-1D fluid dynamic equations are also presented. In particular, the influence coefficient and the Runge-Kutta solution methodologies are described with great details, as they form the basis upon which this thesis research is built.

4.1 Quasi-One-Dimensional Theory

In one-dimensional flow, flow properties such as the velocity, pressure and temperature vary in one direction while the cross-sectional area remains constant (Anderson, 2003). The flow is considered to be adiabatic and inviscid. In other words, the flow is isentropic. Quasi-one-dimensional flow takes the same principle count except the cross-sectional area also varies in one direction, in this case as a function of x (Anderson, 2003). Figure 4.1 gives an illustration of quasi-one-dimensional flow in a duct. The governing equations for quasi-one-dimensional flow are derived from the three conservation laws of mass, momentum and energy. Although the three conservation laws represent fully what happens in nature, the quasi-one-dimensional representation of them is approximate. One can achieve more accurate solutions by considering three-dimensional flow. However, wind tunnel and rocket engine studies have shown quasi-one-

dimensional flow to be fairly accurate (Anderson, 2003). Equations 4.1-4.3 show the three conservation laws when they are applied to quasi-1D flow in a duct.

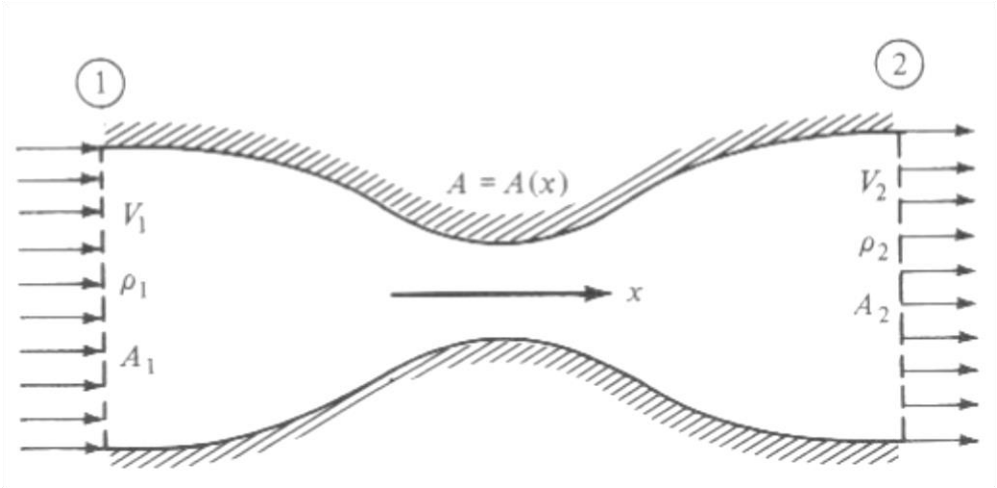

Figure 4.1. Quasi-one dimensional flow in a duct (Anderson, 2011).

$$\rho_1 u_1 A_1 = \rho_2 u_2 A_2 \tag{4.1}$$

$$p_1 A_1 + \rho_1 {u_1}^2 A_1 + \int_{A_1}^{A_2} p dA = p_2 A_2 + \rho_2 {u_2}^2 A_2 \tag{4.2}$$

$$h_1 + \frac{{u_1}^2}{2} = h_2 + \frac{{u_2}^2}{2} \tag{4.3}$$

When considering quasi-one-dimensional flow, the only mechanism responsible for any changes in the flow properties is the change in cross-sectional area. The area-velocity relationship, derived from the manipulation of the continuity and momentum equations, relates the area variation to the velocity variation for subsonic and supersonic flows as described by Equation 4.4 (Anderson, 2003). This relationship reveals trends that occur in converging and diverging ducts. Figure 4.2 details the area-velocity relationship in the form of a diagram.

$$\frac{dA}{A} = (M^2 - 1)\frac{du}{u} \tag{4.4}$$

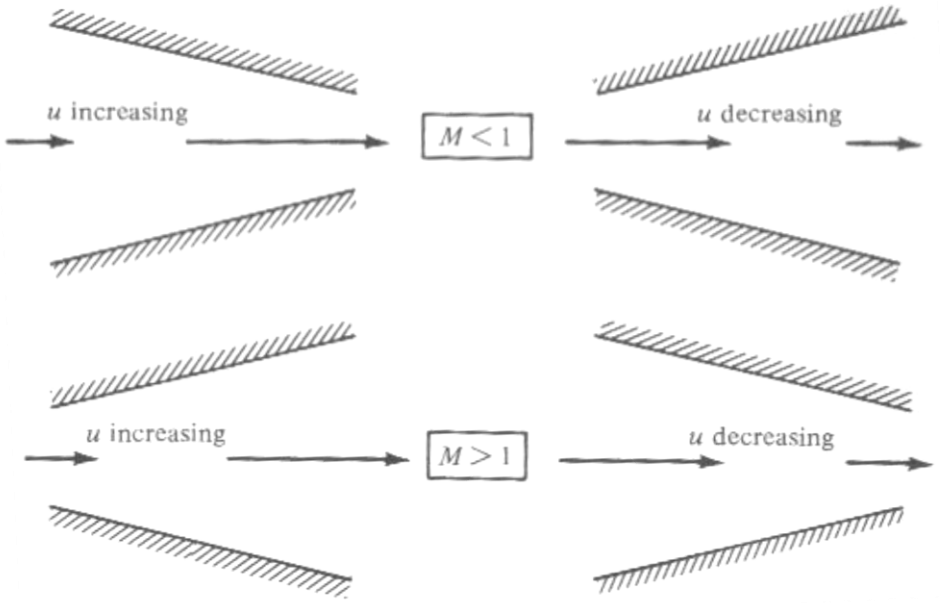

Figure 4.2. Compressible flow in converging and diverging ducts (Anderson, 2011).

4.2 Fanno Flow Theory

Fanno flow refers to flow that is adiabatic and inviscid with effects of friction being considered (Anderson, 2003). In a duct, friction is modeled as a shear stress along the wall. This shear stress acts on the fluid in a uniform manner over any cross section (Anderson, 2003). An illustration of a duct subjected to Fanno flow is displayed in Figure 4.3 below.

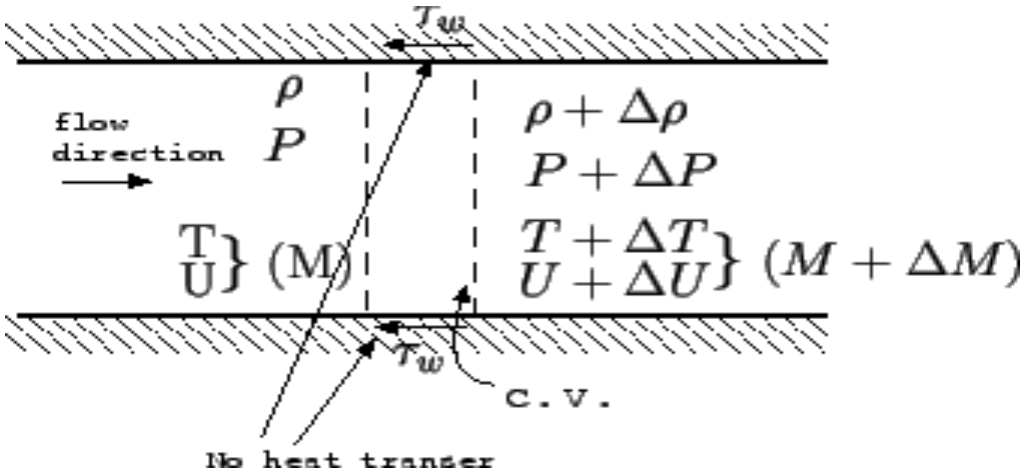

Figure 4.3. Fanno flow illustration ("Fanno", 2007).

The governing equations for Fanno flow are very similar to that of quasi-one-dimensional flow. The only difference lies in the representation of the momentum equation. Equation 4.5 provides the Fanno flow implementation of the momentum equation which contains the shear stress, unlike its quasi-1D counterpart from Equation 4.2.

$$p_1 A_1 + \rho_1 {u_1}^2 A_1 = p_2 A_2 + \rho_2 {u_2}^2 A_2 + \int_0^L \pi D \tau_w dx \qquad (4.5)$$

Similar to quasi-one-dimensional flow, there are trends for the behavior of subsonic and supersonic flows under Fanno flow. For subsonic inlet flows, the Mach number increases while the pressure and temperature both decrease (Anderson, 2003). For supersonic inlet flows, the Mach number decreases while the pressure and temperature both increase (Anderson, 2003).

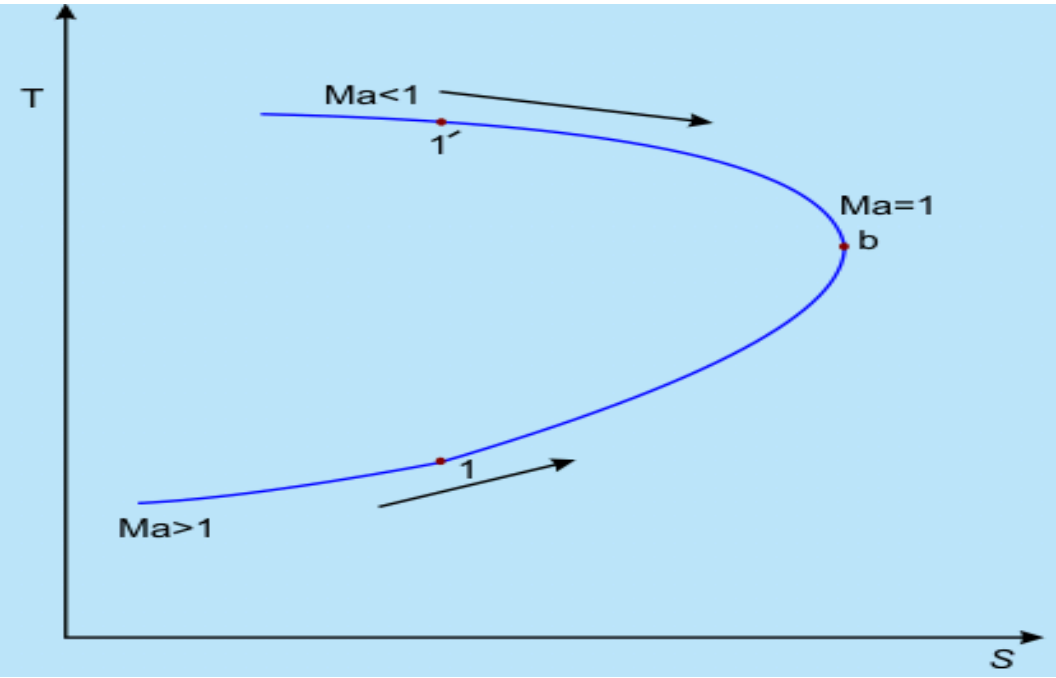

Figure 4.4. Fanno flow curve ("Fanno", 2007).

In nature, when a flow under the influence of friction, the Mach number is driven toward unity (Anderson, 2003). From the Fanno flow curve (displayed in Figure 4.4), it can be seen that the Mach number gets closer to sonic conditions with increasing entropy. Once the Mach number

reaches unity the flow becomes choked. Any points between *1* and *b* on the curve represent a duct of length *L*. The length that will allow the flow to be choked is what is known as the choking length (commonly referred to as *L**). If *L* were to be made larger than *L**, the inlet conditions would have to be adjusted accordingly (Anderson, 2003). For instance, if the conditions at point *1* were expanded by a supersonic nozzle and *L* were larger than *L**, a normal shock would form which would result in the inlet conditions becoming subsonic (Anderson, 2003). Furthermore, it is impossible to drive a flow to sonic conditions and then further decelerate to subsonic conditions. Doing so would violate the 2nd Law of Thermodynamics which states that the entropy of an isolated system should never decrease because an isolated system always strives toward thermodynamic equilibrium (maximum entropy) (Anderson, 2003).

4.3 Runge-Kutta 4th Order Method

Consider a quasi-one-dimensional duct with *n* number of unique cross sections as displayed in Figure 4.5.

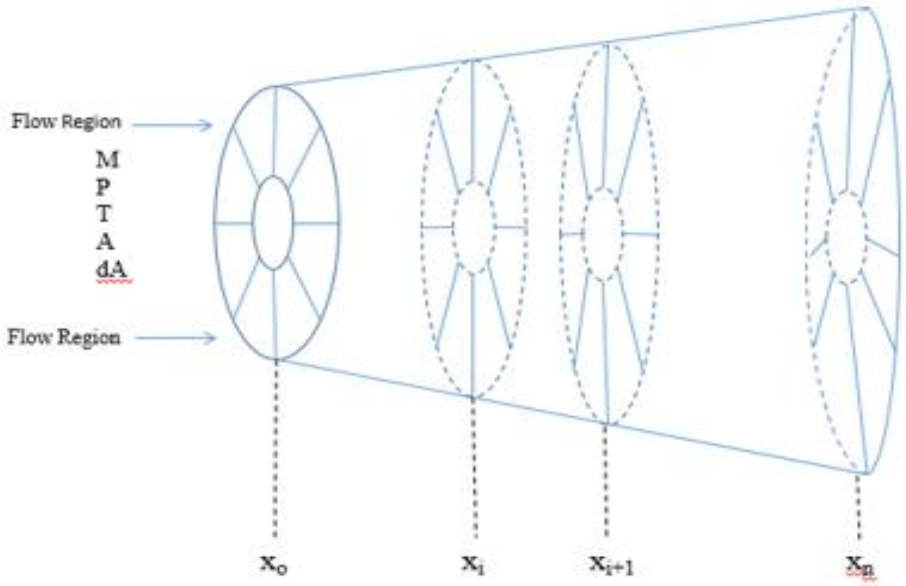

Figure 4.5. Quasi-1D duct.

In Figure 4.5, every aerodynamic parameter of interest at the inlet is a known value. For any arbitrary cross-section x_i, those parameters are unknown. A marching, iterative scheme is necessary in predicting the variables of interest throughout the duct for *n* number of cross-sections.

The Taylor series, portrayed by Equation 4.6, uses the derivative of a function to approximate the solution of a function. By knowing the conditions at one point, one can march forward in space and approximate the conditions at the next point.

$$y_{i+1} = y_i + \frac{dy}{dx} h \tag{4.6}$$

An important thing to consider would be the accuracy between each march forward. The error produced from a single march forward will most certainly propagate throughout each forward march thereafter. For that reason, it is necessary to implement a method capable of minimizing the error between each step forward. One such method is the Runge-Kutta 4th order method. The Runge-Kutta 4th order method expresses the derivative of a function with 4th order accuracy.

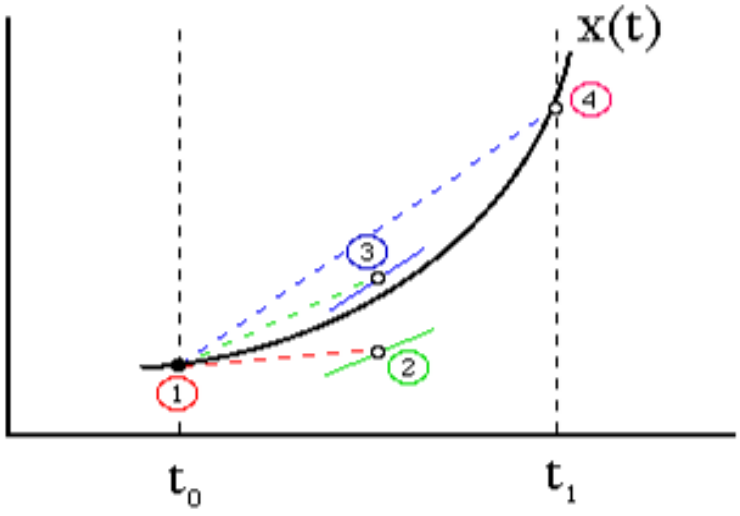

Figure 4.6. Runge-Kutta 4th order diagram ("Runge-Kutta", 2008).

Consider the problem statement shown in Equation 4.7.

$$\frac{dy}{dx} = f(x,y) \quad , \; y(x_i) = y_i$$

$$x \in (x_i, x_n) \; , \; y = f(x) \tag{4.7}$$

Equation 4.7 describes the derivative of a function is presented as a function of two variables, *x* and *y*. The independent variable *x* ranges between the values x_i and x_n. The dependent variable *y* is a function of *x* and has a value of y_i at $x = x_i$. The goal is to determine *f(x)* using the given information. The function *f(x)* can be approximated using the Runge-Kutta 4th order method as shown in Equations 4.8 and 4.9.

$$y_{i+1} = y_i + \frac{1}{6}(k_1 + 2k_2 + 2k_3 + k_4)h \tag{4.8}$$

Where,

$$h = \frac{\Delta x}{N} \ll 1$$

$$k_1 = f(x_i, y_i) \qquad k_3 = f\left(x_i + \frac{h}{2}, y_i + \frac{h}{2}k_2\right)$$

$$k_2 = f\left(x_i + \frac{h}{2}, y_i + \frac{h}{2}k_1\right) \qquad k_4 = f(x_i + h, y_i + hk_3) \tag{4.9}$$

Using the information given and selecting the proper step size *h* according to the above criteria will provide the conditions at y_{i+1}. Once the value of y_{i+1} is obtained, it can be used to find the value of y at the next step. This process can be repeated until *n* number of steps is reached.

The quasi-1D implementation of the Runge-Kutta 4th order scheme is handled similarly to the problem presented above. The only difference lies in the fact that the quasi-1D version of this is represented in vector form. A vector notation is necessary to solve the three primitive variables: Mach number (*M*), Pressure (*P*) and Temperature (*T)* (refer to Figure 3.7)

`

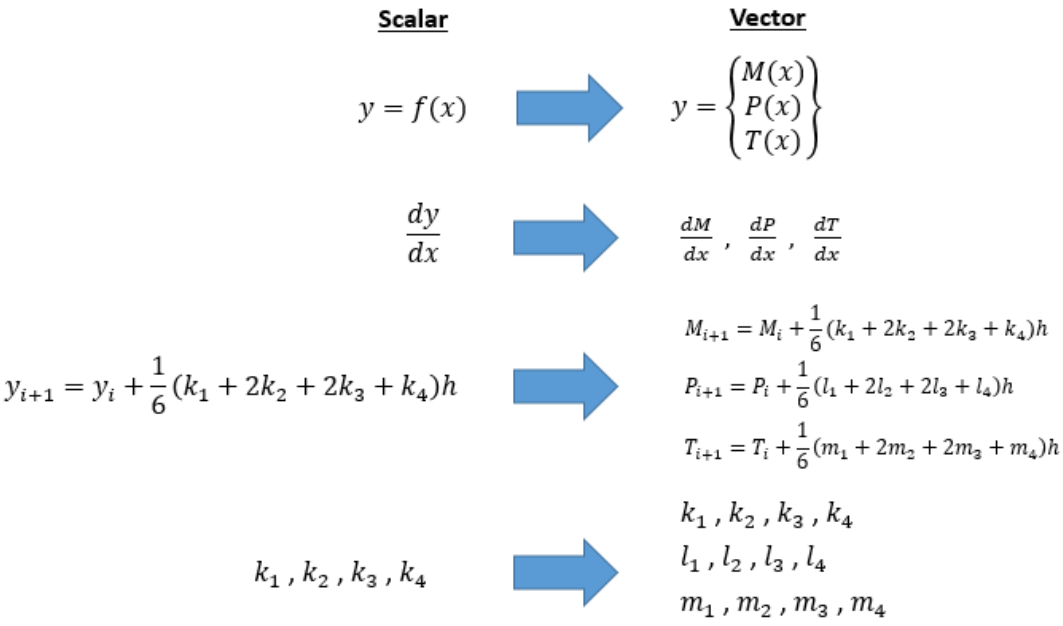

Figure 4.7. Vector implementation of RK 4th order scheme

In order to solve for the three primitive variables, three equations are necessary. By using the three conservation laws of mass, momentum and energy, along with some manipulation, the Equations 4.10 – 4.12 can be derived.

$$\frac{\mathrm{dM}}{\mathrm{dx}} = -\frac{\left(1+\frac{\gamma-1}{2}M^2\right)}{1-M^2}\frac{M}{A}\frac{dA}{dx} + \left(\frac{\gamma M^2\left(1+\frac{\gamma-1}{2}M^2\right)}{2(1-M^2)}M\right)\left(\frac{4C_f}{D_h} - \frac{2y}{\dot{m}}\frac{d\dot{m}}{dx}\right) \tag{4.10}$$

$$\frac{\mathrm{dP}}{\mathrm{dx}} = \frac{\gamma M^2}{1-M^2}\frac{P}{A}\frac{dA}{dx} + \left(-\frac{\gamma M^2[1+(\gamma-1)M^2]}{2(1-M^2)}P\right)\left(\frac{4C_f}{D_h} - \frac{2y}{\dot{m}}\frac{d\dot{m}}{dx}\right) \tag{4.11}$$

$$\frac{\mathrm{dT}}{\mathrm{dx}} = \frac{(\gamma-1)M^2}{1-M^2}\frac{T}{A}\frac{dA}{dx} + \left(-\frac{\gamma(\gamma-1)M^4}{2(1-M^2)}T\right)\left(\frac{4C_f}{D_h} - \frac{2y}{\dot{m}}\frac{d\dot{m}}{dx}\right) \tag{4.12}$$

The previous equations show the changes in each primitive variable across the length of an arbitrary duct with only the influences of area change and friction being considered. The influences manifest themselves in the previous equations as coefficients shown in Table 4.1 below.

Table 4.1

Shapiro's Influence Coefficients

	$\frac{dA}{A}$	$\frac{dH+\delta Q}{c_p T_x}$	$\frac{4C_f dx}{D_h}-2y\frac{dm}{m}$	$\frac{dm}{m}$	$\frac{\delta\gamma}{\gamma}$
$\frac{dM}{M}$	$-\frac{\left(1+\frac{\gamma-1}{2}M^2\right)}{1-M^2}$	$-\frac{\left(1+\gamma M^2\right)}{2\left(1-M^2\right)}$	$-\frac{\gamma M^2\left(1+\frac{\gamma-1}{2}M^2\right)}{2\left(1-M^2\right)}$	$-\frac{\left(1+\gamma M^2\right)\left(1+\frac{\gamma-1}{2}M^2\right)}{1-M^2}$	-1
$\frac{dT}{T}$	$\frac{(\gamma-1)M^2}{1-M^2}$	$\frac{1-\gamma M^2}{1-M^2}$	$-\frac{\gamma(\gamma-1)M^4}{2\left(1-M^2\right)}$	$-\frac{(\gamma-1)M^2\left(1+\gamma M^2\right)}{1-M^2}$	0
$\frac{dp}{p}$	$\frac{\gamma M^2}{1-M^2}$	$-\frac{\gamma M^2}{1-M^2}$	$-\frac{\gamma M^2\left[1+(\gamma-1)M^2\right]}{2\left(1-M^2\right)}$	$-\frac{2\gamma M^2\left(1+\frac{\gamma-1}{2}M^2\right)}{1-M^2}$	0
$\frac{dS}{c_p}$	0	1	$-\frac{(\gamma-1)M^2}{2}$	$(\gamma-1)M^2$	0

The coefficients shown in Table 4.1 were developed by Shapiro and are known as influence coefficients (Shapiro, 1953). All of the coefficients are functions of the specific heat ratio γ and the Mach number *M*. The columns in Table 4.1 represent the different influences. The influences are shown in Table 4.1 (from left to right) to be changes in area, heat addition, friction, mass addition and changes in the specific heat ratio. Each row in Table 4.1 reflected how a particular primitive variable is affected by each of the influences mentioned. With some manipulation, Shapiro's coefficients can be altered to show the changes in the primitive variables, as well as the influences, with respect to length. Table 4.2 below shows the altered coefficients. The coefficients shown in Table 4.2 are same as the coefficients implemented in Equations 4.10 – 4.12. The differential equations do not provide the primitive variables themselves. The Runge-Kutta 4th order method can use the differential equations to accurately approximate the solution of the primitive variables at each unique cross section of an arbitrary duct.

Table 4.2

Modified Influence Coefficients

	$\frac{dA}{dx}$	$\frac{dH+dQ}{dx}$	$\frac{4C_f}{D_h}-\frac{2y}{\dot{m}}\frac{d\dot{m}}{dx}$	$\frac{d\dot{m}}{dx}$	$\frac{d\gamma}{dx}$
$\frac{dM}{dx}$	$-\frac{\left(1+\frac{\gamma-1}{2}M^2\right)}{1-M^2}\frac{M}{A}$	$-\frac{(1+\gamma M^2)}{2(1-M^2)}\frac{M}{c_pT_x}$	$\frac{\gamma M^2\left(1+\frac{\gamma-1}{2}M^2\right)}{2(1-M^2)}M$	$-\frac{\left(1+\gamma M^2\right)\left(1+\frac{\gamma-1}{2}M^2\right)}{1-M^2}\frac{M}{\dot{m}}$	$-\frac{M}{\gamma}$
$\frac{dT}{dx}$	$\frac{(\gamma-1)M^2}{1-M^2}\frac{T}{A}$	$\frac{1-\gamma M^2}{1-M^2}\frac{1}{c_p}$	$-\frac{\gamma(\gamma-1)M^4}{2(1-M^2)}T$	$-\frac{(\gamma-1)M^2\left(1+\gamma M^2\right)}{1-M^2}\frac{T}{\dot{m}}$	0
$\frac{dP}{dx}$	$\frac{\gamma M^2}{1-M^2}\frac{P}{A}$	$-\frac{\gamma M^2}{1-M^2}\frac{P}{c_pT_x}$	$-\frac{\gamma M^2[1+(\gamma-1)M^2]}{2(1-M^2)}P$	$-\frac{2\gamma M^2\left(1+\frac{\gamma-1}{2}M^2\right)}{1-M^2}\frac{P}{\dot{m}}$	0
$\frac{dS}{dx}$	0	$\frac{1}{T_x}$	$-\frac{(\gamma-1)M^2}{2}c_p$	$(\gamma-1)M^2$	0

4.4 Quasi-One-Dimensional Solver

A quasi-1D solver was developed in FORTRAN to implement the Runge-Kutta 4th order scheme. This was programmed in an object-oriented form which allowed for the grouping of important variables, the referencing of functions and easy interpretation of the program structure. The overall objective of this solver was to solve for primitive variables at *n* number of cross-sections of a duct with a variable geometric configuration. To make this possible, the solver required the aerodynamic conditions at the inlet (primitive variables), the duct geometry and the skin friction coefficient at each cross-section. The basic principle behind solving for the primitive variables at each cross-section is represented in Equation 4.13.

$$PV_{new} = PV_{old} + \Delta PV_{old} \tag{4.13}$$

By providing the initial set of primitive variables, one can obtain the new set of primitive variables by simply adding the quantity ΔPV, a change in the primitive variables. In the case of

the Runge-Kutta 4th order solver, ΔPV is represented more accurately as shown in Equation 4.14 below.

$$PV_{new} = PV_{old} + \frac{1}{6}(k_1 + 2k_2 + 2k_3 + k_4)h \tag{4.14}$$

It important to note the similarities in Equation 4.14 and 4.8. When comparing Equation 4.6 and 4.14, it is observed that the Runge-Kutta 4th order scheme was used to represent the derivatives of the primitive variables with a higher degree of accuracy. This allows the primitive variables at the next step to be calculated with minimal error in comparison to other methods such as Euler. It is important to note that this solver only took changes in area and friction into account. Any other influences could simply be added into the differential equations with their respective influence coefficients.

4.4.1 Variable grouping. In order to fully utilize the capabilities of object-oriented programming, variables of interest were grouped accordingly. The most important variables of interest were the primitive variables: Mach number, pressure and temperature. The geometry along with other friction related variables were the next to be grouped. More specifically, those variables included the local distance *x*, cross-sectional area *A*, hydraulic diameter D_h and skin friction coefficient, C_f. The primitive variables, geometry and friction related variables acted as inputs to the code. Aside from the inputs, other variables used within the algorithm itself also needed to be grouped. The coefficients shown in Table 4.2 that pertained to area change and friction influences were grouped as a single matrix quantity. Since only the area and friction related coefficients were used, the coefficient matrix was defined a three-by-two matrix as shown in Table 4.3. The three-by-two indicates that each of the three primitive variables has the two influences of area change and friction acting upon them. The influences themselves were grouped into a single vector quantity.

Table 4.3

Area Change and Friction Influence Coefficients

	$\frac{dA}{dx}$	$\frac{4C_f}{D_h} - \frac{2y}{\dot{m}}\frac{d\dot{m}}{dx}$
$\frac{\mathrm{dM}}{\mathrm{dx}}$	$-\frac{\left(1+\frac{\gamma-1}{2}M^2\right)}{1-M^2}\frac{M}{A}$	$\frac{\gamma M^2\left(1+\frac{\gamma-1}{2}M^2\right)}{2(1-M^2)}M$
$\frac{\mathrm{dT}}{\mathrm{dx}}$	$\frac{(\gamma-1)M^2}{1-M^2}\frac{T}{A}$	$-\frac{\gamma(\gamma-1)M^4}{2(1-M^2)}T$
$\frac{\mathrm{dP}}{\mathrm{dx}}$	$\frac{\gamma M^2}{1-M^2}\frac{P}{A}$	$-\frac{\gamma M^2[1+(\gamma-1)M^2]}{2(1-M^2)}P$

The variables used to calculate the coefficients and influences were each given their own groups as well. In Equations 4.10 – 4.12, each term was simply a coefficient multiplied by an influence with respect to *x*. In order to have control over which influences were active, a vector of switches were created and assigned to a group. The switches were placed inside the three differential equations. By assigning a value of "1" or "0", any influence could be turned on or off. The basic idea behind the switches is portrayed in Equation 4.15.

$$\mathrm{Q1D} = \mathrm{Coefficient} * \mathrm{Influence} * \mathrm{Switch} \tag{4.15}$$

The switches were done arithmetically in this way to insure that the logic of the code was not separated from the algebra. The multiplication of a coefficient, influence and a switch constitutes a quasi-1D term. The quasi-1D terms are essentially the terms of Equations 4.10 – 4.12. Each of the quasi-1D terms were grouped into a single matrix very similar to the coefficient matrix. Equation 4.13 showed that the calculation of ΔPV was needed to calculate the new PV.

`

Knowing that, the delta quantities for each primitive variable were grouped. The Runge-Kutta 4th order solver was designed to work with single variables that are actually comprised of a group of variables.

4.4.2 Important functions and subroutines. The functions used in the solver were named to accurately describe the task they are capable of while ensuring inputs are kept at a minimum. Three of the functions were dedicated to the creation of the coefficient matrix along with the influence and switch vectors. The outputs from these functions were used as inputs for a quasi-1D matrix function that calculated the terms of each of the three differential equations to be solved. The terms of the differential equations obtained from the quasi-1D matrix function were placed into their respective delta functions (refer to Equations 4.10 – 4.12).

As previously stated in Equation 4.14, the Runge-Kutta 4th order method is used to approximate the ΔPV quantities for each of the three primitive variables. Three functions were created to extract the proper elements from the quasi-1D matrix and prepare the delta quantities to be calculated. A subroutine used the delta functions to calculate the ΔPV values and group them into a single variable called *DeltaPV*. *DeltaPV* and the initial primitive variables were used as inputs for a subroutine that calculated the new primitive variables in the same format shown in Equation 4.13. As a means of consolidation, a single subroutine was made to encase all of the aforementioned functions and subroutines. This subroutine, known as *Quasi1DFriction*, could carry out the Runge-Kutta operations on its own using a single input that contained all of the input variables mentioned in the previous section.

4.4.3 Program structure. The solver was constructed such that all the functions needed to perform the Runge-Kutta 4th order scheme were stored in a single module. A driver program that was separate from the Runge-Kutta module gathered the inputs and ran the *Quasi1DFriction*

subroutine. This program design allowed for the Runge-Kutta module to function on its own without the help of other modules. In the future, it can be used in conjunction with other codes to provide aerodynamic analysis.

CHAPTER 5

Validation of Runge-Kutta 4th Order Solver

The Runge-Kutta 4th order flow solver, described in Chapter 4, was designed and programmed in object oriented FORTRAN. The resulting code considers the effects of area change and friction in arbitrary quasi-one-dimensional ducts. Other influences experienced by ducts such as mass injection, heat addition and variable specific heat were omitted due to the lack of validation sources for each respective problem. The solver completes its task by providing it with basic information such as the length of the duct, area at each cross section, skin friction at each cross section, hydraulic diameter at each cross section, number of cross sections and the step size between each cross section. In order to ensure the validity of the newly developed Runge-Kutta 4th order flow solver, validation studies were conducted. The flow solver gives one the ability to control the influence coefficients through the use of a simple set of 'on-off' switches. In particular, validation studies were conducted for each individual influence coefficient, namely; area change and friction, as well as their combined effects.

5.1 Quasi-1D Validations

This section of the validation study considers flow through a duct with changes in the cross sectional area along the length of the duct. In other words, the flow is purely quasi-one-dimensional. This updates Equations 4.10 – 4.12 to what is shown in Equations 5.1 – 5.3 below. Each problem will be solved using the Runge-Kutta 4th order solver and then compared to the analytical solution. The analytical solution to pure quasi-1D flow is shown in Equation 5.4.

$$\frac{\mathrm{dM}}{\mathrm{dx}} = -\frac{\left(1+\frac{\gamma-1}{2}M^2\right)}{1-M^2}\frac{M}{A}\frac{dA}{dx} \tag{5.1}$$

$$\frac{\mathrm{dP}}{\mathrm{dx}} = \frac{\gamma M^2}{1-M^2}\frac{P}{A}\frac{dA}{dx} \tag{5.2}$$

$$\frac{\mathrm{dT}}{\mathrm{dx}} = \frac{(\gamma-1)M^2}{1-M^2}\frac{T}{A}\frac{dA}{dx} \tag{5.3}$$

$$\frac{A}{A^*} = \frac{1}{M}\left[\left(\frac{2}{\gamma+1}\right)\left(1+\frac{\gamma-1}{2}M^2\right)\right]^{\frac{\gamma+1}{2(\gamma-1)}} \tag{5.4}$$

The analytical solution provides the Mach number at each unique cross section of a duct. In order to retrieve the Mach number, specific heat index (γ), Area at each cross section of the duct (A) and the area of the duct at its throat (A^*). Once the Mach number is obtained, the analytical solutions for the pressure and temperature can be acquired using the isentropic flow relations shown in Equations 5.5 and 5.6 below.

$$\frac{P}{P_0} = \left(1+\frac{\gamma-1}{2}M^2\right)^{\frac{-\gamma}{\gamma-1}} \tag{5.5}$$

$$\frac{T}{T_0} = \frac{1}{1+\frac{\gamma-1}{2}M^2} \tag{5.6}$$

5.1.1 Pure quasi-1D converging duct. In this validation, pure quasi-1D flow through a convergent duct is considered. Both subsonic and supersonic inlet flow will be observed.

5.1.1.1 Pure quasi-1D converging duct with subsonic inlet. Figure 5.1 below shows an illustration of the case of pure quasi-1D flow through a converging duct with subsonic inlet conditions. The length of the duct is given as 50 m long. The area varies only along the x-direction and is given to be Area(x) = 17.0 – 3.0x. The inlet Mach number, pressure and temperature are given as 0.03, 300 kPa and 300 K respectively. Figures 5.2 – 5.4 show what was obtained by the analytical solution and quasi-1D solver for the Mach number, pressure and temperature under the conditions mentioned.

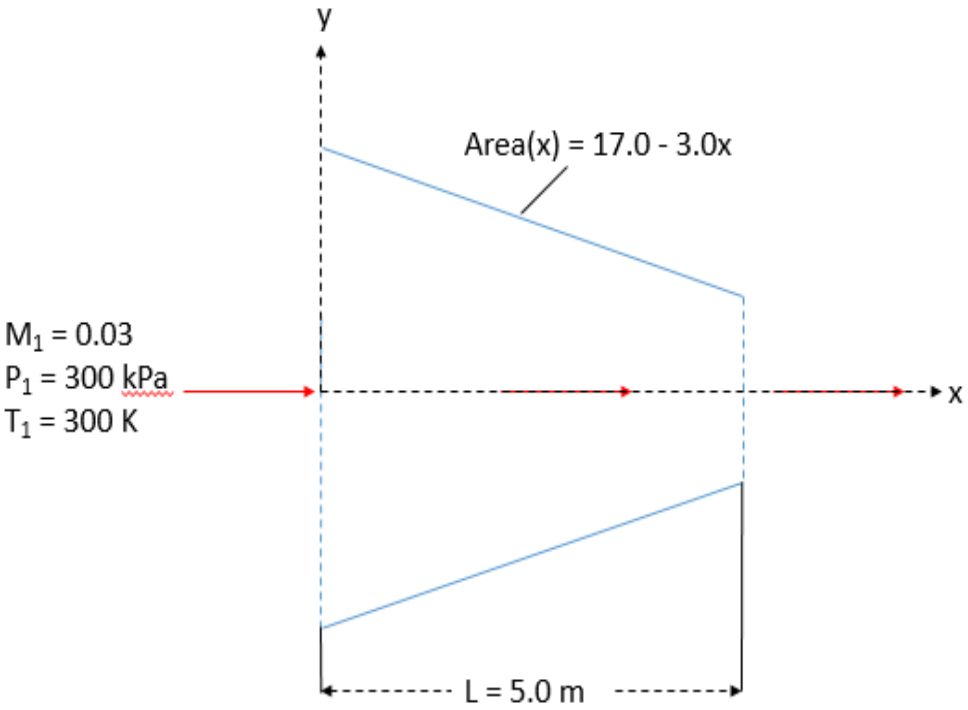

Figure 5.1. Quasi-1D converging duct under subsonic conditions.

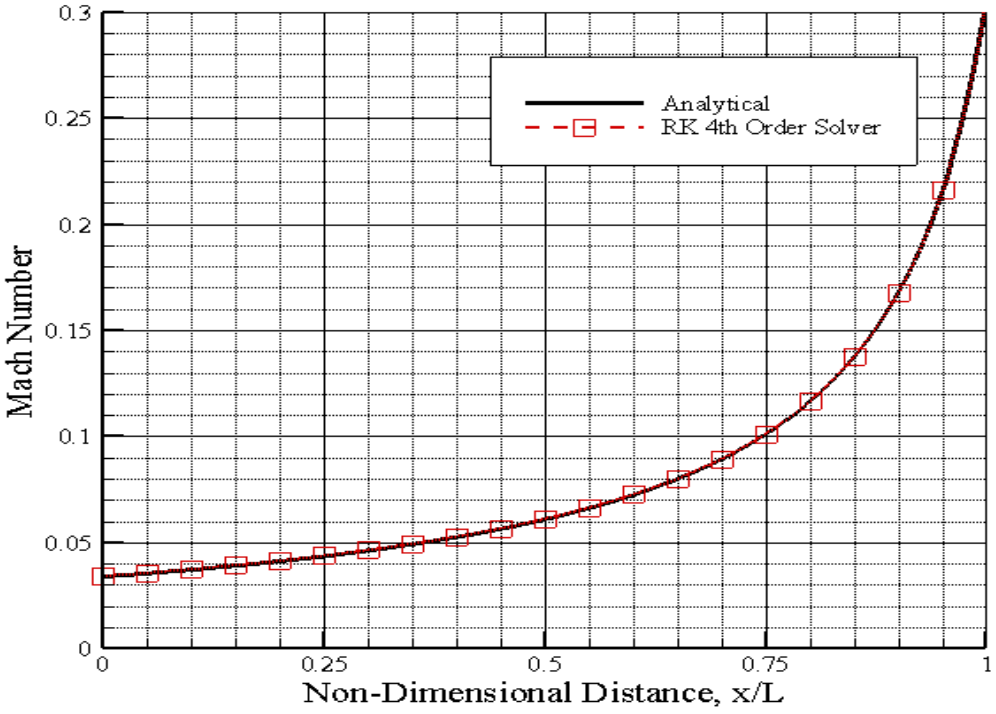

Figure 5.2. Mach number vs distance for a converging duct under subsonic conditions.

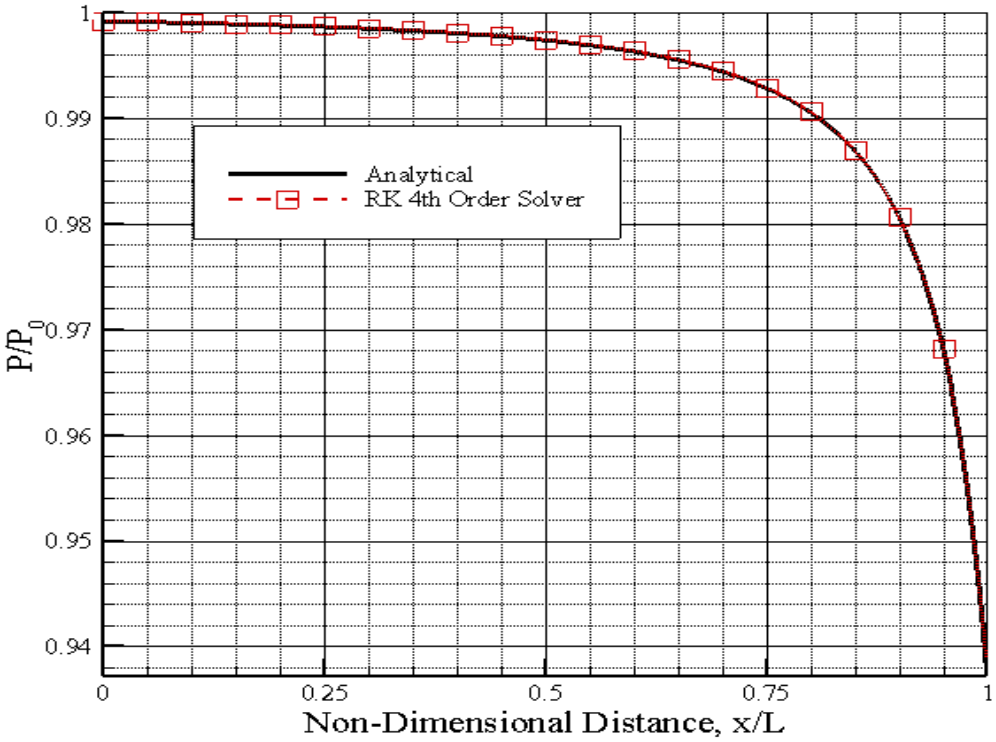

Figure 5.3. Pressure vs distance for a converging duct under subsonic conditions.

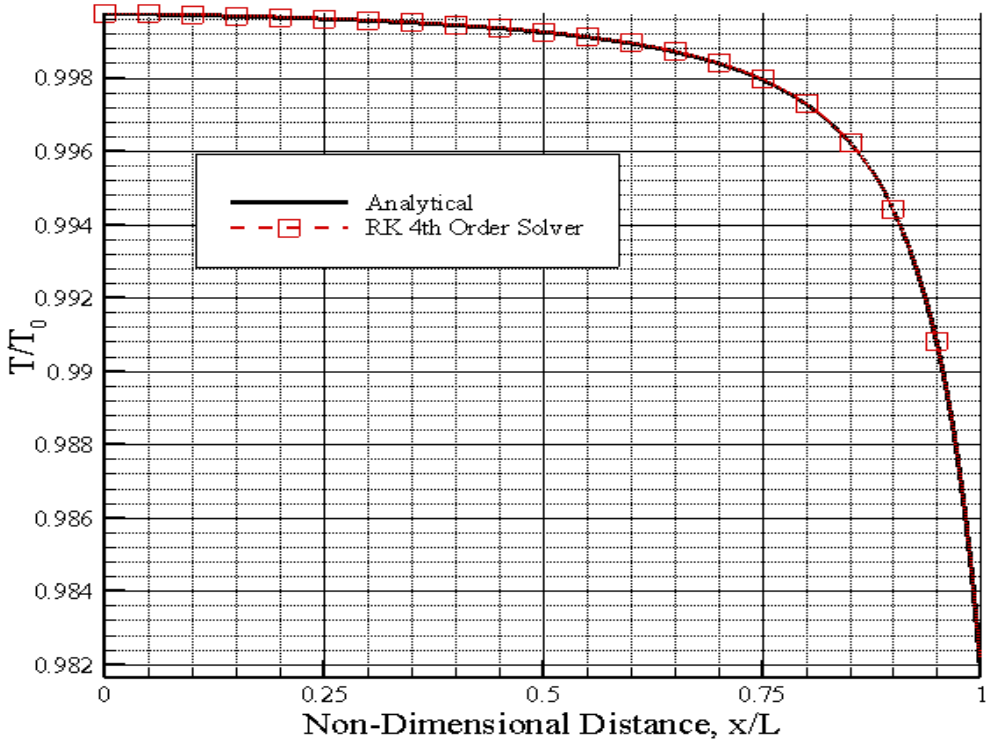

Figure 5.4. Temperature vs distance for a converging duct under subsonic conditions.

It is important to note that both the pressure and temperature are scaled by the total pressure and total temperature respectively. Figures 5.2 – 5.4 above show that results obtained from the solver are consistent with that of the analytical solution. Not only do the results compare well with the analytical solution, they also follow the expected trends presented by any aerodynamic textbook.

5.1.1.2 Pure quasi-1D converging duct with supersonic inlet. For the converging duct with supersonic inlet case, a converging duct with geometry identical to the previous problem is used. The duct along with its inlet conditions are shown in Figure 5.5.

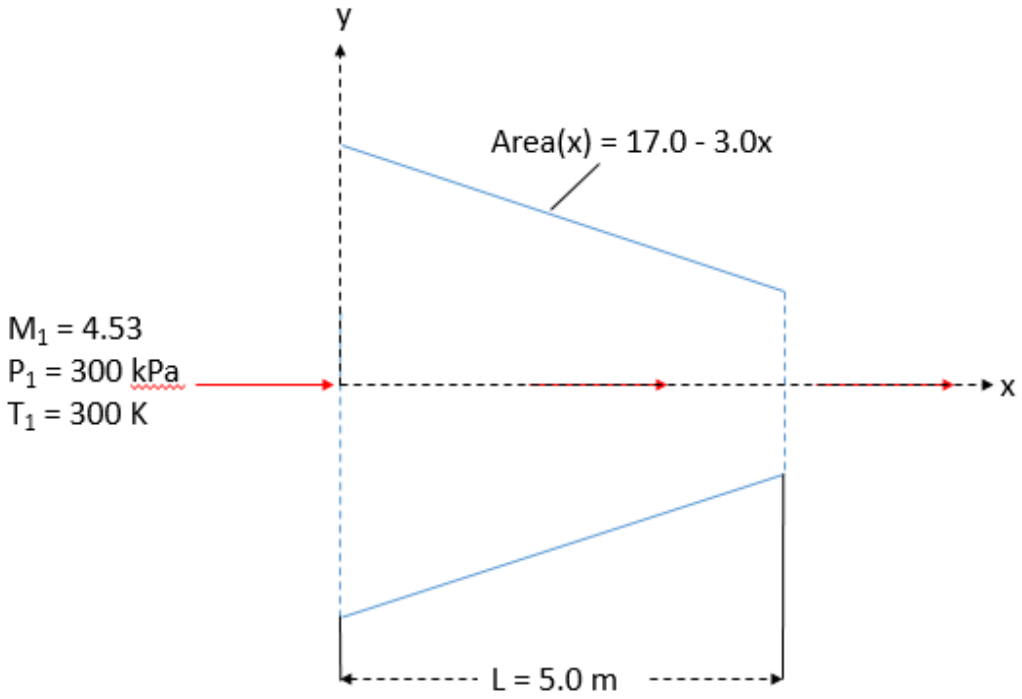

Figure 5.5. Quasi-1D converging duct under supersonic conditions.

The inlet Mach number, pressure and temperature are given to be 4.53, 300 kPa and 300 K respectively. Similar to the previous validation problem, the results of the quasi-1D solver are compared directly to the analytical solution. From the observation of Figures 5.6 – 5.8, it is noted the solver's solution compares well with the analytical solution.

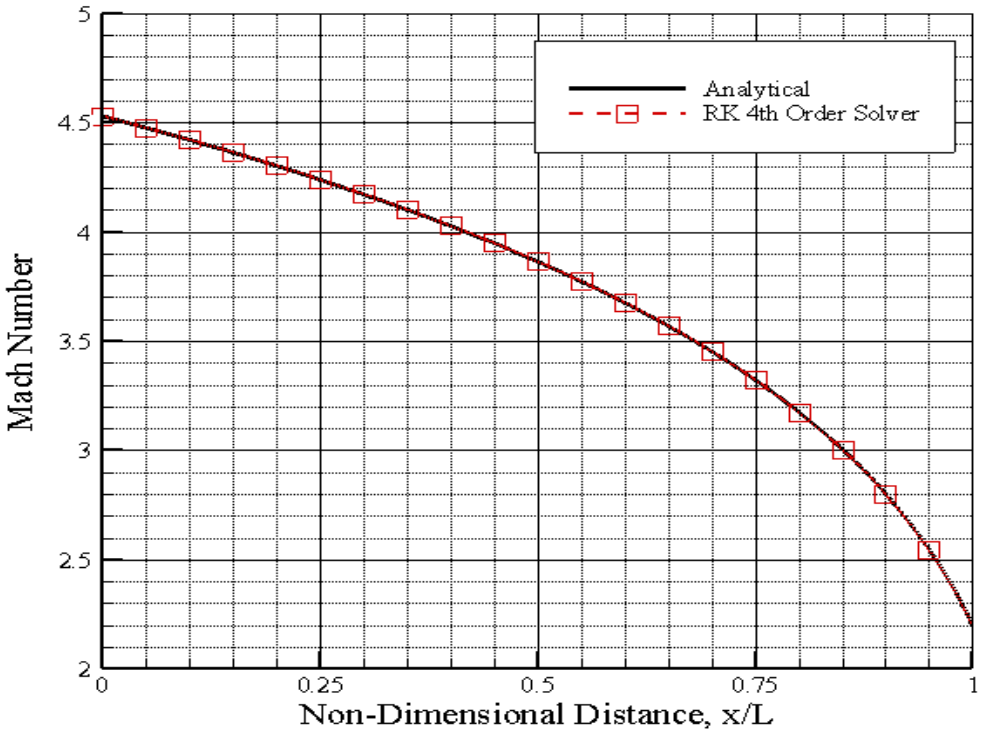

Figure 5.6. Mach number vs distance for a converging duct under supersonic conditions.

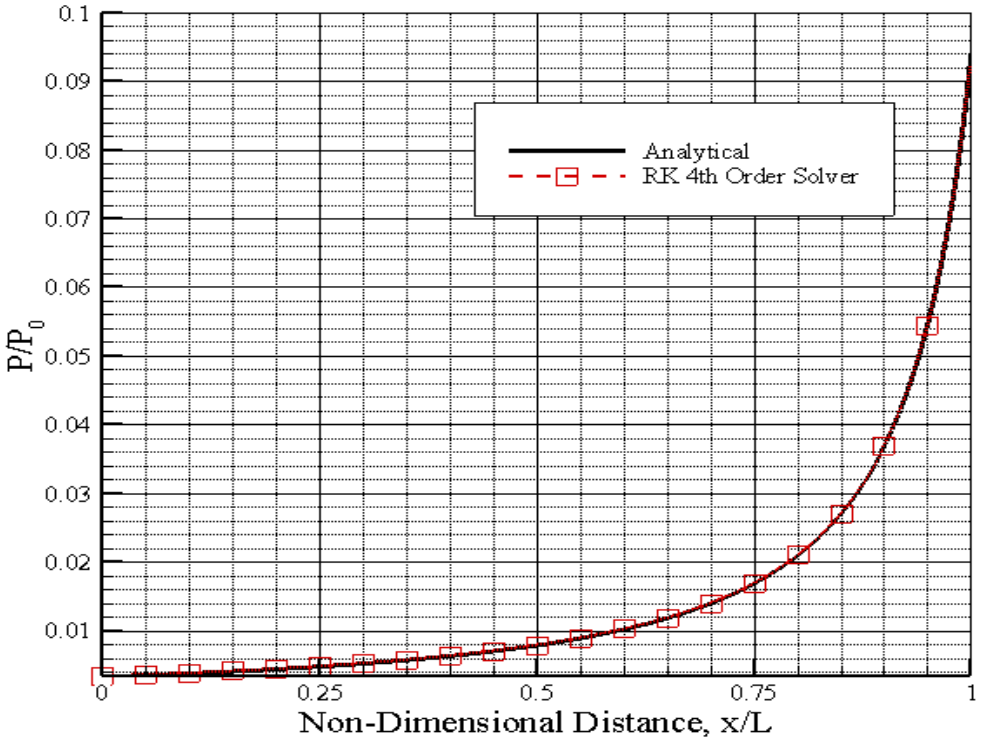

Figure 5.7. Pressure vs distance for a converging duct under supersonic conditions.

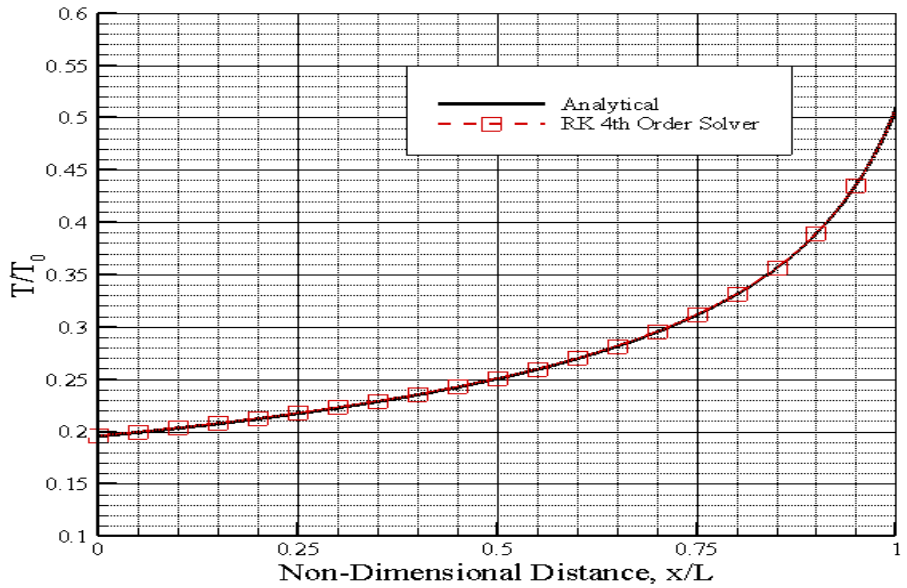

Figure 5.8. Temperature vs distance for a converging duct under supersonic conditions.

5.1.2 Pure quasi-1D diverging duct. In this validation, opposite to the previous, the case of a quasi-1D diverging duct was observed. The study was conducted for subsonic and supersonic inlet flow.

5.1.2.1 Pure quasi-1D diverging duct with subsonic inlet. Figure 5.9 below depicts a diverging duct with subsonic inlet conditions. The diverging nozzle has a length of 5.0 m. The area varies along the x-direction and is given to be Area(x) = 2.0 + 3.0x.

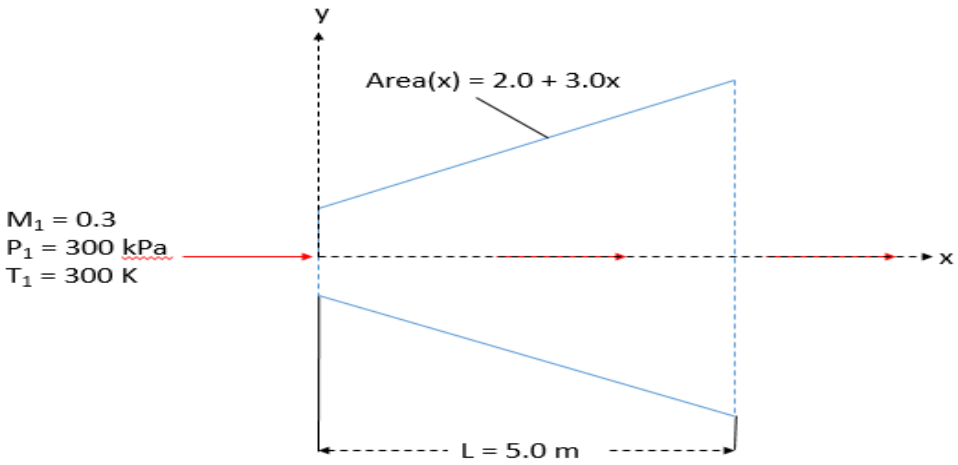

Figure 5.9. Quasi-1D diverging duct under subsonic conditions.

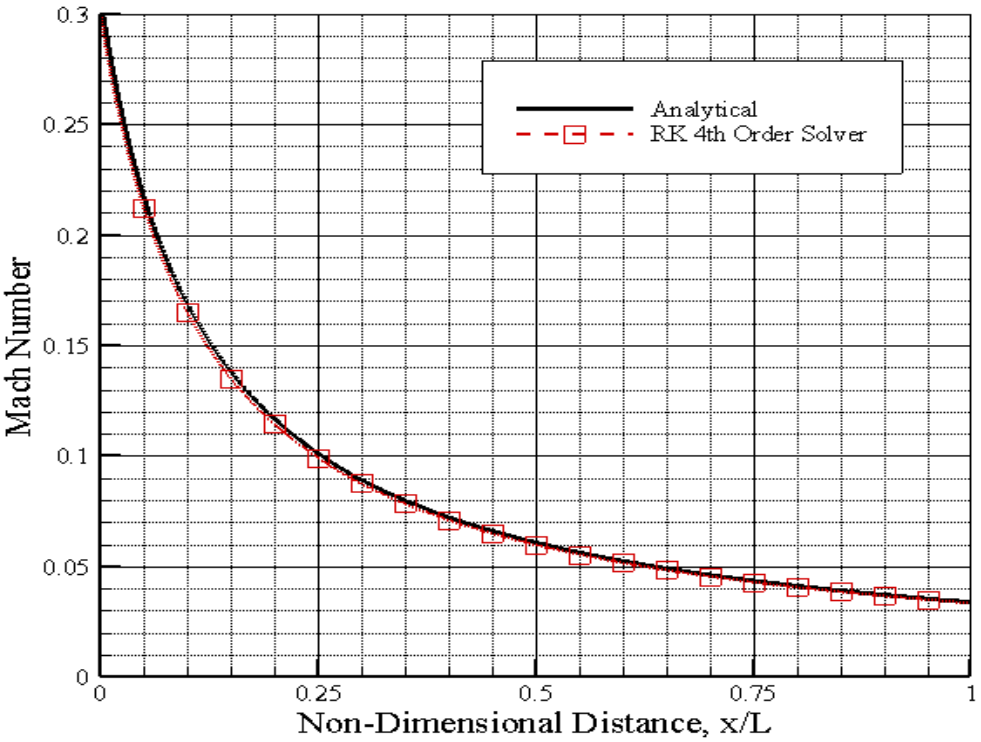

Figure 5.10. Mach number vs distance for a diverging duct under subsonic conditions.

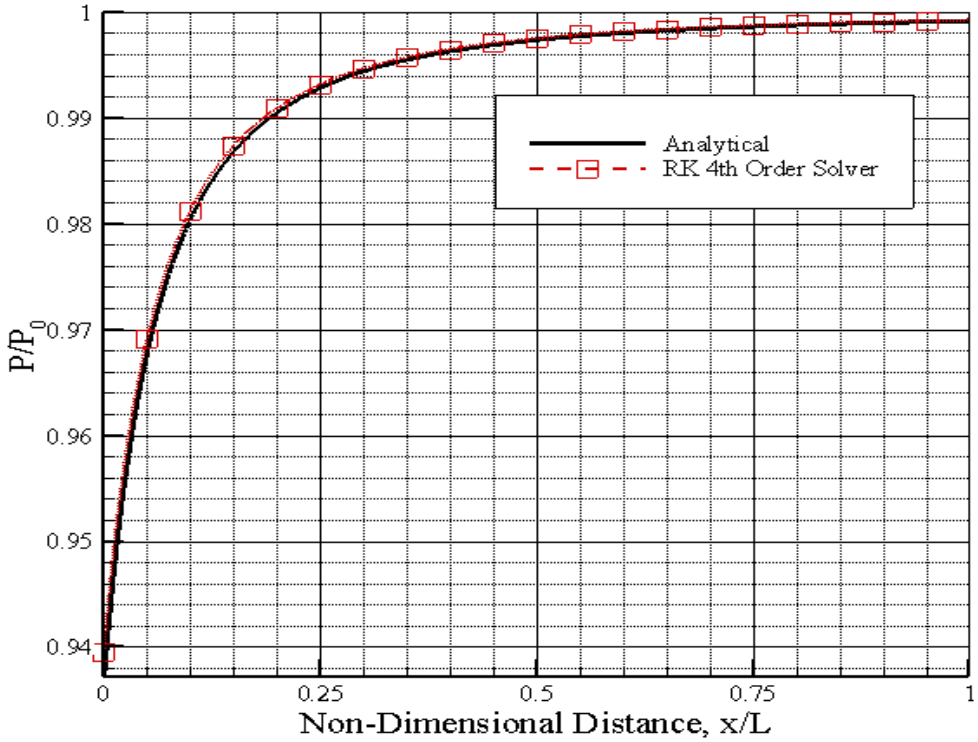

Figure 5.11. Pressure vs distance for a diverging duct under subsonic conditions.

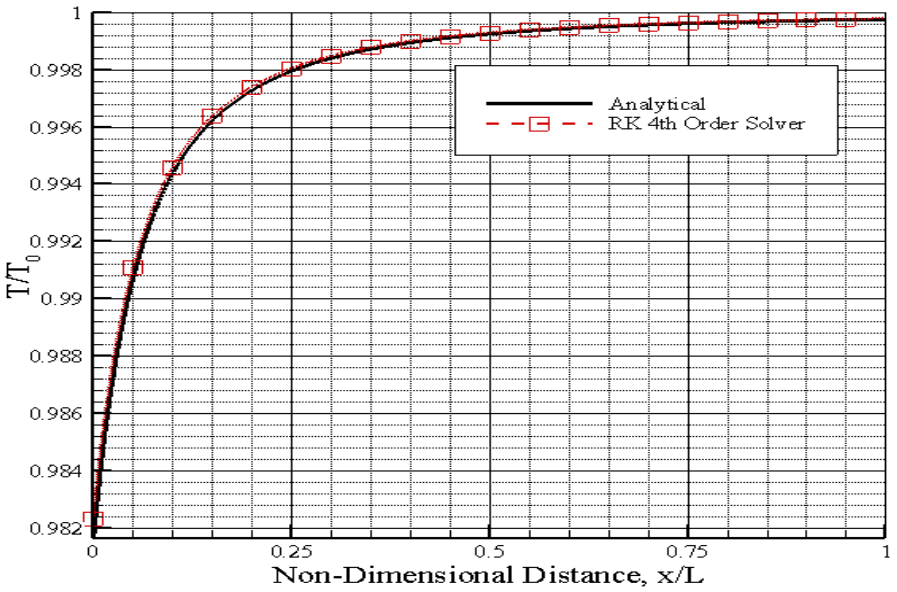

Figure 5.12. Temperature vs distance for a diverging duct under subsonic conditions.

The diverging duct with subsonic inlet conditions validation shows that the analytical solution compares well with the results obtained from the solver.

5.1.2.2 Pure quasi-1D diverging duct with supersonic inlet. In this divergent case, the geometry of the previous validation is maintained while the inlet conditions are set to be supersonic. The Mach number, pressure and temperature are now 2.2, 300 kPa and 300 K respectively. The results provided by the quasi-1D solver are, again, compared with the analytical solution in Figures 5.14 – 5.16 below.

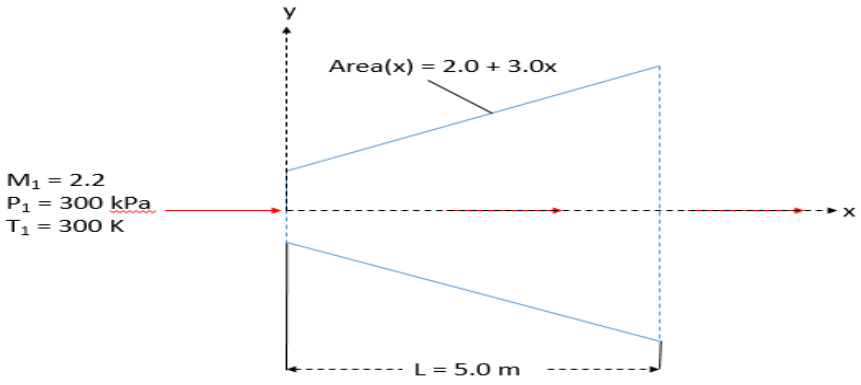

Figure 5.13. Quasi-1D diverging duct under supersonic conditions.

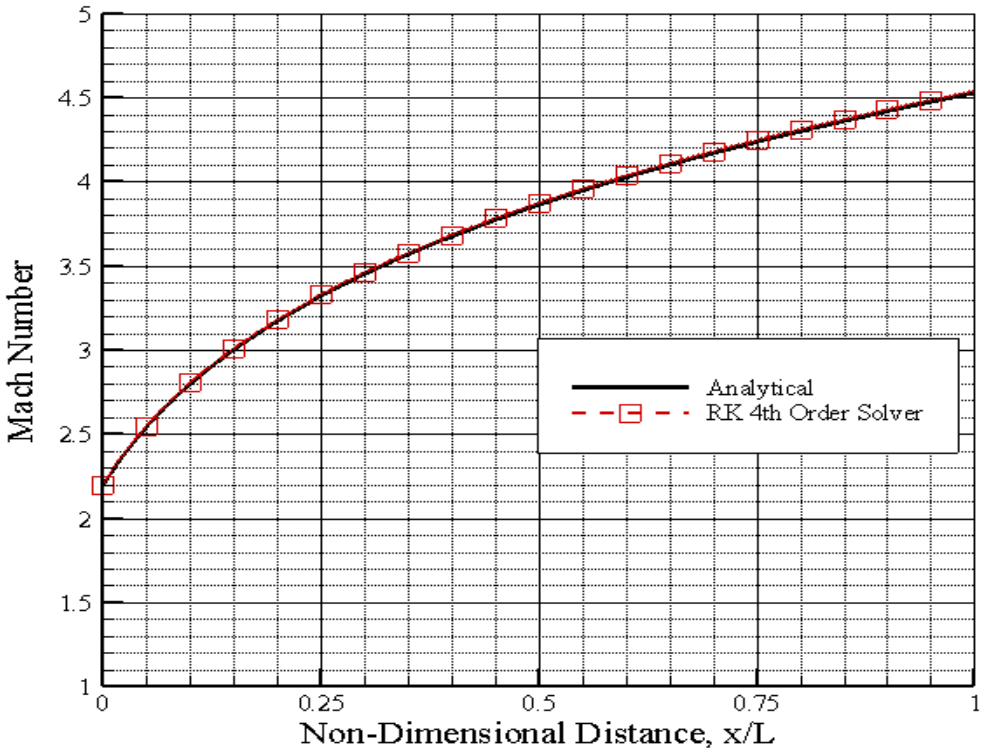

Figure 5.14. Mach number vs distance for a diverging duct under supersonic conditions.

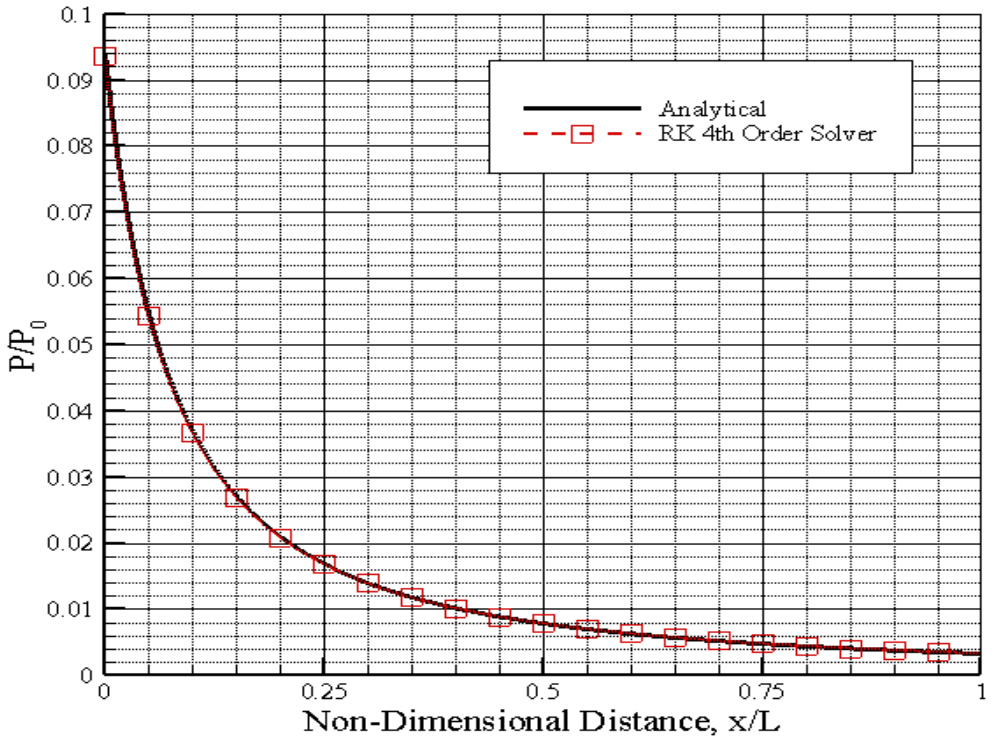

Figure 5.15. Pressure vs distance for a diverging duct under supersonic conditions.

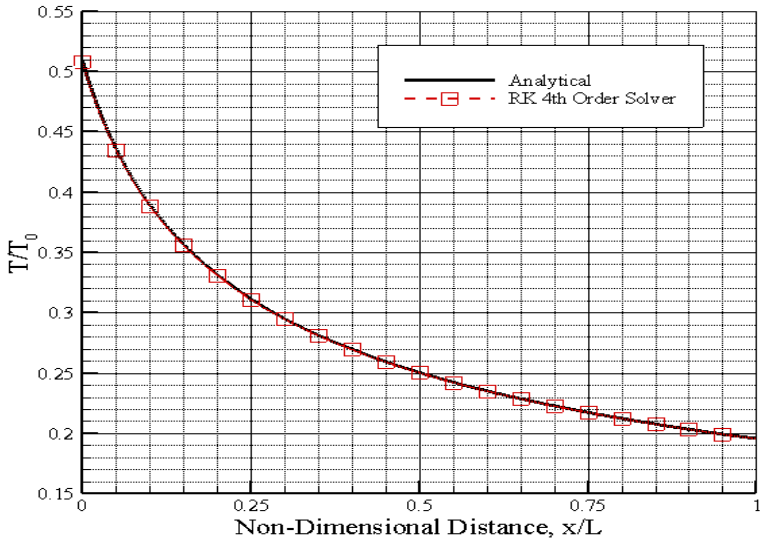

Figure 5.16. Temperature vs distance for a diverging duct under supersonic conditions.

From the observation of Figures 5.14 -5.16, the results from the solver's solution compares well with the analytical solution in the case of a diverging duct with supersonic inlet conditions.

5.2 Fanno Flow Validations

Fanno flow, as previously described in Chapter 4, is flow that is adiabatic and inviscid with effects of friction being considered. Three unique Fanno flow scenarios are used for validation purposes in this section.

5.2.1 Fanno flow through a constant area duct. In this validation, air flow through a constant area duct with friction is presented as depicted in Figure 5.17 below.

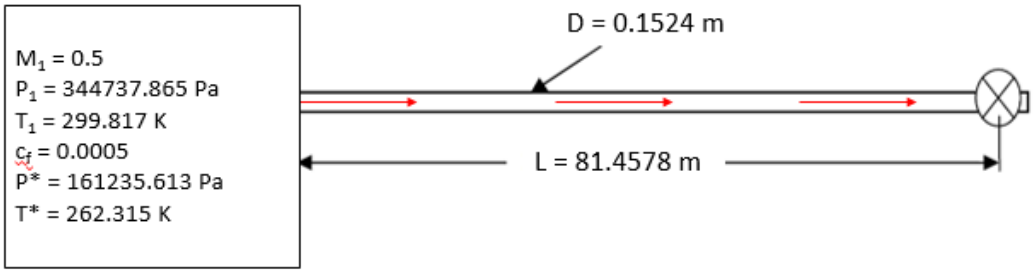

Figure 5.17. Constant area duct with constant skin friction (Bandyopadhyay, 2007).

The constant area duct has a diameter of 0.1524 m and a length of 81.4578 m. The length prescribed is equivalent to the choking length for this particular set of data given. The skin friction coefficient is constant throughout the length of the pipe and has a value of 0.0005. The inlet Mach number, pressure and temperature are given to be 0.5, 344737.865 Pa and 299.817 K respectively. Bandyopadhyay and Majumdar implemented a quasi-one-dimensional, finite volume algorithm in a flow solver called Generalized Fluid System Simulation Program (GFSSP) (Bandyopadhyay, 2007). Figures 5.18 – 5.20 pictured below compares the solutions obtained by the Runge-Kutta 4th order solver and GFSSP with the analytical solution. It is important to note that the temperature and pressure are scaled by T* and P*, respectively. The asterisks labeled next to these parameters indicates a value taken at choked flow conditions. The values of T* and P*, as shown in the above diagram, are 262.315 K and 161235.613 Pa respectively.

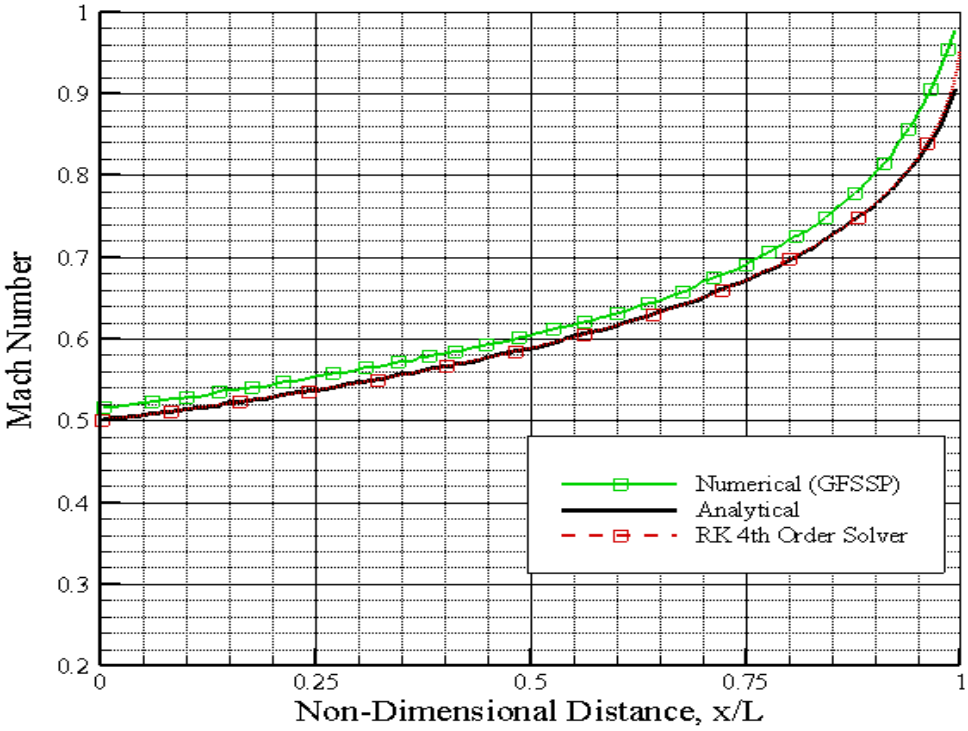

Figure 5.18. Mach number vs distance for constant area duct with constant skin friction.

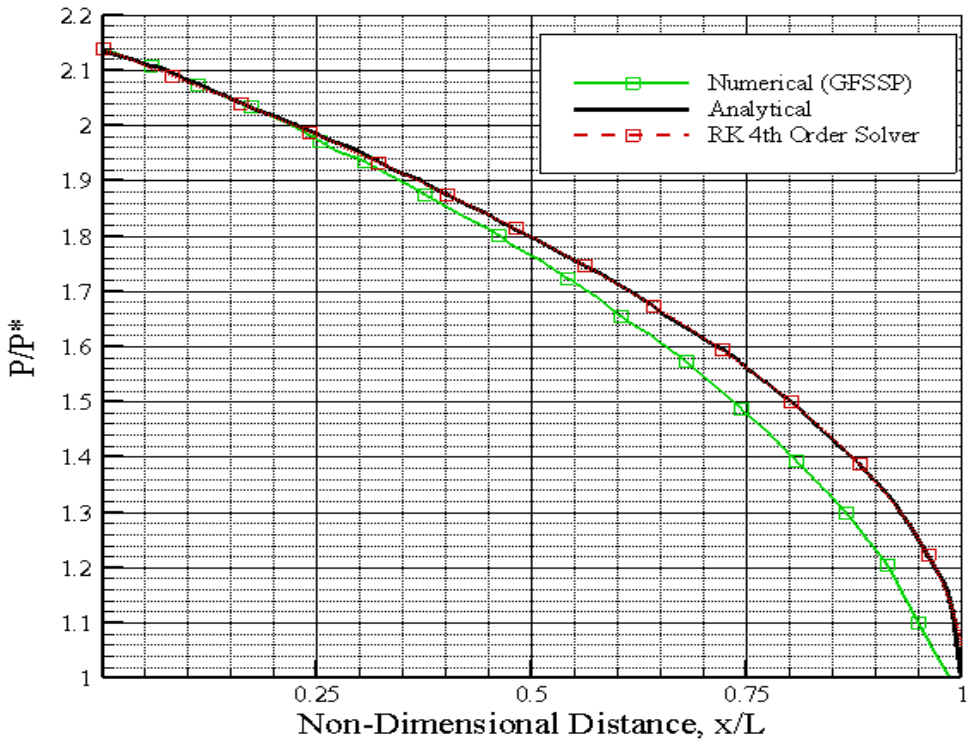

Figure 5.19. Pressure vs distance for constant area duct with constant skin friction.

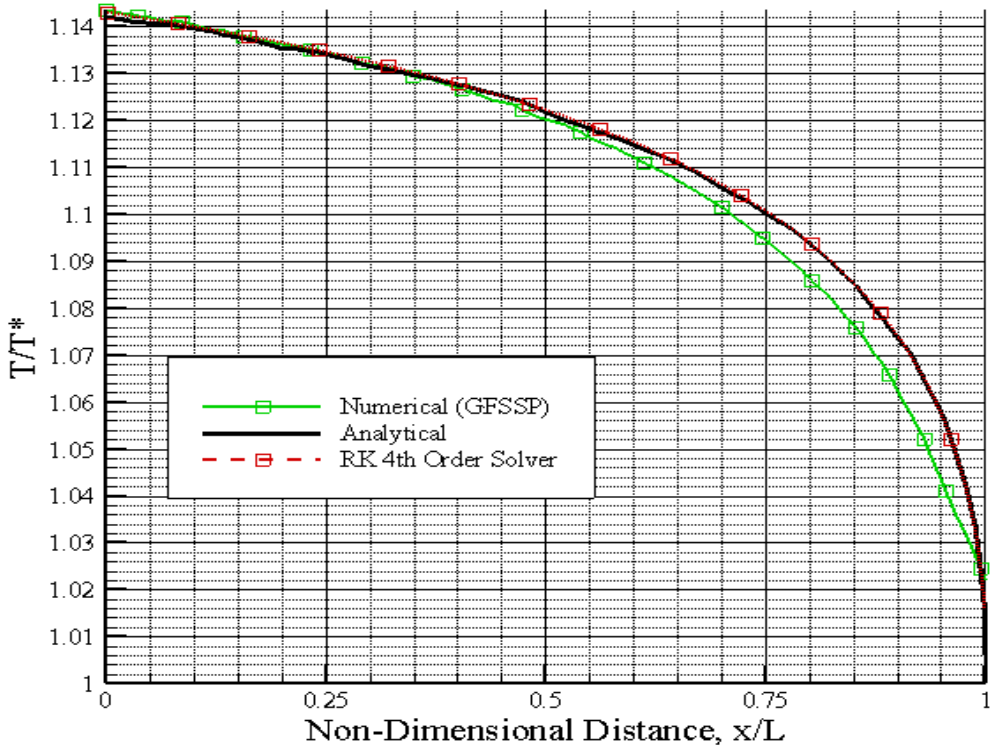

Figure 5.20. Temperature vs distance for constant area duct with constant skin friction.

From Figures 5.18 – 5.20 above it is clearly seen that the Runge-Kutta 4th order solver compares well with the analytical solution. Not only does it compare well, it also out performs the solution given by GFSSP.

5.2.2 Fanno flow with subsonic and supersonic inlet conditions by Anderson. Anderson (Anderson, 2003) provided two different problems that can be used to validate the Fanno flow portion of the Runge-Kutta 4th order solver. The two problems address subsonic and supersonic under the influence of skin friction.

5.2.2.1 Fanno flow with subsonic inlet conditions. The first of Anderson's problems addresses Fanno flow with subsonic inlet conditions. A diagram of this problem is shown below in Figure 5.21.

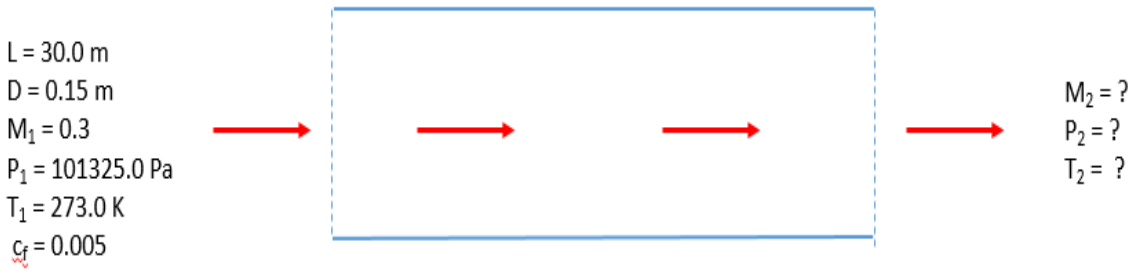

Figure 5.21. Subsonic pipe flow with constant skin friction described by Anderson.

Figure 5.21 depicts a pipe with a length of 30.0 m and a diameter of 0.15 m. The skin friction coefficient is held constant along the axial direction of the pipe and is given to be 0.005. The inlet Mach number, pressure, and temperature are given to be 0.3, 101352.0 Pa and 273.0 K respectively. Figures 5.22 – 5.24 show the comparison between the Runge-Kutta 4th order solver and Anderson's solution. Since Anderson only provided the inlet and exit conditions, the distribution of each aerodynamic parameter is not given for his solution. The inlet and exit conditions provided by Anderson are depicted by the red diamonds. Just as the previous Fanno

flow validation scaled the Temperature and Pressure by T* and P*, the same is done in the following validation study as well.

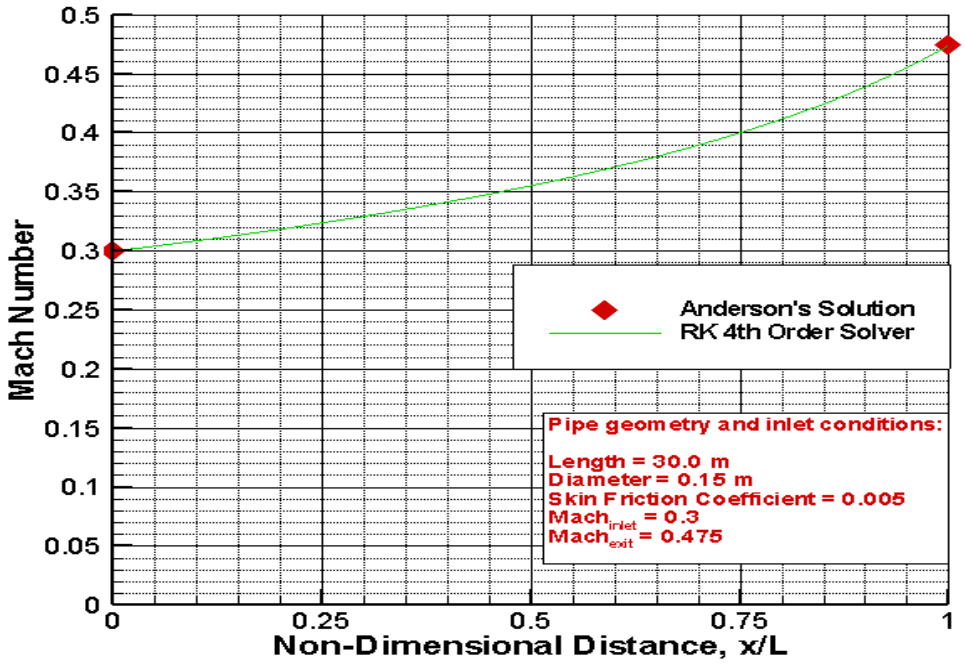

Figure 5.22. Mach number vs distance for subsonic pipe flow with constant skin friction.

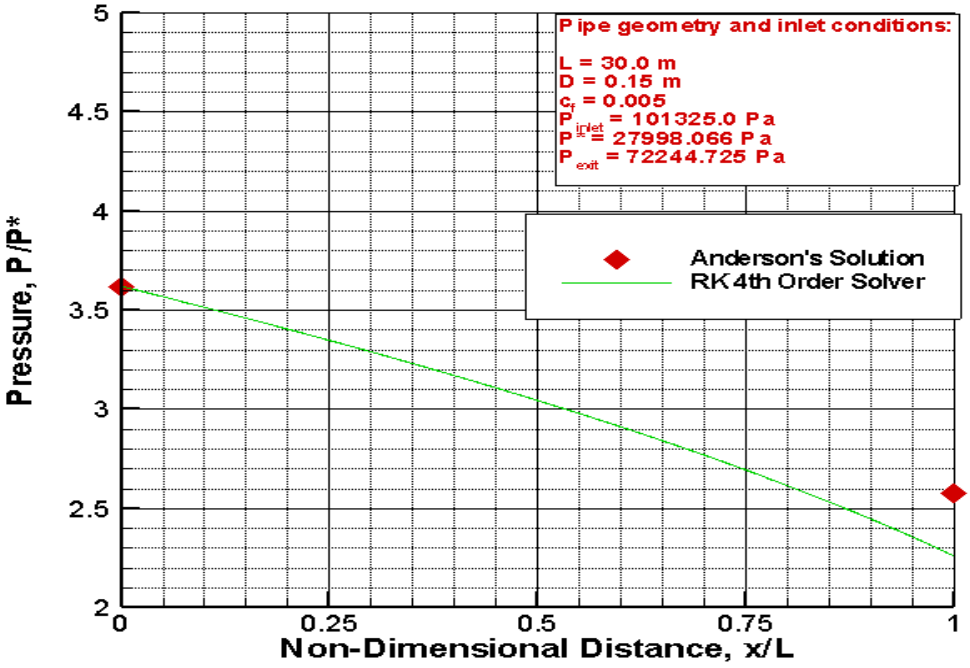

Figure 5.23. Pressure vs distance for subsonic pipe flow with constant skin friction.

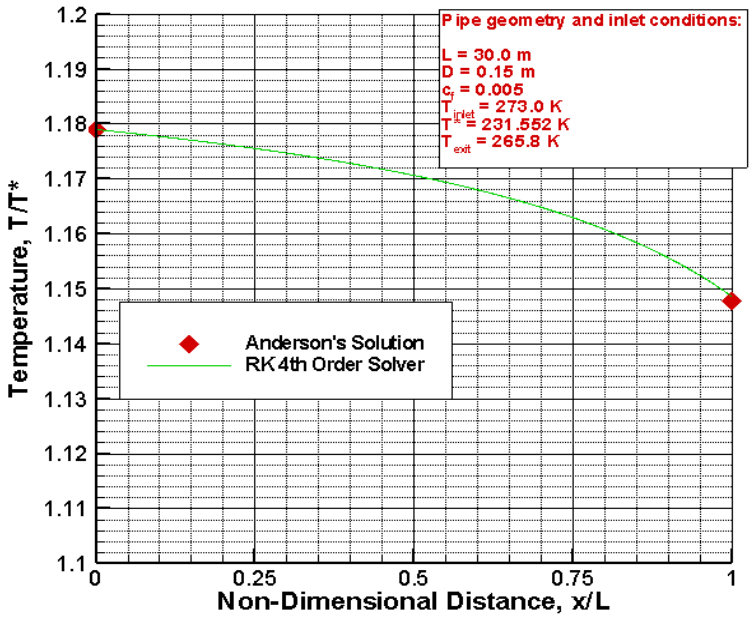

Figure 5.24. Temperature vs distance for subsonic pipe flow with constant skin friction.

Overall, the Runge-Kutta 4th order solver compares well to that of Anderson's solution. The only inconsistency takes place in the calculation of the pressure (see Figure 5.23) that the solver appears to have under-predicted.

5.2.2.2 Fanno flow with supersonic inlet conditions. The second of Anderson's problems shows the scenario of Fanno flow through a pipe with supersonic inlet conditions. Figure 5.25 shows a diagram of this problem. The inlet conditions are given in Figure 5.25. The length of the pipe is given to be 1.524 m and the diameter is given to be 0.12192 m. The Mach number, pressure and temperature are given as 3.0, 101325 Pa and 300 K respectively.

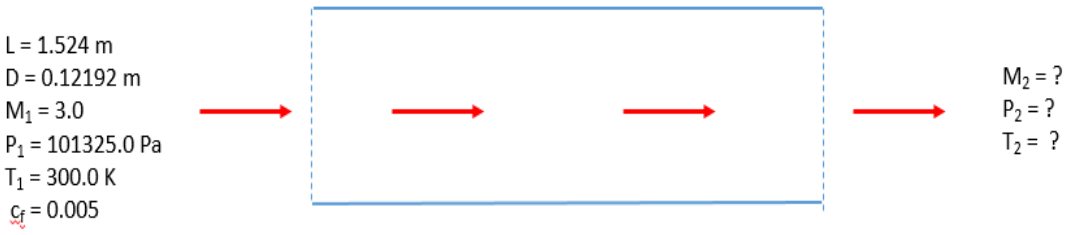

Figure 5.25. Supersonic pipe flow with constant skin friction described by Anderson.

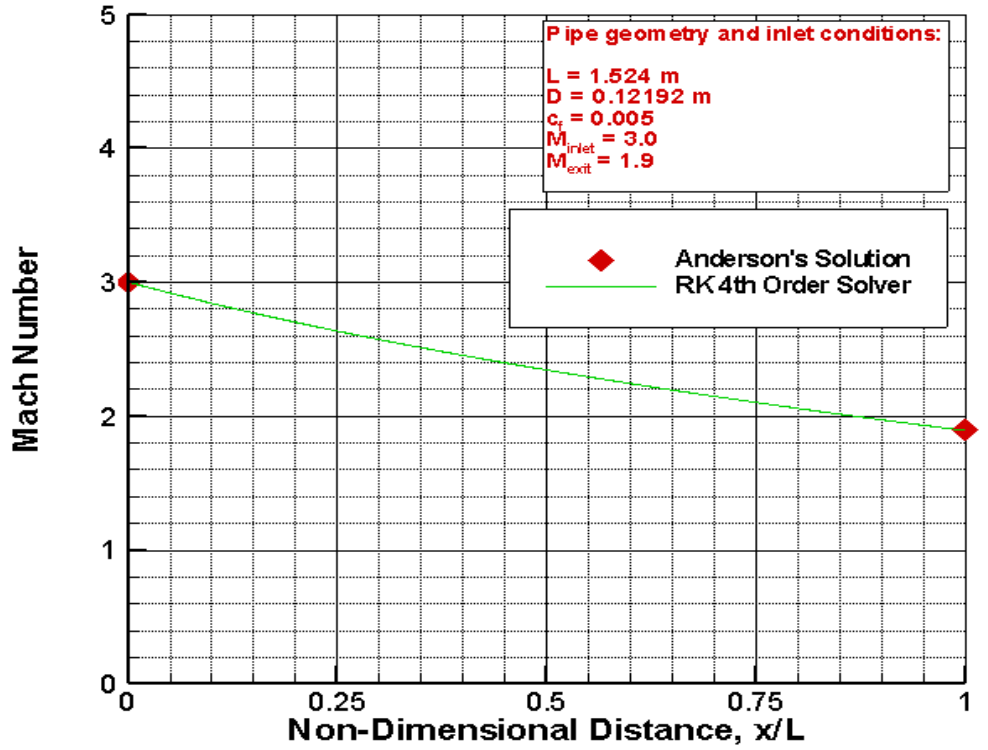

Figure 5.26. Mach number vs distance for supersonic pipe flow with constant skin friction.

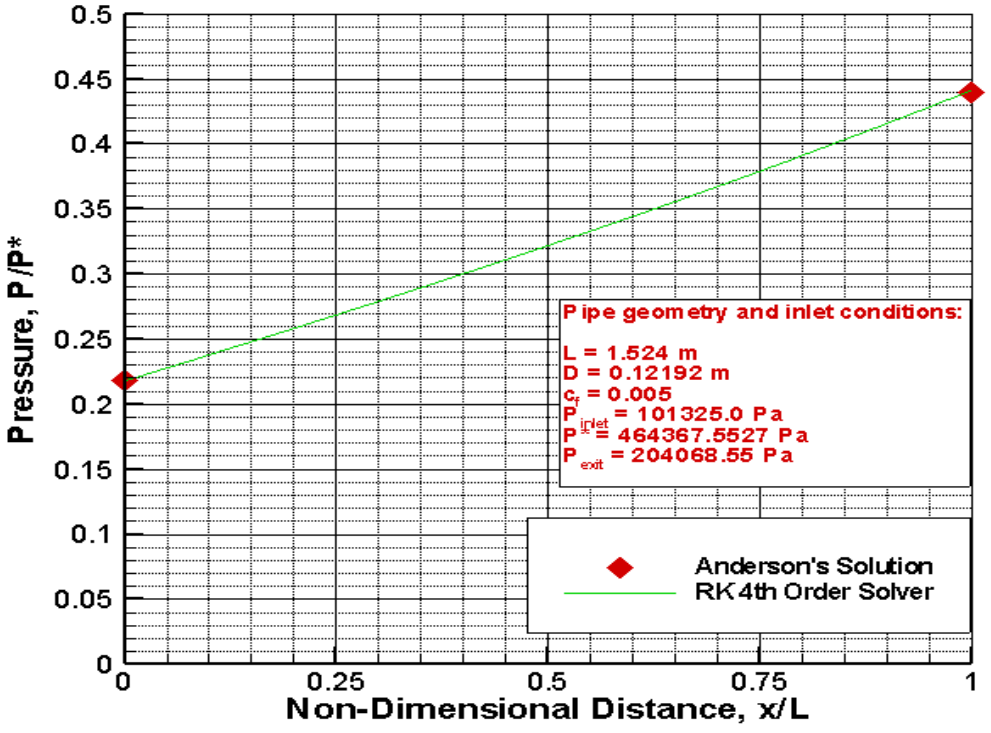

Figure 5.27. Pressure vs distance for supersonic pipe flow with constant skin friction.

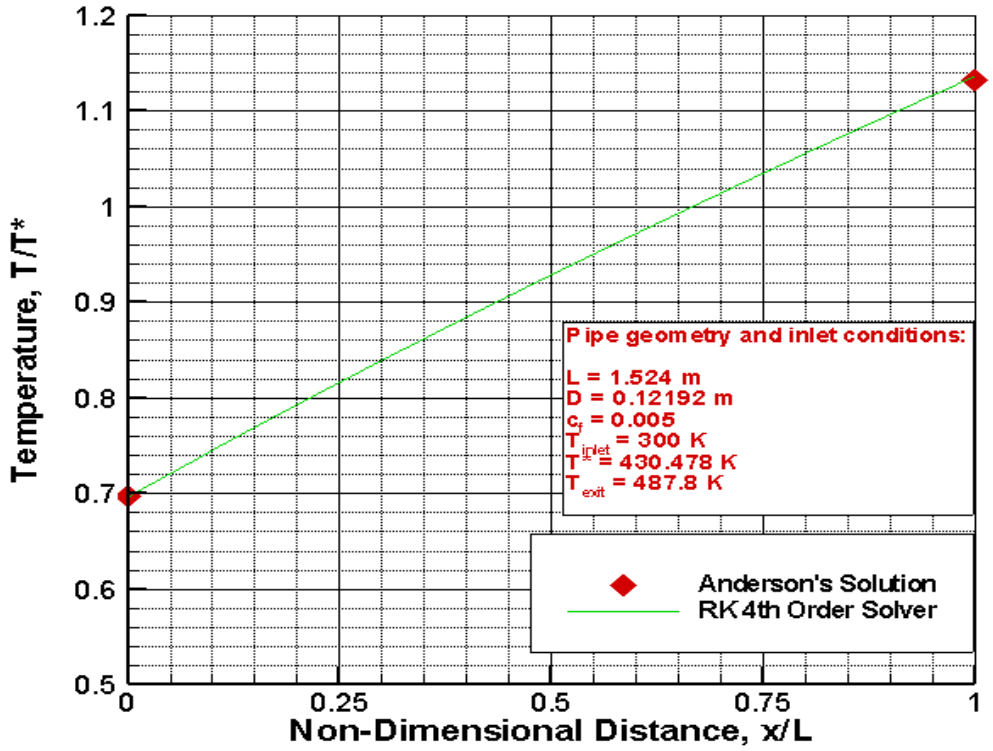

Figure 5.28. Temperature vs distance for supersonic pipe flow with constant skin friction.

From Figures 5.26 – 5.28, it is evident that the results obtained from the Runge-Kutta 4th order solver compare well with the solution obtained by Anderson.

5.3 Combined Quasi-1D and Fanno Flow Validation

5.3.1 Converging-diverging duct subjected to quasi-1D and Fanno flow. Figure 5.29 below depicts a converging-diverging nozzle. The converging section has an inlet diameter that is given to be 0.2286 m. The length of the converging section is given to be 1.27 m from the inlet to the throat. The inlet Mach number, pressure and temperature are 0.25, 344737.865 Pa and 299.817 K respectively. The throat diameter is given to be 0.1524 m and the exit diameter is given as 0.3048 m. The distance from the throat to the exit is 5.08 m. Bandyopadhyay and Majumdar used GFSSP to compute the nozzle exit conditions. The results obtained from GFSSP are compared against the results acquired from the Runge-Kutta 4th order solver in Figures 5.30 – 5.32.

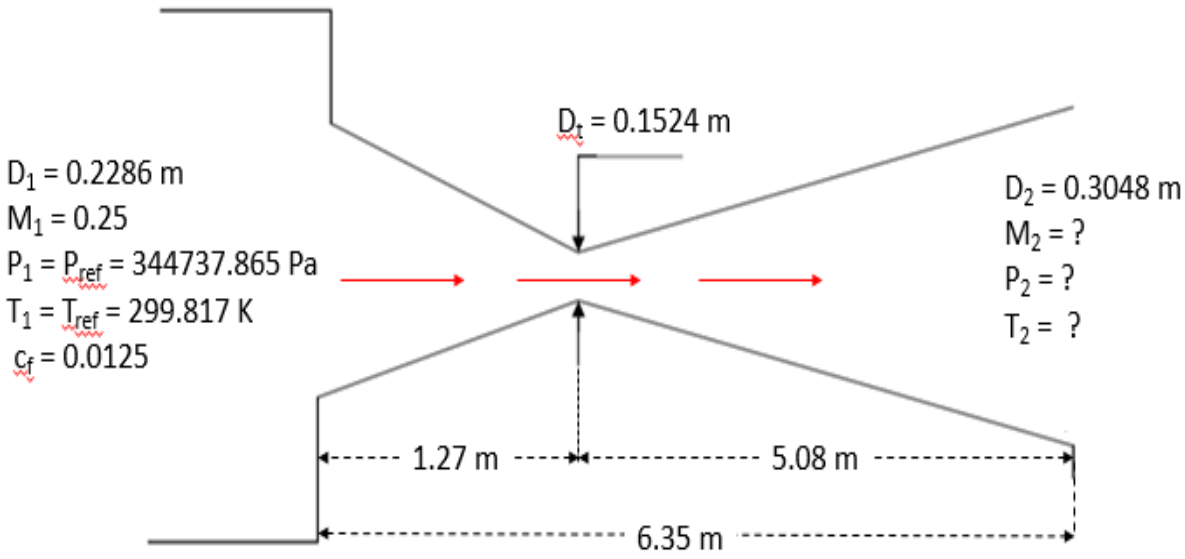

Figure 5.29. Detailed sketch of and converging-diverging nozzle (Bandyopadhyay, 2007).

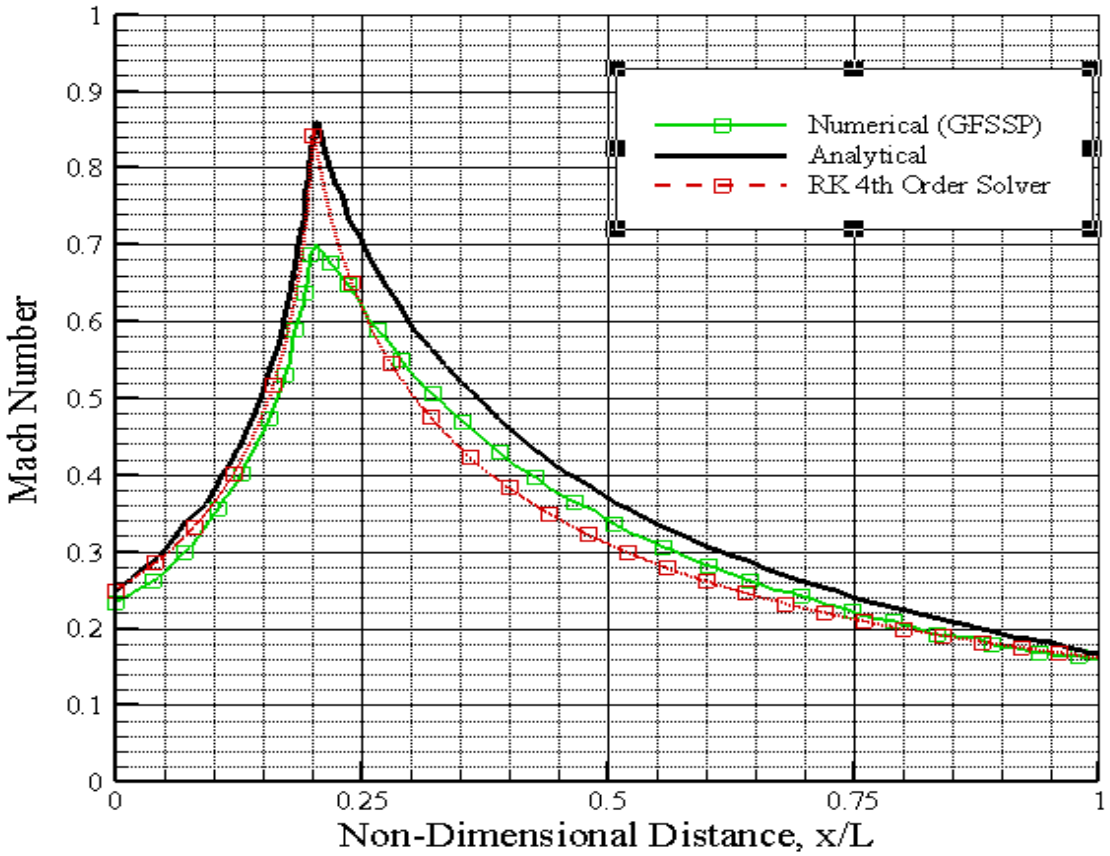

Figure 5.30. Mach number vs distance for a converging-diverging nozzle.

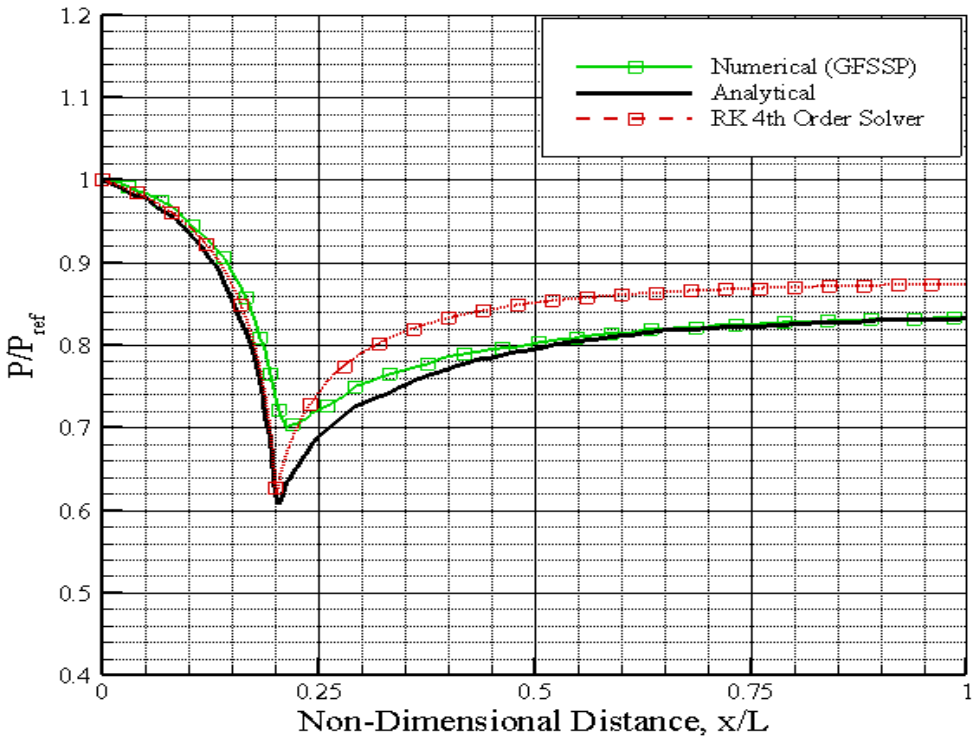

Figure 5.31. Pressure vs distance for a converging-diverging nozzle.

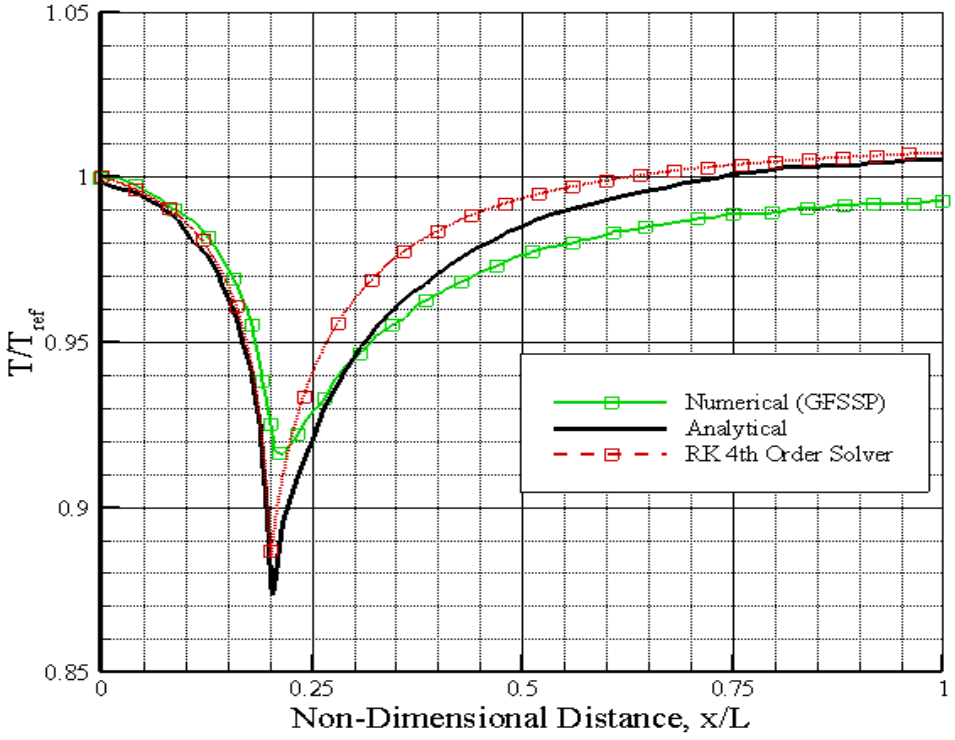

Figure 5.32. Temperature vs distance for a converging-diverging nozzle.

From Figures 5.30 – 5.32, it is clear that the results from the Runge-Kutta 4th order solver compare well with the results obtained from GFSSP. There appears to be an inconsistency in the calculation of the pressure. It should be noted that in each figure, the conditions at the throat are captured more accurately with the Runge-Kutta 4th order solver.

CHAPTER 6

Implementation of Runge-Kutta 4th Order Validation Tool

This chapter explores the use of the newly developed Runge-Kutta 4th order solver in supporting the development of NCAT scramjet design goals. Currently, the Runge-Kutta 4th order solver is successfully coupled to the NCAT scramjet design code. Its successfully integration was verified and preliminary validation studies were conducted. To date, all validation studies were conducted in a quantitative manner. The limited data obtained showed mixed results. At low Mach numbers the data seems to correlate well with flow field expectations, but this conclusion does not hold for the higher Mach numbers. This chapter describes the validations studies of interest to this thesis and highlights the challenges and short-comings of the newly developed Runge-Kutta 4th order solver.

6.1 Verification of the Scramjet Design Code

It was imperative to verify the scramjet design code prior to validating it. Independent calculations were done to reassure that functions within the scramjet design code were operating efficiently. A few select parameters relating to the forebody section of the scramjet model (displayed in Figure 6.1) were independently verified.

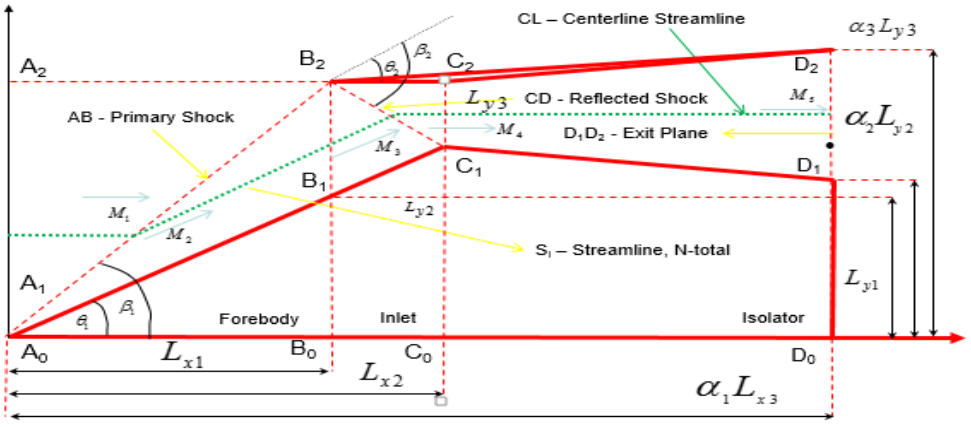

Figure 6.1. Modified forebody-inlet-isolator section of NCAT scramjet model.

Figure 6.1 represents a modified version of Figure 3.2. The alpha parameters, α1, α2 and α3 shown in Figure 6.1 will be detailed in Section 6.2. The parameters verified, in relation to the forebody section, included the outlet mass flow rate and the forebody height (L_{y3}). Both parameters are plotted over the free stream Mach number range of 4 to 12. The plots for the outlet mass flow rate and forebody height are illustrated below in Figures 6.2 and 6.3, respectively. Both figures are normalized around a free stream Mach number of 8.

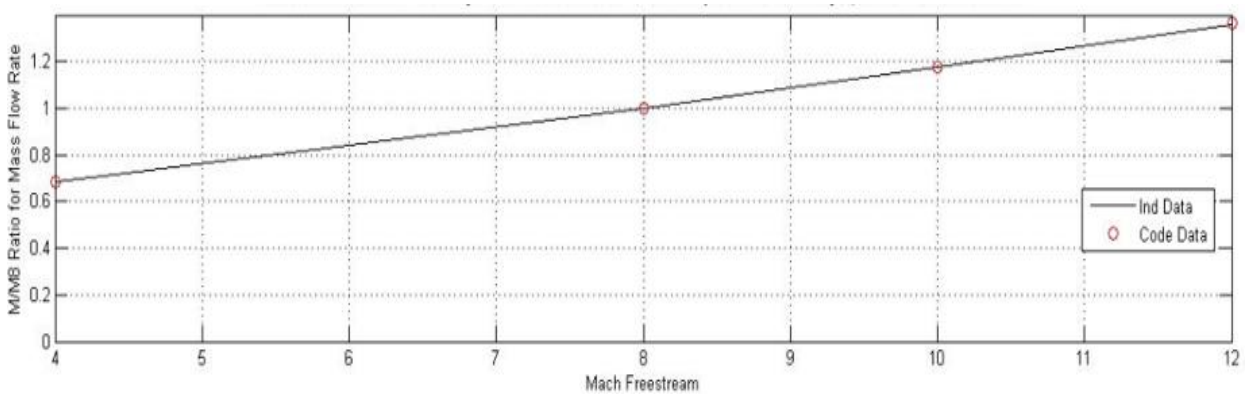

Figure 6.2. Outlet mass rate vs free stream Mach number.

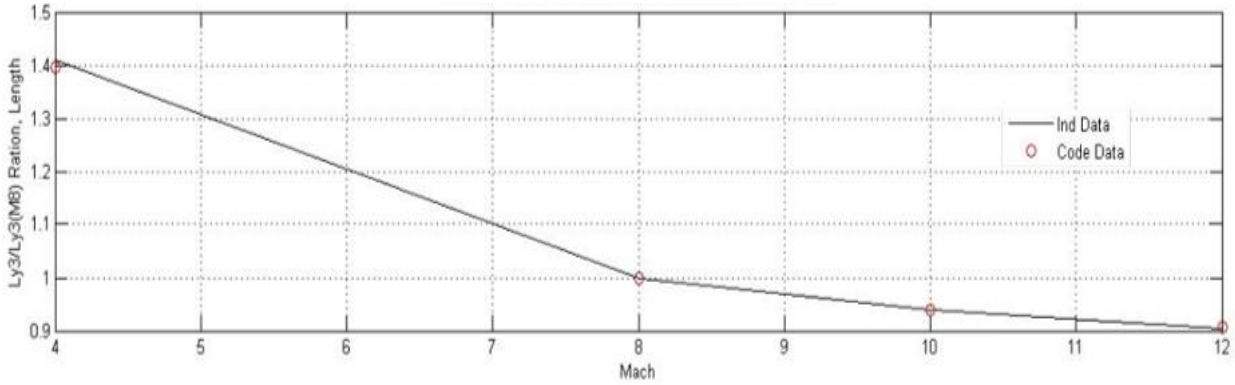

Figure 6.3. Forebody exit height vs free stream Mach number.

In Figure 6.2, the forebody outlet mass flow rate over the range of Mach numbers 4 to 12 has a linear correlation. Linear mass injection models would be simple to implement in reality. Figure 6.3 indicates that the forebody height, L_{y3}, decreases as the Mach number increases. Figure 6.3 can be interpreted as saying that a deceleration from Mach 8 to 4 would result in a 40

percent increase of the forebody height. An increase of that magnitude would require an unreasonable increase in forebody height to accommodate the deceleration from Mach 8 to 4. Increases in Mach number would translate to a decrease in forebody height of around 10 percent. These criteria only hold true for an inlet designed for Mach 8 airflow due to normalizing.

6.2 Validation of Quasi-1D Tool

The Runge-Kutta 4th order solver was integrated with the quasi-1D scramjet code developed by Dhanasar to be used as a means of validation. As previously mentioned in Chapter 1, only the isolator zone was validated. To allow for more variation in the validation study, three optimization parameters were added to give flexibility to the geometry. Refer to the detailed schematic pictured in Figure 6.1 to give clarity on how the optimization parameters are used.

From Figure 6.1, the three optimization parameters α1, α2 and α3 can be identified. The parameter α1 controls the length of the isolator while α2 and α3 each control the heights of the lower and upper walls of the isolator exit, respectively. A value of 1.0 for any alpha value signified that no modifications were made to the geometry. A value that's smaller than 1.0 indicated a reduction in length while a value greater than 1.0 meant an increase. For the validations, the primitive variable results from the quasi-1D code and Runge-Kutta 4th order solver were plotted against the isolator length. Each validation case was taken with a fixed set of optimization parameters under the free stream Mach numbers of 4, 6, 8 and 10. The altitude and wedge angle were held constant at values of 30 km and 12 degrees, respectively, for each free stream Mach number. The values for α_1, α_2 and α_3 were 1.0, 0.8 and 1.2 respectively. This configuration allows the isolator exit to be widened equally on the top and bottom without affecting the symmetry of the isolator duct. Isolator Mach number, pressure and temperature were plotted against the free stream Mach number.

6.2.1 Isolator validations. The activity within the isolator of the scramjet model is highlighted below in Figures 6.4 - 6.6. Isolator Mach number, pressure and temperature are given under the free stream Mach numbers of 4, 6, 8 and 10. The Runge-Kutta 4th order solver is plotted against the quasi-1D scramjet code for validation purposes.

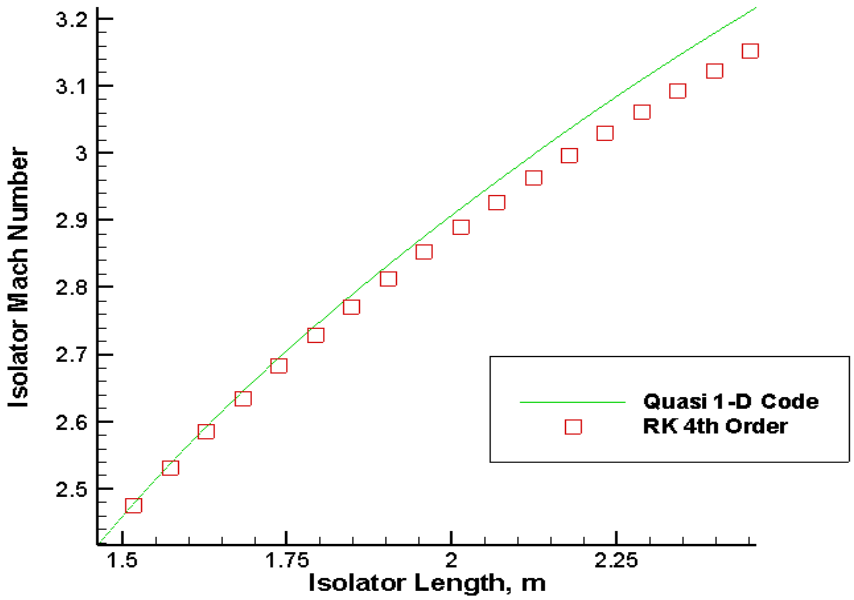

Figure 6.4. Free stream at Mach 4: isolator Mach number vs isolator length.

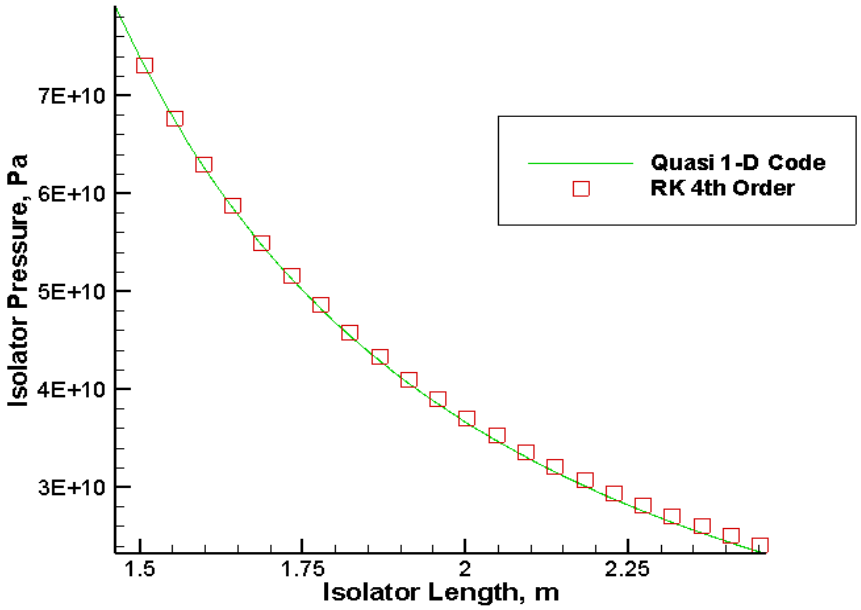

Figure 6.5. Free stream at Mach 4: isolator pressure vs isolator length.

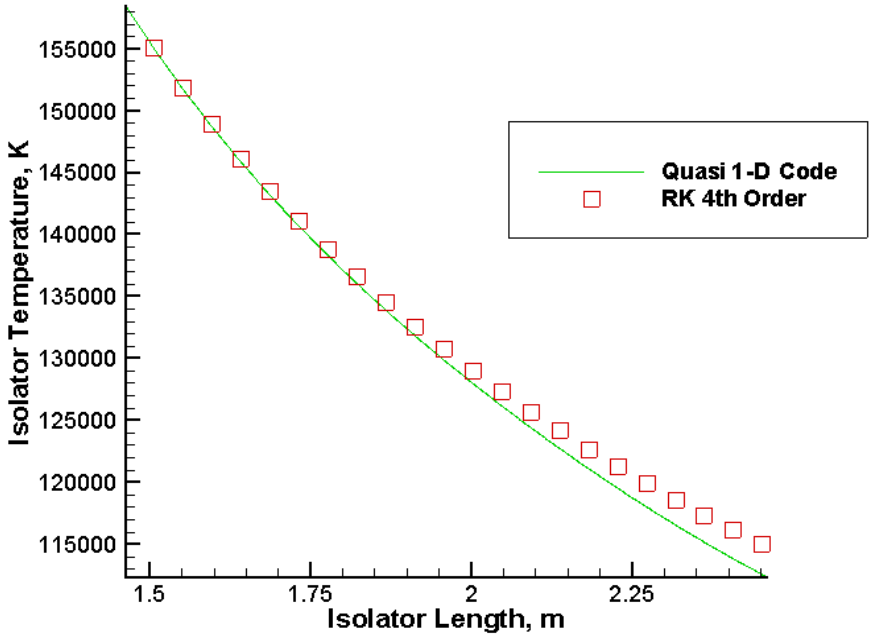

Figure 6.6. Free stream at Mach 4: isolator temperature vs isolator length.

Figures 6.4 - 6.6 indicate that the solution provided by the Runge-Kutta 4th order solver and scramjet quasi-1D code agree closely with one another. Figures 6.7 – 6.15 illustrate the activities for the remaining free stream Mach numbers of 6, 8 and 10.

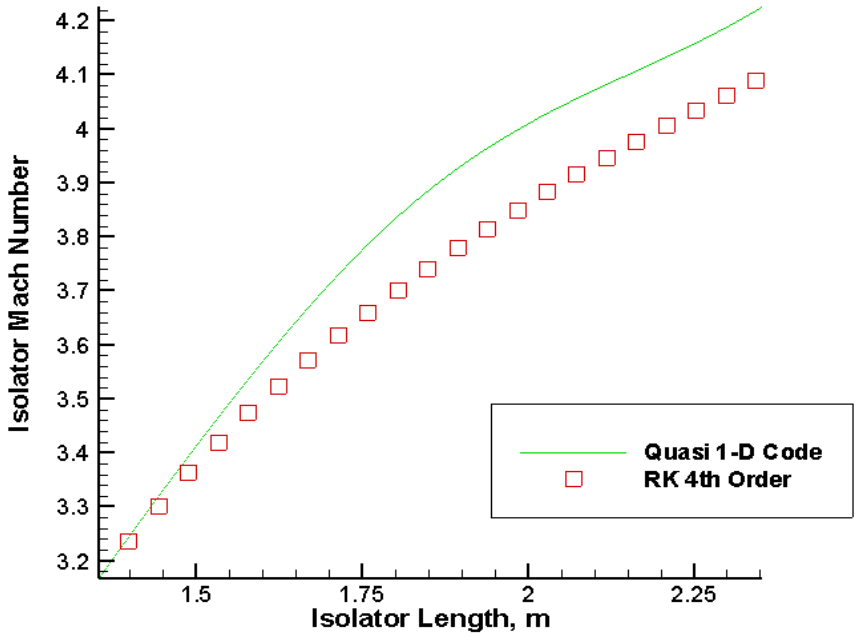

Figure 6.7. Free stream at Mach 6: isolator Mach number vs isolator length.

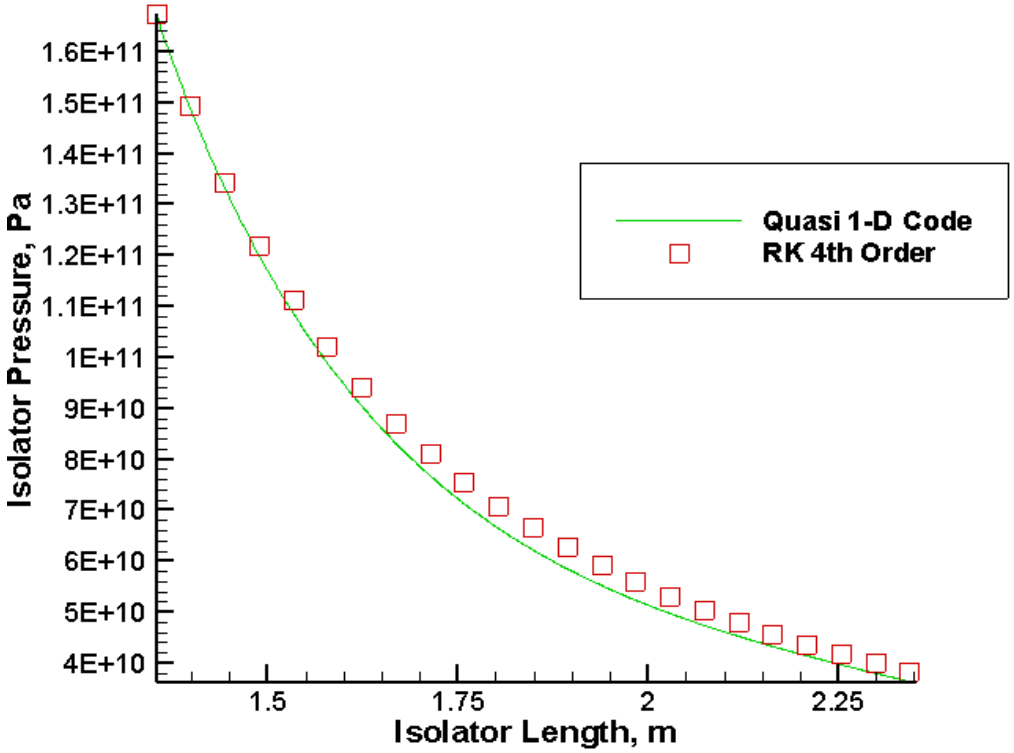

Figure 6.8. Free stream at Mach 6: isolator pressure vs isolator length.

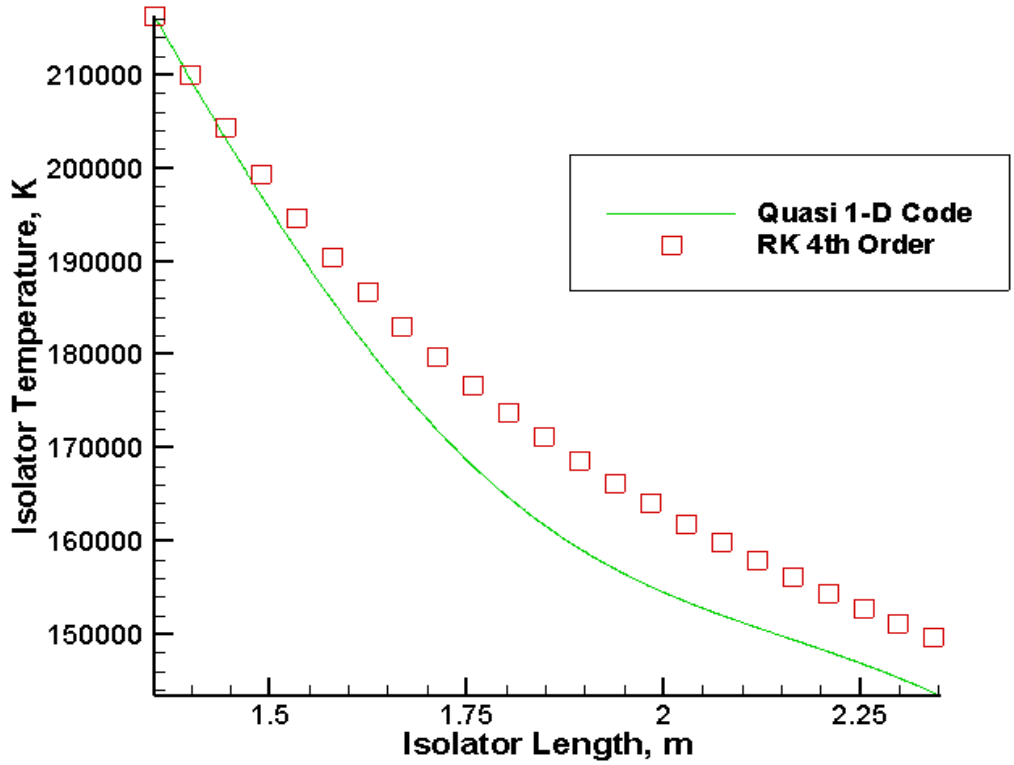

Figure 6.9. Free stream at Mach 6: isolator temperature vs isolator length.

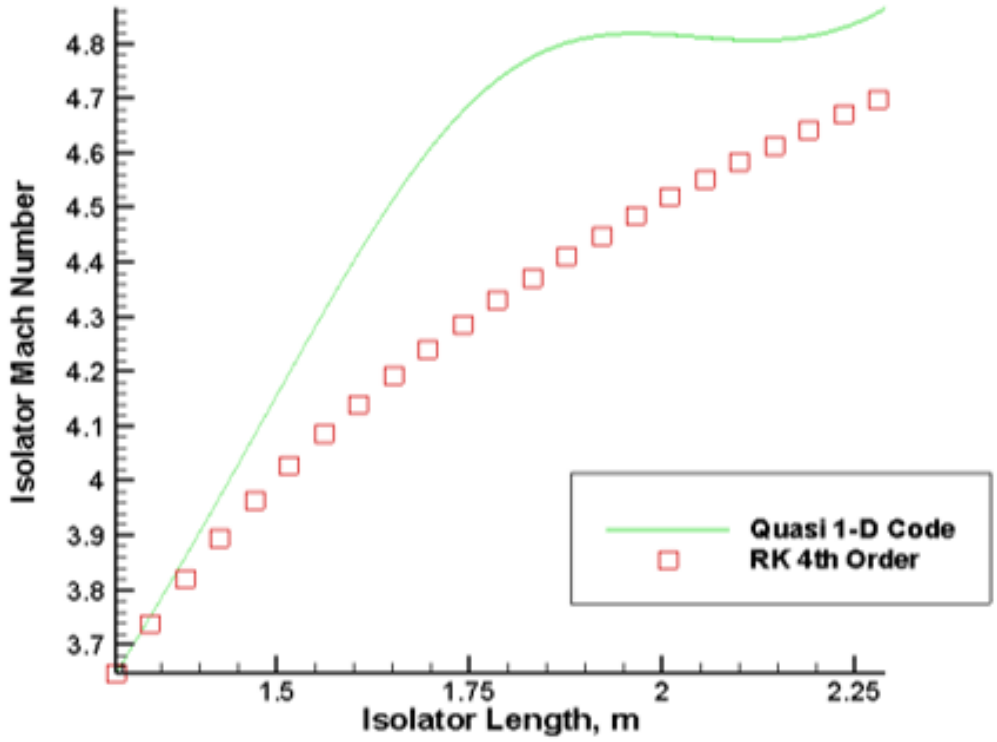

Figure 6.10. Free stream at Mach 8: isolator Mach number vs isolator length.

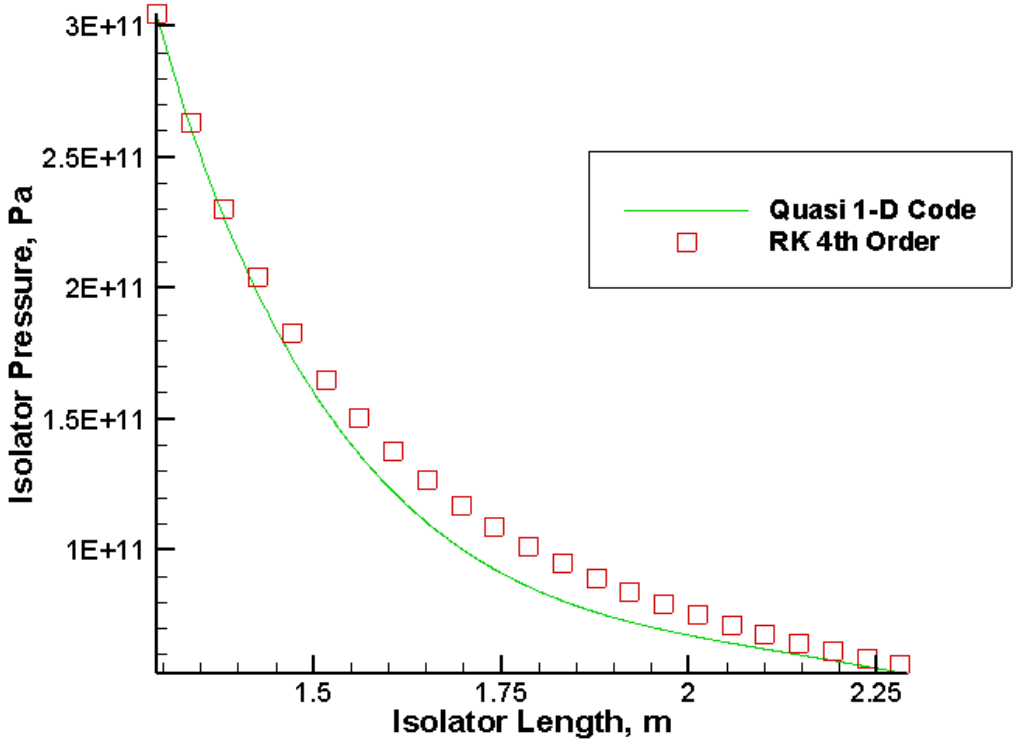

Figure 6.11. Free stream at Mach 8: isolator pressure vs isolator length.

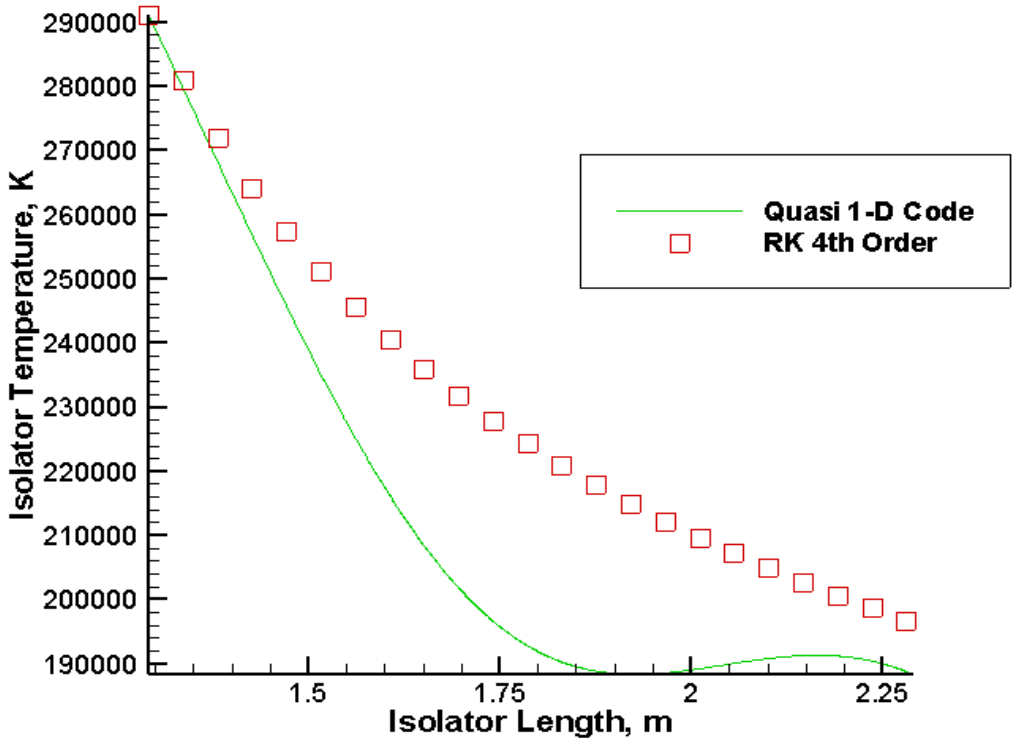

Figure 6.12. Free stream at Mach 8: isolator temperature vs isolator length.

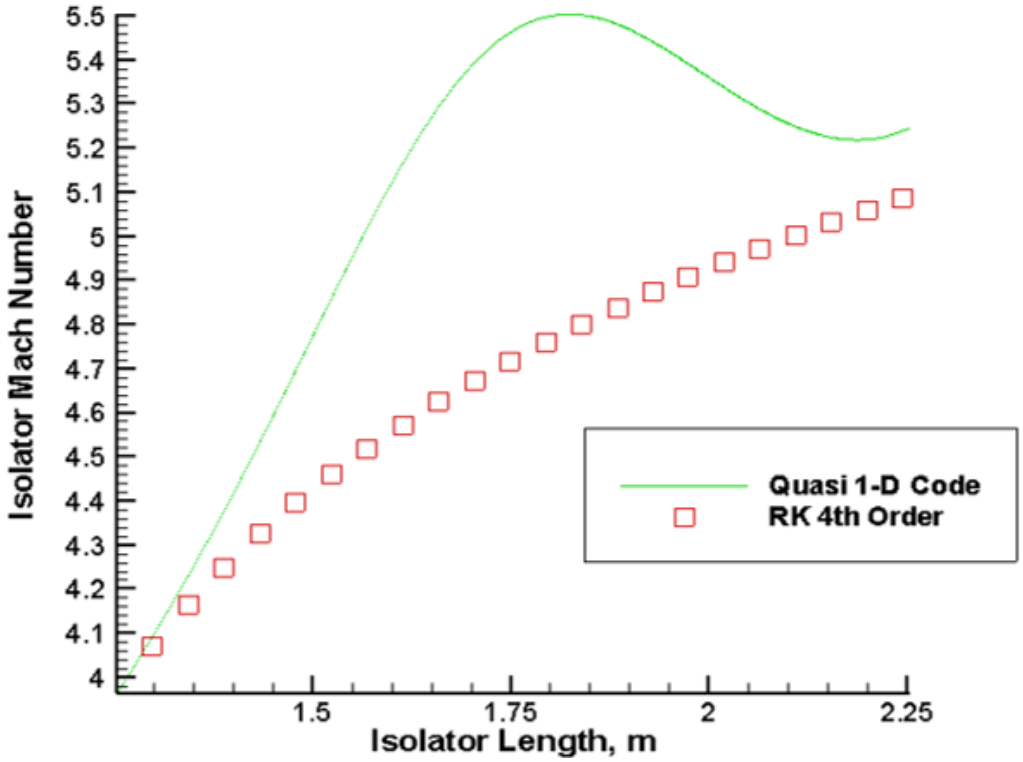

Figure 6.13. Free stream at Mach 10: isolator Mach number vs isolator length.

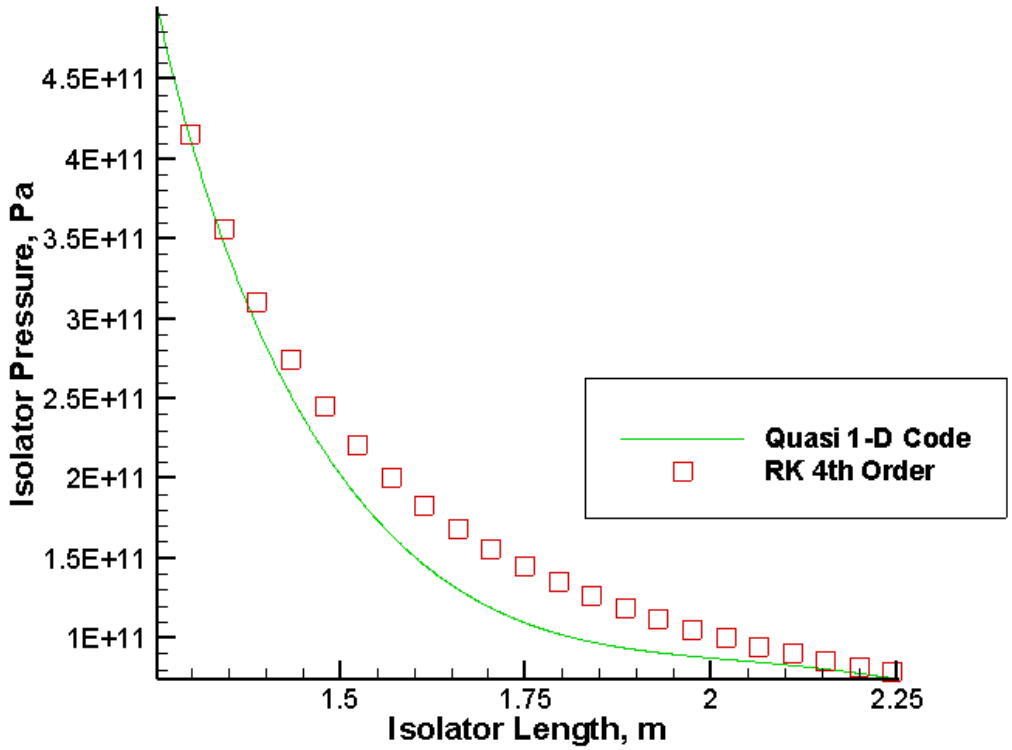

Figure 6.14. Free stream at Mach 10: isolator pressure vs isolator length.

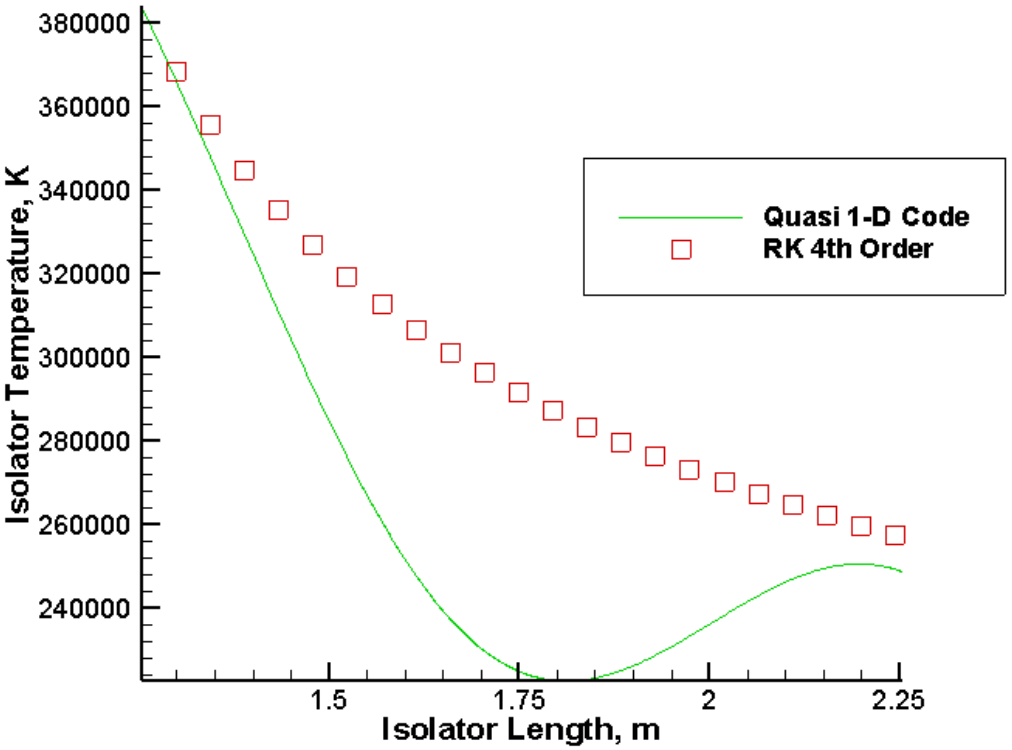

Figure 6.15. Free stream at Mach 10: isolator temperature vs isolator length.

From observation of Figures 6.7 – 6.15, it can be noticed that the Runge-Kutta 4th order solver and scramjet quasi-1D code begin to disagree as the free stream Mach number increases. A closer look can be observed in Figures 6.16, 6.17 and 6.18 below.

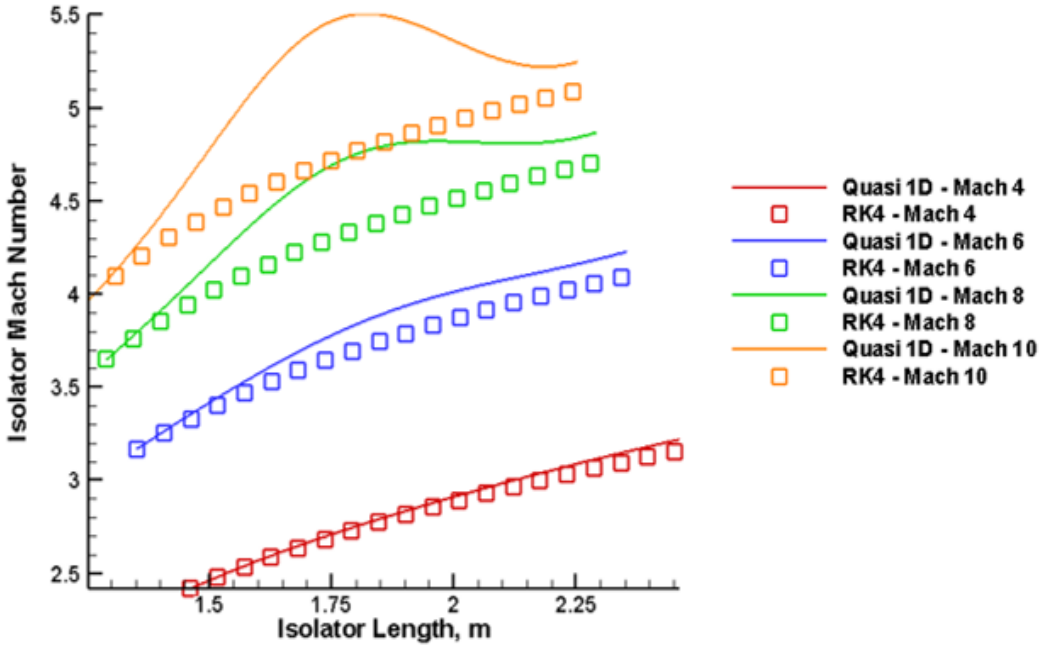

Figure 6.16. Free stream Mach 4, 6, 8 and 10: isolator Mach number vs isolator length.

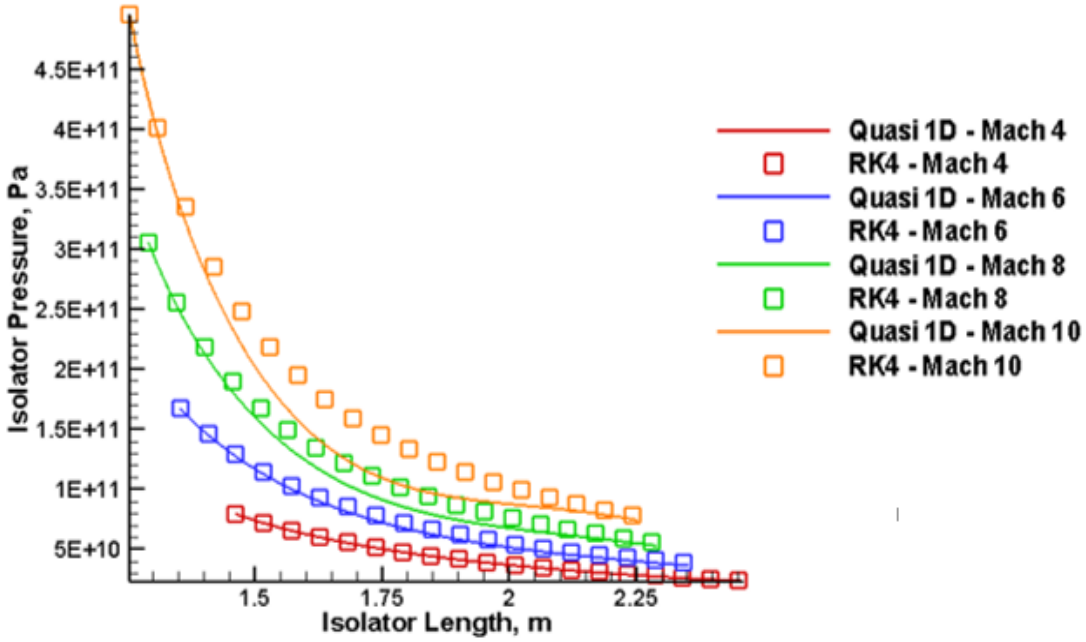

Figure 6.17. Free stream Mach 4, 6, 8 and 10: isolator pressure vs isolator length.

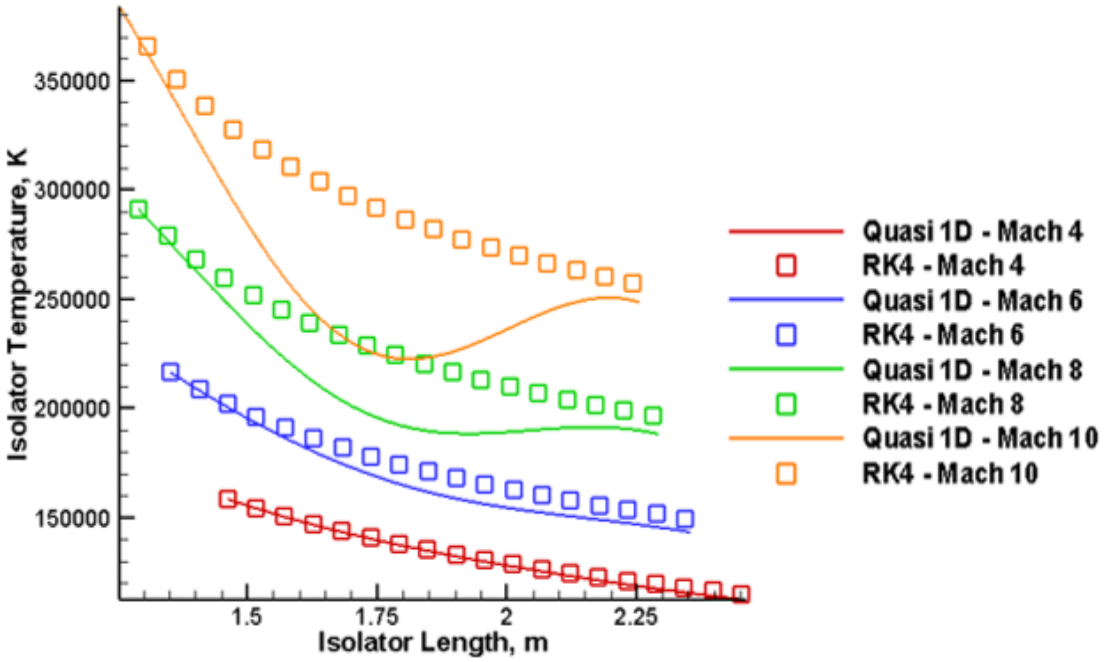

Figure 6.18. Free stream Mach 4, 6, 8 and 10: isolator temperature vs isolator length.

The discrepancy between the Runge-Kutta 4th order solver and the scramjet quasi-1D code can mainly be attributed to the Runge-Kutta 4th order's ability to simulate heat addition. The scramjet code inherently has a means of accounting for the heat addition influence. As previously mentioned, the Runge-Kutta 4th order solver only takes the influences of area change and friction into account.

CHAPTER 7

Conclusion and Future Work

7.1 Conclusion

A Runge-Kutta 4th order solver was successfully designed and programmed. The solver successfully implemented two of the five influence coefficients; namely, area change and friction. Further, the Runge-Kutta 4th order flow solver was validated against classical fluid dynamic problems and was proven correct in each case. In addition, the solver was successfully coupled to NCAT scramjet design code where it is used as a validation tool. In a set of preliminary tests, the fluid quantities, such as, Mach number, pressure and temperature were observed in the scramjet isolator duct. The results from the scramjet code as well as the newly developed solver were compared under identical scenarios. At low Mach numbers, the results match each other very well. However, the two codes began to deviate as the free stream Mach number increased. The deviation was attributed to the Runge-Kutta 4th order solver's lack of heat addition influence while the quasi-1D scramjet code accounted for it. The Runge-Kutta 4th order solver performed well, given that every component wasn't assembled yet. The independent validations of the Runge-Kutta 4th order solver (refer to Chapter 5) along with the results for low free stream Mach numbers (refer to Chapter 6) both supported the fact that the new Runge-Kutta 4th order solver was accurately developed and implemented. Nevertheless, its capability is limited to area change and frictional effects.

7.2 Future Work

For future work, it is recommended that the three influence coefficients that were eliminated from this analysis be added to the current solver (refer to Table 4.2). In addition, it is recommended that the new solver be used to analyze the entire scramjet flow path.

References

"China". (2014). China confirms new hypersonic glide vehicle test-flight. Retrieved March 4th, 2014, from http://rt.com/news/hypersonic-vehicle-missile-china-665/

"Defense". (2014). Defense, Space and Security. Retrieved March 6th 2014, from http://www.boeing.com/boeing/defense-space/ic/icbmsys/index.page

"Fanno". (2007). Fanno Flow. Retrieved March 11, 2014, from http://www.potto.org/gasDynamics/node138.html

"JAPHAR". (2009). Airflow Around the Hypersonic Vehicle JAPHAR. Retrieved March 12, 2014, from http://hathor.onera.fr/photos-en/simulations/hypersonic-vehicle-scramjet.php

"Missile". (2014). Missile defense buster: China tests new hypersonic glide vehicle. Retrieved 3/4/2014, 2014, from http://rt.com/news/supersonic-china-delivery-vehicle-554/

"Revolutionary". (2006). Revloutionary jet engine tested. Retrieved March 12, 2014, from http://news.bbc.co.uk/2/hi/4832254.stm

"Runge-Kutta". (2008). The Runge-Kutta Method. Retrieved October 15, 2013, from http://www.physics.drexel.edu/students/courses/Comp_Phys/Integrators/rk4.html

"Spinoff". (1999). Spinoff 1999.

Anderson, John D. (2003). *Modern Compressible Flow with Historical Perspective* (3rd ed.). New York, NY: McGraw-Hill.

Anderson, John D. (2011). *Fundamentals of Aerodynamics* (5th ed.). New York, NY: McGraw-Hill.

Bandyopadhyay, Alak ; Majumdar, Alok. (2007). Modeling of Compressible Flow with Friction and Heat Transfer using the Generalized Fluid System Simulation Program (GFSSP). *Thermal Fluid Analysis Workshop*

Barthelemy, R. (1989). The National Aero-Space Plane Program. *AIAA*.

Bouchez, Marc , Roudakov, Alexandre S. , Kopchenov, Valery I. , Semenov, Vyacheslav L. , Scherrer, Dominique. (2005). French-Russian Analysis of Kholod Dual-Mode Ramjet Flight Experiments. *AIAA*.

Bowcutt, Kevin ; Smith, Thomas ; Kothari, Ajay ; Raghavan, Venkataraman ; Tarpley, Christopher. (2011). *The Hypersonic Space and Global Transportation System: A Concept for Routine and Affordable Access to Space*. Paper presented at the AIAA International Space Planes and Hypersonic Systems and Technologies Conference, San Francisco, California.

Chase, R. L. , Tang, M. H. (1995). *A History of the NASP Program from the Formation of the Joint Program Office to the Termination of the HySTP Scramjet Performance Demonstration Program*. Paper presented at the Aerospace Planes and Hypersonics Technologies Conference Chattanooga, TN.

Curran, Edward T. (2001). Scramjet Engines: The First Forty Years. *Journal of Propulsion and Power, 17*(6).

Dhanasar, M. (2009). *Quasi-1D Modeling of a Morphing Ramjet-Scramjet.* (Ph.D. Dissertation), North Carolina A&T State University.

Eggers, Th. , Novelli, Ph. , Haupt, M. (2001). Design Studies of the JAPHAR Experimental Vehicle for Dual Mode Ramjet Demonstration *AIAA*.

Ferguson, F. ; Fiagbe, Y ; Dasque, N. (2009). *Design of Optimized 3D Tip-To Tail Scramjet Engines*. Paper presented at the 47th American Institute of Aeronautics and Astronautics Aerospace Sciences Meeting and Exhibit, Orlando, Florida.

`

Fry, Ronald S. (2004). A Century of Ramjet Propulsion Technology Evolution. *Journal of Propulsion and Power, 20*(1), 27-58.

Grant, Jamil D. (2010). *Validation of the Forebody Design of a Ramjet-Scramjet Propulsion System Using Computational Fluid Dynamics.* (Master of Science), North Carolina A&T State University.

Hank, Joseph M. , Murphy, James S. , Mutzman, Richard C. (2008). The X-51A Scramjet Engine Flight Demonstration Program. *AIAA*.

Harsha, Phillip T. , Keel, Lowell C. , Castrogiovanni, Anthony , Sherrill, Robert T. (2005). X-43A Vehicle Design and Manufacture. *AIAA*.

Lin, Hubao, Xue, Jizhong , Zhou, Xiaodong (1991). Development of Recovery Technology in China. *AIAA*.

McClinton, C. R. (1997). Hyper-X Wind Tunnel Program. *AIAA*.

Mercier, R. A. (1998). Hypersonic Technology (HyTech) Program Overview. *AIAA*.

Rosenburg, Zach. (2002). Fins failed in HyShot scramjet flight. Retrieved October 4, 2013, from http://www.flightglobal.com/news/articles/fins-failed-in-hyshot-scramjet-flight-150149/

Rosenburg, Zach. (2013). Hypersonic X-51 program ends in success. Retrieved October 4, 2013, from http://www.flightglobal.com/news/articles/hypersonic-x-51-programme-ends-in-success-385481/

Sato, Tetsuya , Tanatsugu, Nobuhiro , Kobayashi, Hiroaki , Hatta, Hiroshi , Sawai, Shujiro , Maru, Yusuke. (2003). *Develoment Study on the Atrex Engine*. Paper presented at the International Academy of Astronautics, Bremen, Germany.

`

Shapiro, Asher H. (1953). *The Dynamics and Thermodynamics of Compressible Flow* (Vol. 1): The Ronald Press Company.

Walker, Steven ; Tang, Ming ; Morris, Sue ; Mamplata, Caesar. (2008). *Falcon HTV-3X - A Resuable Hyprsonic Test Bed*. Paper presented at the AIAA International Space Planes and Hypersonic Systems and Technologies Conference, Dayton, Ohio.

`